ISOLATION AND CHARACTERIZATION OF NANOBODIES THAT BIND THE BTB DOMAIN OF PATZ1 TRANSCRIPTION FACTOR

by
SARAH BARAKAT

Submitted to the Graduate School of Engineering and Natural Sciences
in partial fulfillment of
the requirements for the degree of Doctor of Philosophy

Sabancı University
July 2022

ABSTRACT

ISOLATION AND CHARACTERIZATION OF NANOBODIES THAT BIND THE BTB DOMAIN OF PATZ1 TRANSCRIPTION FACTOR

SARAH BARAKAT

Molecular Biology, Genetics, and Bioengineering, Ph.D. Thesis, July 2022

Thesis supervisor: Prof. Dr. Selim Çetiner

Keywords: ZBTB, Transcription Factor, PATZ1, Nanobody, Phage display

PATZ1 is a transcription factor that belongs to the ZBTB protein family. It is found to be overexpressed in some human malignancies such as colorectal and testicular tumors, suggesting a proto-oncogenic role. However, this association remains poorly understood. The aim of this study was to generate potent and selective nanobodies against the PATZ1-BTB domain to assist the characterization of its structure and function. For this, a phage display nanobody library was screened for PATZ1-BTB domain binders. Candidate binders were analyzed by ELISA, expressed in *E. coli* and purified using affinity and size exclusion chromatography. Binding affinities were determined using surface plasmon resonance. Size-exclusion chromatography and a fluorescent two-hybrid assay were used for further assessment of specificity and affinity. The effect of the selected nanobodies on the expression levels of the known PATZ1 target genes (CTH, ETV1) was assessed using real-time PCR. Three nanobody clones with nanomolar affinities were produced as soluble proteins at high concentration. Co-elution analysis showed specific complex formation between these nanobodies and the PATZ1-BTB domain. In the fluorescent two- hybrid assay, these nanobodies showed colocalization with their target protein in the nuclei of live cells. Intracellular stable expression of PATZ1-BTB domain-targeting nanobodies resulted in significant increase of ETV1 gene expression and decrease of the CTH target gene. Our results suggest that the specific binding of nanobodies to the BTB domain of PATZ1 might regulate its gene transcriptional activity. Further investigation will clarify if these nanobodies might be used as PATZ1 modulators.

ÖZET

PATZ1 TRANSKRİPSİYON FAKTÖRÜNÜN BTB DOMAİNİNE BAĞLANAN NANOKORLARIN İZOLASYONU VE KARAKTERİZASYONU

SARAH BARAKAT

Moleküler Biyoloji, Genetik ve Biyomühendislik, Doktora Tezi, Aralık2022

Tez Danışmanı: Prof. Dr. Selim Çetiner

Anahtar Kelimeler: ZBTB, Transkripsiyon Faktörüdür, PATZ1, Nanobodiler, Faj Gösterimi Kütüphanesi

PATZ1, ZBTB protein ailesine ait bir transkripsiyon faktörüdür. Kolorektal ve testiküler tümörler gibi bazı tümör tiplerinde aşırı üretildiği bulunmuş ve bu özelliğiyle proto-onkogen özelliği önerilmiştir. Fakat bu durumun ayrıntıları hala bilinmemektedir. Bu çalışmanın amacı, PATZ1-BTB domaininin yapı ve fonksiyon karakterizasyonu için tesirli ve seçilmiş nanokorlar üretmektir. Bu amaçla, bir faj gösterimi kütüphanesi PATZ1-BTB bağlanıcıları için tarandı. Aday bağlanıcılar ELISA ile analiz edildi, *E. coli* bakterisinde üretildi ve afinite ve boyut dışlama kromatografisi ile temizlendi. Yüzey plazmon rezonans ile bağlanma afiniteleri ölçüldü. Daha öte özgüllük ve afinite analizi için flüoresan iki-hibrit analizi ve boyut dışlama kromatografisi kullanıldı. Seçilen nanokorların PATZ1'ın hedef genlerine (CTH, ETV1) etkisi gerçek zamanlı PCR ile ölçüldü. Nanomolar afiniteye sahip üç nanokor çözünür proteinler şeklinde yüksek konsantrasyonlarda üretildi. Birlikte elüsyon analizi ile nanokorlar ile PATZ1-BTB domaini arasında özel kompleks oluşumu gözlemlendi. Flüoresan iki-hibrit analizi ile nanokorlar ile hedef proteinlerinin kolokalizasyonu canlı hücrelerin çekirdeklerinde gözlemlendi. Hücre içinde stabil bir şekilde üretilen PATZ1-BTB domainini hedefleyen nanokorlar ETV1 gene okunmasını kayda değer derecede arttırırken CTH gene okunmasını azalttı. Sonuçlarımız nanokorlar ile PATZ1-BTB domaini arasındaki özel bağlanmanın gen regülasyonuna etkisi olabileceğini önermektedir. Bu konuda yapılacak araştırmalar sonucunda nanokorların PATZ1 modülatörü olarak kullanılıp kullanılamayacağı netlik kazanacaktır.

ACKNOWLEDGEMENTS

I would like to start by expressing my deep gratitude to Prof. Dr. Batu Erman for giving me the chance to join his lab as a PhD student despite the fact that I come from a different discipline. He believed in me, trusted my potentials, and never stopped guiding and supporting me. I will forever be grateful to him for helping me finding myself and finding what my true calling in life is.

I would also like to extend my sincere gratitude to Prof. Dr. Ario de Marco for all the generosity, encouragement, and support that he surrounded me with during my short-term visit to his lab and throughout my PhD journey I am also thankful to all his kind lab members, especially Sandra Folarin Oloketuyi, who devoted all her time during my visit to assisting me in conducting all my bio-panning experiments in the most efficient and timely manner.

I also want to express my heartfelt appreciation to Prof. Dr. Selim Çetiner and all esteemed jury members, Prof. Dr. Uygar Tazebay, Asst. Prof. Christopher Mayack, and Asst. Prof. Ogün Adebali for their valuable feedback. Special thanks to Asst. Prof. Emrah Eroğlu who was by my side during the hardest times, reassuring me, restoring my confidence, and opening new horizons in front of my eyes.

I want to thank all the former and present Ermanlab members: Sinan Öcal, Görkem Odabaş, Pegah Zahedimaram, Büşra Şimşek, Ecem Ültanır, Gizem cile, Sofia Piepoli, Melike Berksöz, Liyne Nogay, Gülin Baran, Saden Bedir, Sanem Sariyar, and Sinem Usluer, Canberk Yeşilada, Izem Devecioğlu, Berkay Engin. I have learned a lot from each one of them. I want to thank in particular Asma Almurtadha, Ronay Çetin, Melike Gezen, Nazife Tolay, and Hakan Taskiran who were by my side during my early times in the lab. They introduced me to the lab atmosphere slowly and were so patient in conveying all their knowledge to me in the easiest way they could. Special thanks to the undergrads: Mustafa Tunçay, Asal Ghaffari Zaki, and Ege Ezen. Working in a project that involves dealing with a lot of samples is always extremely tiring, but these guys made it much easier for me. I was so fortunate to have such smart and dedicated students assisting me at all the time.

This PhD could not have been possible without the help of many collogues. In particular, I would like to thank Alp Ertunga Eyupoglu and all of our friends from Turgut İlaç company for assisting me with my SPR experiments. Sincere appreciations also to Emre Vatandaşlar from Medipol University for conducting the cell sorting experiments.

My PhD years were the toughest in every aspect. It was only the help and mercy of my Lord Allah (swt) that got me through. Part of his mercy is surrounding me always with lovely friends. Among these wonderful friends is my dear Pegah Zahedimaram and her husband Navid Haghmoradi, Melike Gezen, Nermeen Ahmed and her wonderful family, Sarah, Nadeen, and Maryam, Atia Shafique, Şeyda Demirok, Kubra Erçetin, Zeyneb Büşra Çakır, and Sarah Hemdan.We experienced a lot of heartache and grief, but we also enjoyed a lot of wonderful and unforgettable times together. Thank you all for your true love and for all the happy moments you bought to my life.

My family is God's greatest gift to me in this life. I am so blessed to have such loving, caring, and close-knit family. My mother, the real glory of this family, her prayers were reaching me each and every day wherever I was, lightning my days and filling my heart with peace and tranquility. Today I stand very humbly before her as no words can express my sincere gratitude for all what she has granted me throughout my life. To my brothers and sisters: Asma, Eman, Huda, Ibrahem, Suaad, Majed, and Shaima, my brothers in-law Jameel, Ahmed, and Aladin, and my sister in-law Nada, thank you for everything, but most of all for bringing all these adorable nieces and nephews into our lives who overwhelmed our family with so much joy, laughter, and fun. Safa, Hanan, Esam, Alaa, Rawa, Elyas, Elaf, Hamzah A, Abdulatheem, Wed, Hamzah B, Yusuf, Hashim, Laith, Mohammed, Kenan, Layan, Juman, love you all so much. My beloved father, who was impatiently looking forward to this day, but unfortunately, I couldn't make it in time for him. He left this world but left me the key values of this life that I will be holding on for the rest of my life, religion, morals, and knowledge.

Finally, I would like to mention with lots of appreciation that this work was supported by the TÜBİTAK BIDEB 2215 PhD fellowship and 118Z015 and 20AG007 grants.

Dedicated to,

My Almighty lord, the source of knowledge and understanding …… Allah(swt)

Thank you

صدق الله العظيم

TABLE OF CONTENTS

LIST OF TABLES

LIST OF FIGURES

LIST OF SYMBOLS AND ABBREVIATIONS

ADP	Adenosine Diphosphate
Ag	Antigen
Amp	Amperes
Amp	Ampicillin
APL	Acute Promyelocytic Leukemia
APS	Ammonium Persulfate
aTTP	Acquired Thrombotic Thrombocytopenic Purpura
B2H	Bacterial Two-Hybrid
BACH2	BTB and CNC Homology 2
BCL6	B-cell lymphoma 6
bp	Base pair
BRC	Broad Complex
BSA	Bovine Serum Albumin
BTB	Broad-complex, Tramtrack, and Bric-à-Brac
CAR	Chimeric Antigen Receptors
CDR	Complementary Determining Regions
CEA	Carcinoembryonic Antigen
CFU	Colony Forming Units
Chl	Chloramphenicol
CIAP	Calf Intestine Alkaline Phosphatase
cm	Centimeter
CMV	Cytomegalovirus
CTLA-4	Cytotoxic T-Lymphocyte-Associated protein 4
DLBCL	Diffuse Large B-Cell Lymphomas

DMEM	Dulbecco’s Modified Eagle Medium
DMSO	Dimethylsulfoxide
DNA	Deoxyribonucleic Acid
DsbC	Disulfide Bond isomerase
E. Coli	Escherichia coli
EC	Endothelial Cells
EDTA	Ethylenediaminetetraacetic Acid
ELISA	Enzyme-Linked Immuno-Sorbent Assay
EMT	Epithelial-Mesenchymal Transition
F2H	Fluorescent Two-Hybrid
FABP4	Fatty Acid-Binding Protein 4
FACS	Fluorescence-Activated Cell Sorting
FBS	Fetal Bovine Serum
FR	Framework Regions
G	Gram
GBP	GFP-Binding Protein
GFP	Green Fluorescent Protein
GSC	Glioma-initiating Stem Cells
h	Hour
HBS	HEPES-Buffered Saline
HC	Heavy Chain
HcAb	Heavy Chain only Antibody
HDAC	Histone deacetyltransferase
HER2	Human Epidermal growth factor Receptor type 2
HIV	Human Immunodeficiency Virus

HMGA	High Mobility Group proteins characterized by an AT-hook
HRP	Horse-Radish Peroxidase
IMAC	Immobilized Metal Affinity Chromatography
Kan	Kanamycin
kDa	Kilo Dalton
KRAB	Kruppel-Associated Box
L	Liter
LB	Luria Broth
LC	Light Chain
M	Molar
m	Milli
m	Mouse
mAb	Monoclonal Antibody
MAZR	MAZ Related factor
MEF	Mouse Embryo Fibroblast
min	Minute
MM	Minimal Medium
MMR	Macrophage Mannose Receptor
MOMP	Mitochondrial Outer Membrane Permeabilization
mRNA	Messenger RNA
n	Nano
Nb	Nanobody
NCOR	Nuclear Receptor COrepressor
OD	Optical Density
p	Pico

PARP1	Poly (ADP-Ribose) Polymerase 1
PATZ1&2	POZ/BTB And AT Hook Containing Zinc Finger 1&2
PBS	Phosphate Buffered Saline
PCNA	Proliferating Cell Nuclear Antigen
PCR	Polymerase Chain Reaction
PD-L1	Programmed Death-Ligand 1
PEG	Polyethylene glycol
PEI	Polyethylenamine
Pen-Strep	Penicillium and Streptomycin
PET	Positron Emission Tomography
PLZF	Promyelocytic Leukemia Zinc Finger
POZ	Poxviruses and Zinc-finger
qPCR	Real-time Quantitative PCR
RNA	Ribonucleic Acid
RNF4	RING Finger Nuclear Factor 4
RPKM	Reads Per Kilobase Per Million
rpm	Rotation Per Minute
RT-PCR	Real-Time Polymerase Chain Reaction
s	Seconds
SCAN	SRE-ZBP, CTfin51, AW-1 (ZNF174), Number 18 cDNA
scFv	Single-Chain Variable Fragment
SDS-PAGE	Sodium Dodecyl Sulfate Polyacrylamide Gel Electrophoresis
SEC	Size Exclusion Chromatography
SIN3A	SIN3 homolog A
SMRT	Silencing-Mediator for Retinoid/Thyroid hormone receptors

SPECT	Single-Photon Emission Computed Tomography
SPR	Surface Plasmon Resonance
SSD	Subsyndromal Symptomatic Depression
SV40	Simian Virus 40
TBE	Tris Borate EDTA
TCEP	Tris (2-carboxyethyl) phosphine hydrochloride
TEMED	Tetramethylethylenediamine
TGFB1	Transforming Growth Factor Beta 1
TMB	Tetramethylbenzidine
Ttk	Tramtrack
UV	Ultraviolet Light
v	Voltage
VH	Variable Heavy chain domain
VHH	Variable Heavy chain domain of Nanobodies
ZF	Zinc Finger
ZID	Zinc finger protein with Interaction Domain
ZSG	Zinc Finger Sarcoma Gene
α	Alpha
β	Beta
μ	Micro

1. INTRODUCTION

1.1. The BTB-ZF Transcription Factors

The BTB-ZF is a family of proteins that share a main character of comprising two major parts: an N terminus BTB domain and a C terminus ZF motif. The (BTB) stands for Bric-a-brac [1], Tramtrack [2], and Broad complex [3], which are transcription factors cloned from mutant *Drosophila melanogaster* where the conserved BTB sequences were identified for the first time [1,4]. On the other side, (ZF) stands for the zinc finger motif which was first identified as part of the transcription factor IIIA protein1 in *Xenopus laevis* [5]. The BTB domain is also known as the POZ domain since it was also discovered in the poxvirus virus genome [6,7]. The ZF domain was also characterized in *Drosophila* Krüppel protein that is responsible for segmentation [8], therefore, synonymously the BTB-ZF protein family is also known as the POK (POZ/Krüppel) family.

The human genome comprises 49 genes that encode BTB-ZF proteins, however, the BTB domain is encoded by 107 more genes in various combinations of motifs other than the ZF motif [9]. The BTB-ZF proteins mostly function as transcription factors where their ZF motifs recognize and bind to regulatory regions of target genes [10], whereas their BTB domains are responsible for interactions with other transcription regulatory proteins [11], thus the transcriptional activity of these factors is highly context-dependent. The BTB domains can recruit co-activators such as p300, and act as transcriptional activators; or they can recruit co-repressor proteins such as SMRT (Silencing Mediator for Retinoid and Thyroid Hormone

Receptor), or NCOR (Nuclear Receptor Corepressor), and thus act as transcriptional repressors [12,13].

The exact role that these proteins play in normal, or disease conditions is not fully understood and many aspects of the mechanisms behind their mode of action are yet to be discovered. However, gene knockout methods, chromosomal aberrations, and epigenetic alterations have increased our knowledge about these proteins. Members of this protein family are now well known to have important roles in a variety of critical biological processes, including the maturation of immune cells and the regulation of immune responses, [14,15]. Other members of this protein family were found to be associated with craniofacial development and neuronal apoptosis [16,17]. From another aspect, involvement in cell cycle control and DNA damage responses suggested a tumor-related function of some of these proteins. Indeed, some were found to have an oncogene role such as B-cell lymphoma 6 (BCL6) in B cell lymphoma [18–22], or tumor suppressor role such as APM-1 in association with cervical carcinoma [23].

1.1.1. The Structure and Function of The ZF Domain

After the first ZF motif was identified as part of the IIIA transcription factor in *Xenopus laevis* [5], many studies were carried to investigate its structure and function. A variety of extended sequence motifs were found to accompany these ZF motifs, thus determining their functions. One of the domains that were found to accompany ZF motifs was discovered by Bardwell and Treisman [7]. They found a ZF protein that was coupled with an interaction domain of a conserved 120 amino-acid sequence at its N terminus and thus they decided to name it ZID (zinc finger protein with interaction domain)[7]. The same coupled protein was also recognized in a group of poxvirus proteins [6], therefore it was subsequently known as Pox virus and Zinc finger or " POZ " domain for short [7]. The POZ domain was identified as a conserved sequence in a large family of proteins such as ZF5, Ttk, and GAGA, and many organisms spanning *Drosophila* and Humans [7]. In *Drosophila*, the POZ domain was identified in association with Broad Complex (BRC), Tramtrack (Ttk), and Bric-a-brac

protein [1,2], therefore a second name the for POZ domain is the BTB domain (Broad-Complex, Tramtrack, and Bric-a-brac). In *Drosophila*, the POZ domain was found to be involved in the regulation of many vital processes such as oogenesis, and eye and limb development [4].

Kruppel-associated box (KRAB) is another protein-protein interaction domain that is associated with the ZF motif. Like the BTB/POZ domain, the KRAB domain is a widespread domain of a conserved amino acid sequence at the amino-terminal end of proteins [24]. This domain seems to be vertebrate-specific and has been identified in many human genes performing a wide range of functions in hematopoietic cell development and differentiation [24,25]. Another motif that is found in association with zinc finger transcription factors is the SCAN domain. The name is derived from the initials of four proteins where this domain was initially found (SRE-ZBP, CTfin51, AW-1 (ZNF174), and Number 18 cDNA or ZnF20). Like KRAB, it seems to be vertebrate-specific, however, in contrast to KRAB and BTB/POZ domains, the SCAN domain is not associated with either transcriptional activation or repression [26].

Structurally each ZF motif is composed of tandem repeats of two cysteines in close proximity to two histidines (C2H2) that coordinate a zinc (Zn) ion. The domain folds into a finger-like projection that can grasp DNA [27]. By this structure, ZF domains are able to bind DNA in a new approach based on recognizing varying lengths of nucleic acid sequences. While other DNA-binding mechanisms depend on limited homo/heterodimers formation of binder proteins on the double helix DNA strand, ZFs' unique structure provides a huge number of combinatorial possibilities for DNA recognition and binding. Therefore, it is not surprising that ZFs are not only the most common DNA-binding motif but also one of the most widespread motifs in nature[10]. The discovery of the new binding mechanism of ZFs to DNA inspired many researchers about many other possible applications of this mechanism. The zinc finger design can produce specific DNA-binding constructs for targeted gene expression [28]. These constructed ZF-like peptides can switch targeted genes off or on when associated with co-activator or repressor domains. Alternatively, zinc finger peptides can be combined with an appropriate effector or functional domains to construct chimeric proteins, thus the targeted genes can be modified or manipulated [29].

In humans approximately 600 to 700 genes encode ZF motifs, reflecting the essential role that this class of transcription factors plays [24]. Many of these ZF proteins have been associated with tumorigenesis, thus understanding the function of this family of proteins is critical for human health. As an example, two members of the ZBTB family, BCL6 and PLZF (Promyelocytic Leukemia Zinc Finger) proteins were found to be associated with non-Hodgkin's lymphoma [30], and acute promyelocytic leukemia (APL) [31], respectively.

1.1.2. The Structure and Functions of The BTB Domain

The BTB domain was first identified in the genome of poxvirus [6]. The name was derived from *Drosophila* transcription factors (Bric-a-brac, Tramtrack, and Broad complex) that had the same sequence that was identified in poxvirus proteins at their N terminus [1,4]. The BTB domain is mostly identified in eukaryotes, therefore it seems that it had evolved after the origin of eukaryotes. However, its existence in viruses might be attributed to the evolutionary ability of some viruses to capture cellular genes. There are around 2800 known BTB containing proteins, which makes it one of the most widespread domains. Out of these, 350 proteins were identified in humans. The rest were identified in a wide range of organisms such as plants, metazoans, and fungi. The great versatility of this domain is perhaps the reason for this success in evolution [32].

Structurally, BTB domains are composed of around 120 amino acids arranged in a unique three-dimensional structure of five α-helix clusters which are capped from one end by a short three-stranded beta-sheet [7]. The overall arrangement and the secondary structure are similar; however, the primary sequence possesses a very high variability especially in the core domain [33]. Out of the 95 amino acids that form the core domain, only a dozen are conserved and most of those are hidden within the scaffold of the domain [33,34]. On the other hand, the exposed residues contain highly variable residues that constitute the interaction surface of the domain. The large diversity in this interaction surface, allows these domains to have a wide variety of protein-protein interaction partners and thus provides the first level of their functional diversity. For instance, the variable residues at the interaction surface of

the BTB domain in BTB-ZF proteins can allow for homodimerization and heterodimerization, as well as recruitment of transcriptional corepressors such as NCOR and SMRT [35–37]. Tetramerization have also been reported for some BTB domains such as those in the potassium ion channel protein [38].

Additionally, some of these BTB domains show gain or loss of some class-specific extensions at N- terminus or C-terminus of the core domain. The difference in these class-specific extension elements provides the second level of functional diversity of these domains. For example, the T1 domain contains the ‘‘core’’ BTB elements only. Elongin C, on the other hand, is a different BTB domain that lacks the alpha-helix, in contrast to the Skp1 BTB domain that has gained two additional alpha-helices at the C terminus and the BTB-ZF proteins that have gained an extra alpha-helix and a beta-sheet at their N terminus. Accordingly, these proteins are involved in different functions. While T1 is an ion channel protein, Elongin C and Skp1 are well-known adaptor molecules for protein degradation. On the other hand, most BTB-ZF containing proteins are transcription factors [32,33].

The third level of functional diversity is provided by the diverse domains that can pair with the BTB domain. Twenty different domains have been reported to couple with the BTB domain, however, five are most commonly observed, these are; Ion transport, NPH3, MATH, Kelch, and Zinc Finger domain [32]. The mode of coupling with other domains affects in turn the function of the protein. For example, ZF coupled BTB proteins have DNA binding ability owing to the ZF motif, therefore these proteins mostly have transcription regulation functions. In other proteins, this domain is paired with ubiquitin ligase domains or with transmembrane channel proteins. However, some proteins are composed of the BTB domain only such as Skp1 and Elongin C which are involved in protein degradation and regulation of transcriptional elongation respectively [39,40].

It can be stated that; in terms of function, BTB domains are generally protein-protein interaction domains, as such, they were nicknamed as "Born To Bind". For this, they have the ability to form transient or stable interactions or recruit other interacting proteins. The roles they play are diverse as indicated above, however; in summary, these roles fall into one

of three categories; protein degradation, signal transduction, and transcription regulation [32]. The role as a regulator of transcription is thought to be the latest incidence in order to supply the need to regulate complex genomes. This might be the reason that BTB-containing transcription factors are missing in yeast [32]. In contrast, the BTB domain role in protein degradation and signaling is conserved in yeast and other eukaryotes [32].

1.2. POZ (BTB) and AT-hook Containing Zinc Finger 1 (PATZ1)

PATZ1 is a transcription factor that belongs to the BTB-ZF protein family. The name is derived from the initials of the names of the domains that constitute it (POZ, AT-hook containing Zinc Finger 1). It is also known in many alternative names such as PATZ1, MAZ Related factor (MAZR), Zinc finger Nuclear Factor/Zinc finger protein 278 (ZNF278/Zfp278), Zinc finger Sarcoma Gene (ZSG), and dJ400N23.

In humans, the PATZ1 protein is encoded by the ZBTB19 gene which is located on chromosome number 22. This gene is composed of six exons and can be alternatively spliced into six variants; four of which encode proteins (isoforms of 687, 537, 641, or 537 amino acids), while the last two are non-protein coding transcripts (Figure 1.1).

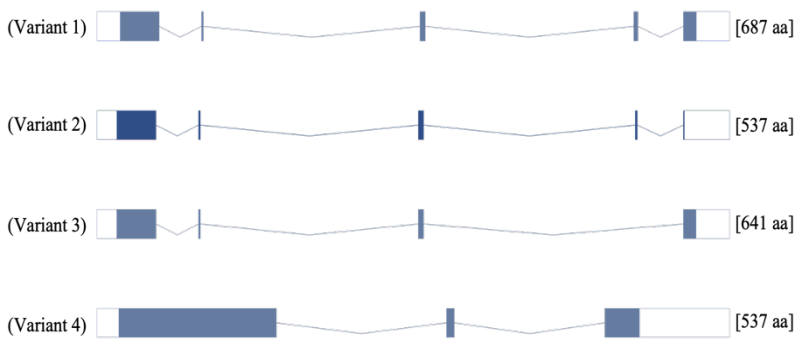

Figure 1. 1: PATZ1 transcript variants.

Schematic representation of the 4 transcript variants of the PATZ1 gene with their size in amino acid numbers. Shaded boxes represent open reading frames and unshaded boxes represent untranslated region of exons.

The PATZ1 protein is mainly localized in the nucleus, however, under certain physiological or pathological conditions, it can translocate to the cytosol [32]. PATZ1 was found to be highly expressed during embryogenesis in many tissues especially in the midbrain [41]. Protein expression in the brain diminishes in adults, where it is mainly enriched in less differentiated cells [41], an expression pattern that indicates a vital role of PATZ1 in development. Relevant to these observations, PATZ1 has also been identified as a pluripotency factor in embryonic and induced pluripotent stem cells [42].

PATZ1 was first discovered in 2000 by three independent groups. The first group discovered PATZ1 while studying chromosomal rearrangements in chromosome 22 that is responsible for the development of Ewing Sarcomas. In this study, part of the PATZ1 gene was found to be translocated and fused to the EWSR1 gene causing loss of function of the Patz1 gene and gain of function in EWS gene [43]. At the same time, Fedele et al., identified PATZ1 as an interacting partner with the RING finger Nuclear Factor 4 (RNF4) protein and as a regulator of its transcription [44]. In the same year, PATZ1 was also discovered and cloned in a two-hybrid screening assay in association with another BTB domain containing transcription factor named BACH2 (BTB and CNC Homology 2) [45]. Instead of a ZF DNA binding domain, BACH2 contains a Leucine Zipper DNA Binding Domain which indicates that it was mainly the BTB domains of these proteins from different families that were responsible for interaction.

PATZ1 is composed of a BTB domain at its N-terminus and 7 ZF domains at its C-terminus, in addition to the central AT-hook domain [43–45]. Being a member of the BTB-ZF transcription factor family, PATZ1 possesses its gene regulatory function through its structure. As described earlier, the ZF domain recognizes and binds the targeted DNA sequence while the BTB domain facilitates oligomerization and interactions with other regulatory proteins. Among those are SMRT, NCOR1, SIN3A (SIN3 homolog A, transcription regulator – yeast) [46] (Figure 1.2).These co-regulators were also found to be able to recruit some histone-modifying enzymes, such as HDAC (Histone DeACetylases). Decreased levels of histone acetylation are usually associated with closed chromatin

configuration that in turn represses gene expression [47]. Accordingly, PATZ1 might also have an epigenetic effect on gene transcription.

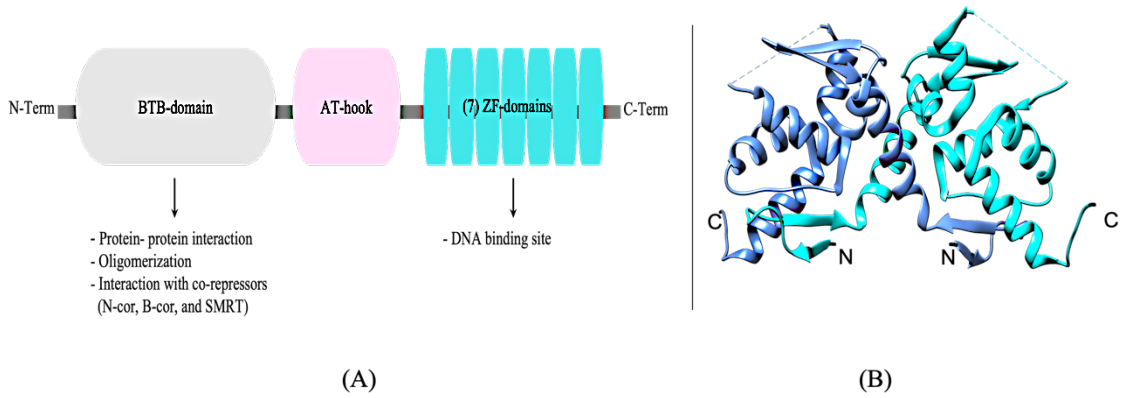

Figure 1. 2: PATZ1 structural domains.

(A) A schematic representation of PATZ1 domains and their related functions. (B) 3D structure of mPATZ1-BTB domain homodimer (PDB code: 6GUV).

The presence of the AT-hook motif, which is a DNA binding motif that specifically binds to AT-rich sequences in the minor groove of DNA, might also cooperate in the DNA binding of PATZ1. This mode of action was found in other proteins that share the presence of the AT-hook motif such as HMGA proteins (high mobility group proteins characterized by an AT-hook). These are non-histone chromatin-associated proteins that do not have an intrinsic transcriptional activity by themselves, rather they modulate transcription by their AT-hook motifs that can alter the chromatin architecture and form multi-protein complexes with other proteins on the promoter or enhancer regions [48]. Accordingly, the chromatin-remodeling function of PATZ1 is possibly accomplished via both its BTB and At-hook domains [49]. Both domains are also involved in a huge variety of protein-protein interactions and multi-protein complex formation. Therefore, the role of PATZ1 as a transcription factor is highly variable and context-dependent according to the type of co-regulatory protein and their mode of interaction. For that, PATZ1 has been reported in certain instances as a transcription activator while in others it was found to exert a transcription repression function. For example, the BACH2 is a transcriptional repressor with which PATZ1 was first

discovered. In the same study, the Igarashi group found that BACH2 switches to transcription activation when complexed with PATZ1 [45]. On the other hand, the Chiariotti group found that the association of PATZ1 with RNF4 switches it into repression [44] and attenuates its androgen receptor-dependent transcription enhancement [50]. Moreover, it has been shown that PATZ1 can activate or repress the same promoter but in a different cellular context. For example, when associated with PATZ1, the c-myc promoter was found to be activated in B lymphocytes while repressed in cervix carcinoma cells [44,45]. other examples are the CDKN1A, MDM2, and BAX genes that are p53 regulated genes. PATZ1 was found to interact with p53 and thus activates the promoters of these genes. However, in the absence of p53, PATZ1 was found to have an opposite effect on these genes[51].

1.2.1. The Physiological Role of PATZ1

To discover the physiological function of PATZ1, several studies were conducted utilizing the gene knockout approach. In mice, Patz1 knockout resulted in a malposition in the cardiac outflow tract and neural tube closure. These mice mostly died in utero or soon after birth, suggesting an essential role of PATZ1 in vesicular and nervous system development [41].

From another aspect, the expression of PATZ1 in the thymus is well studied and its role in controlling B-cell normal development at different stages is of major importance. It is now evident that PATZ1 is part of the transcription machinery that controls the decision of double-positive thymocytes to differentiate into $CD4^+$ or $CD8^+$ cells [52]. In an earlier study in 2010, Ellmeier's group found that PATZ1 knockout mice had a higher number of CD4+ thymocytes compared to CD8+. They found that PATZ1 downregulates the ThPOK gene which is considered as a master regulator of T lymphocytes development; such that its repression dictates cells to CD4- /CD8+ cell lineages [52,53]. PATZ1 is also highly expressed in the early stages of thymocytes development or what is known as double-negative cells where it exerts a negative control on the expression of the Cd8 gene by interacting with other co-regulators and keeping the local chromatin in a condensed configuration [54,55].

Subsequently, the expression of PATZ1 was found to tone down until almost no PATZ1 could be detected in the peripheral T cell population[55].

Another defect of PATZ1 knockout mice was infertility of both males and females, indicating another role of PATZ1 in spermatogenesis and sexual development [56]. Spermatogenesis is essentially dependent on androgens [57] and PATZ1 attenuates androgen receptors by regulating the activity of RNF4 [50]. In another study on human males and females, a critical polymorphic DNA region that is associated with pubertal timing and pubertal growth was found to harbor a site for PATZ1 binding [58], therefore suggesting a potential role for PATZ1 in human sexual development of both sexes.

On the cellular level, PATZ1 is involved in regulating many important cellular activities such as cellular proliferation, apoptosis, and senescence. Regarding cellular proliferation, PATZ1 knock-out mice showed dwarf phenotype, likely due to defected cell proliferation [41]. The same study showed that PATZ1 knock out mouse embryo fibroblasts (MEFs) resulted in slower growth of these cells, and increased the expression of cell cycle negative regulators such as p53 and p16 [41]. These data suggest that cellular proliferation might be activated by PATZ1. From another aspect, PATZ1 was recently identified among 52 differentially expressed genes regulating senescence [59]. In co-ordinance with this finding , is that the downregulation of PATZ1 induces premature senescence [60]. In the same context, PATZ1 knock-out MEFs showed premature senescence consistent with slow growth and decreased cellular proliferation[41]. Concerning apoptosis, the role of PATZ1 seems to be context dependent. PATZ1 knock-out mice had reduced numbers of apoptotic cells after treatment with apoptosis-inducing agents compared to controls; suggesting a proapoptotic role [51]. However, in human cancer cells, PATZ1 silencing enhanced the sensitivity to apoptotic stimuli indicating an anti-apoptotic role of PATZ1 in such conditions [51,61,62].

Recently there is increasing evidence that PATZ1 is involved in the maintenance of pluripotency and cellular reprogramming. Pluripotency is a character of embryonic stem cells that is maintained by a group of transcriptional factors mainly Oct4 [63], Sox2 [64], and Nanog [65,66]. PATZ1 was found to directly regulate Nanog and Pou5f1 and to interact with many

other pluripotency regulators such as Oct4, DPP4, SOX2, and PCGF1 [42,67,68]. A similar role could be played by PATZ1 in cancer stem cells, as suggested by its higher expression in glioma-initiating stem cells (GSCs) compared to differentiated tumor cells [41]. Based on this data, the role of PATZ1 in reprogramming MEFs towards pluripotent stem cells through overexpression of the Yamanaka cocktail [69], has been tested by Hui Ma et al. who found that PATZ1+/- MEFs were more efficiently reprogrammed compared to knock out or overexpression suggesting a critical control of PATZ1 dosage for the generation of Induced pluripotent stem cells [70].

1.2.2. PATZ1 in Cancer

In the development of tumors, PATZ1 plays a context-dependent role as it does in a healthy cell. As a result, it was found that PATZ1 has dual activity in some tumors and functions as an oncogene and as a tumor suppressor in others.

1.2.2.1. PATZ1 as a Tumor Suppressor

The role of PATZ1 as a tumor suppressor is recognized in many types of tumors. Lymphomas are a type of tumor where PATZ1 was found to have a tumor suppressor function. Diffuse large B-cell lymphomas (DLBCLs) are a sub-group of non-Hodgkin lymphomas and the most frequently observed type. In these lymphomas, PATZ1 expression was found to be downregulated in correlation with increased expression of BCL6 oncogene and decreased expression of proapoptotic BAX [71,72]. Thus, it may act as a tumor suppressor by enhancing apoptosis by inhibiting the transcription of BCL6 and activating the transcription of BAX. Moreover, low levels of PATZ1 were significantly associated with the worst outcomes [72]. These data propose PATZ1 not only as a tumor suppressor in DLBCLs but also as a prognostic marker.

In lung cancers, PATZ1 was found to exert its tumor suppressor function via its negative effect on IKK/NF-κB signaling pathway that is associated with cancer cell migration, invasion, and metastasis. Matching with these results is the higher expression of PATZ1 in primary lung cancers compared to lymph node or other metastases sites [73].

PATZ1 was also found to be downregulated in thyroid cancer. The absence of PATZ1 increased cellular proliferation, migration, invasion, thus correlated inversely with the degree of cell differentiation [74,75]. The role of PATZ1 in these cancers is suggested to be P53 dependent. PATZ1 was found to alter the expression of many p53-dependent genes such as EpCam, Caldesmon, RhoE, and Fibronectin, which are involved in epithelial-mesenchymal transition (EMT) and cell migration [75]. EMT is a transformation process of epithelial cells into mesenchymal stem cell-like cell. These cells are multipotent stromal cells that have the ability to differentiate into a variety of cell types in addition to their ability to migrate and invade other sites and tissues. This is a normal process that is associated with development or wound healing. However, in cancer, it is associated with metastasis and cancer progression.

PATZ1 involvement in germ cell cancers is also reported in some studies. As mentioned previously, PATZ1 is thought to play an important role in spermatogenesis and sexual development through RNF4 dependent control of androgen receptor [50], therefore its expression was expected to be altered in tumors of these cells. In fact, in testicular germ cells tumors the expression of PATZ1 was found to be upregulated in contrast to the above-mentioned tumors where PATZ1 was found to be downregulated. However, here PATZ1 was found to be delocalized to the cytoplasm rather than the nucleus where it is normally expressed in healthy tissues [56]. In healthy cells, PATZ1 localization is usually confined to the nucleus where it acts as a transcription factor. Translocation of PATZ1 to the cytoplasm in cancer cells might reflect a loss of its gene regulatory function. It is not clear if this cytoplasmic translocation is associated with the gain of new functions and whether these new functions are oncogenic or tumor suppressive. In Females, PATZ1 was also found to be associated with the development and prognosis of serous ovarian carcinoma. Here PATZ1

expression was found to be downregulated and negatively related to cellular proliferation and invasion in *in-vitro* experiments [76].

1.2.2.2. PATZ1 as an Oncogene

The role of PATZ1 as an oncogene was mainly detected in colon cancer. In colorectal cancer samples, PATZ1 was found to be upregulated compared to non-cancerous samples. When cellular growth was checked in PATZ1 knockout SW1116 colon cancer cells, it was found to be significantly inhibited, and when overexpressed, cellular growth was restored and promoted [77].

The oncogenic effect of PATZ1 might be exerted through its control on p53 and its target genes that are associated with cell cycle control, cellular proliferation, adhesion, and morphogenesis. This is consistent with our group's work on PATZ1 and its relation to the p53 transcription factor. We previously showed that PATZ1 increases proliferation rates in MEFs and in human colon cancer cell lines (HCT116) in a P53 dependent manner. Moreover, RNA-sequencing data of PATZ1 WT and knockout MEFs showed that PATZ1 regulates the expression of many p53 dependent genes that are associated with oncogenic and metastatic functions such as cellular proliferation and adhesion [62].

Regarding thyroid cancer, we have previously referred to p53 as an interactive element with PATZ1 that suppresses target genes that are involved in EMT and cell migration. However, in colon cancer, PATZ1 is reported as an oncogene that increases cellular proliferation, adhesion, and morphogenesis in a p53 dependent manner. This conflict infers that the p53 dependent role of PATZ1 as an oncogene or as a tumor suppressor is highly tissue-specific and cellular context-dependent.

In small round cell sarcomas, or called Ewing Sarcoma, where it was first discovered, the rearrangement of the PATZ1 gene to the EWS gene results in a fusion protein that lacks

the transcriptional repressor domain of PATZ1 (the BTB domain) and was associated with a complete loss of PATZ1 expression[43].

Interestingly, other members of the BTB-ZF protein family that share a similar structure with PATZ1 have been reported to have an oncogenic role. Among those is BCL6 which was first discovered in diffuse large B cell lymphoma [78]. BCL6 was found to prevent the expressions of some tumor suppressor and cell cycle arrest genes such as ATR, p53, CHEK, and CDKN1A/p21. It is worth noting that when PATZ1 was knocked out in mice, BCL6 was found to be upregulated. Those mice developed BCL6-expressing lymphomas and died earlier compared to their wild-type counterpart confirming the oncogenic nature of BCL6 [79,80], however referring to a tumor suppressor role of PATZ1 in this context.

Promyelocytic Leukemia Zinc Finger (PLZF) is another member of this family with an oncogenic behavior. It was found to be involved in acute promyelocytic leukemia where PLZF gene was found to be translocated into the RAR-α gene producing a fusion protein of PLZF-RAR-α that combines the transcriptional activity of RAR-α with the co-factor recruitment capacity of PLZF. The resultant fusion protein changes the expression of its target genes that are associated with impaired DNA repair, cell cycle arrest, and apoptosis [81].

1.2.2.3. Dual Oncogenic/Tumor Suppressor Function of PATZ1

The dual action of PATZ1 as a tumor suppressor and as an oncogene is mainly recognized in gliomas. Phenotypically, gliomas are generally classified into proneural or mesenchymal. In contrast to mesenchymal glioma cells that show an invasive mode of growth, the proneural tumor cells exhibit a non-invasive growth pattern. Therefore, proneural patients tend to have longer survival rates compared to mesenchymal patients. PATZ1 has was found to be enriched in proneural type and associated with the undifferentiated state of glioma-initiating stem cells therefore suggested to play a tumor suppressor role in this context [82]. In consistence with this role, PATZ1 was found to suppress the expression of CXCR4

which is a mesenchymal inducer that is involved in proneural-mesenchymal transition. This is the glioblastoma equivalent of EMT and associates with the worse prognosis [82,83].

On the other hand, PATZ1 oncogenicity is suggested due to its role in chemotherapy resistance of glioblastoma where silencing of PATZ1 in these cells enhanced their sensitivity to chemotherapeutic agents [70]. GSCs are thought to be the main contributor against therapeutic resistance [84]. PATZ1 was found to be overexpressed in these GSC thus might contribute to the maintenance of the therapeutic resistance stem cell phenotype [42,82]. This is consistent with the fact that PATZ1 is enriched in the proneural type, which has a stem cell signature and is unresponsive to both radio- and chemotherapy [82].

It is worth knowing that PATZ1 was found to be associated with other non-cancerous cases such as diabetes, atherosclerosis, and even some psychological disorders such as subsyndromal symptomatic depression. In diabetes, PATZ1 was found to be upregulated in endothelial cells (ECs) where it is thought to contribute to many vascular dysfunctions associated with diabetes. Here PATZ1 was found to act as an anti-angiogenic factor via inhibiting the expression of fatty acid-binding protein 4 (FABP4) that is associated with angiogenic and metabolic signaling pathways in ECs [85]. In atherosclerosis, PATZ1 was found to be expressed at mild levels in the endothelium of the vascular smooth muscle cells [60], where it is normally co-expressed with transforming growth factor beta 1 (TGFB1) which controls many cellular activities such as cell growth, proliferation, differentiation and apoptosis [86]. Interestingly, PATZ1 was found to be one of the significantly differentiated regulating factors in subsyndromal symptomatic depression (SSD). The role of PATZ1 in neurogenesis is well known, therefor it may affect depression through its role in neurogenesis [87,88].

1.3. Nanobodies

1.3.1. The Structure of Nanobodies

Antibodies are serum-derived glycoproteins that are produced by B lymphocytes as a defense mechanism when there is an external stimulus (antigen (Ag)). These antibodies are capable of antigen recognition, binding, and elimination through further complicated immune processes with the help of other immune cells. Structurally, antibodies are composed of four polypeptide chains; two identical light chains (LC) and two identical heavy chains (HC) coupled together by disulfide bonds into a final Y-shaped structure. In these chains, two main regions can be identified: the constant region and the variable region. The variable region is the region responsible for Ag recognition, thus it possesses a huge genetic variability to facilitate different Ag recognition. The variable region is present at the N terminus of the two ends of the Y structure; therefore, it is accommodated by both the HC and the LC. Within the variable region of each heavy and light chains, there are more conserved regions called framework regions (FR) and highly variable regions called the complementary determining regions (CDR1, CDR2, CDR3) which are responsible for the specific Ag recognition, with the CDR3 being the region that shows the highest degree of variability. From another aspect, several regions can be identified in this antibody structure, the Fab region; which refers to the Ag binding fragment composed of part of the constant region in addition to the variable region of both the heavy and the light chains, while the single-chain variable fragment (scFv) refers to the same fragment but without the constant fraction, and the Fc region; which refers to the fragment crystallizable region at antibody tail. This domain plays an essential role in the activation of target immune cells such as macrophages and natural killer cells through interaction with a cell surface receptor called the Fc receptor that results in Ag elimination. This region is entirely composed of the heavy chain constant domain and the type of these constant domains determines the isotype of the antibody such as IgG, IgA, and IgD isotypes [89].

The structure explained above is for the conventional antibodies, which are found throughout mammalian species, however, another type of antibodies lacking the light chain were discovered in 1993 by Hamers-Casterman et al. thus called heavy chain only antibodies (HcAbs) [90]. These new antibodies are so far detected in camelids (alpacas, llamas, or camels), sharks, in addition to the conventional type [90,91]. The structure of these new antibodies is similar to the heavy chain structure of the conventional type but lacks the first constant domain (Figure 1.3). Thus, their overall structure comprises 2 heavy chains each composed of two constant domains (CH2, CH3) and an antigen-binding domain [90,92]. In this case, the variable domain that is responsible for antigen binding is totally enclosed in the heavy chain thus called variable heavy chain domain and abbreviated as (VHH) with an addition of an extra (H) to distinguish them from the conventional ones (VH). These VHH domains were expressed as single-domain antibodies (sdAbs) and are now commonly known as nanobodies (Nbs).

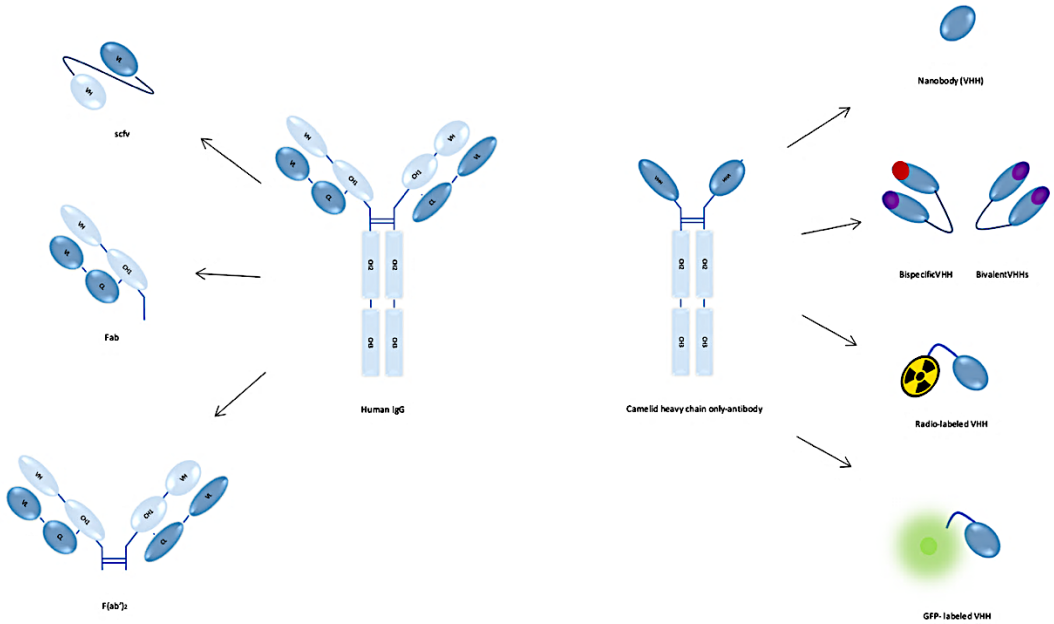

Figure 1. 3: Antibodies and their derivatives.

The left panel shows conventional antibody and its derived fragments; scFv, Fab, and F(ab')2. The right panel shows camelid heavy-chain antibody and different forms of its derived constructs; VHH, bispecific/ bivalent VHHs, radio-labeled VHH, GFP- labeled VHH.

When comparing the structure of the variable region of the conventional heavy chain HV with that of the nanobodies HVV, it is clear that the overall structure is conserved [92], however, there are some minor but important differences that enabled the nanobodies to have the full functional capacity with their single-chain structure (3CDRs) compared the conventional antibodies that share the job between the heavy and light chains (6CDRs).

Both VHH and VH preserve the characteristic of immunoglobulin fold [93]. Both are composed of four conserved framework regions (FR) and three hypervariable regions (CDR). The framework regions are arranged in a typical immunoglobulin fold of two β -sheets where the first sheet is composed of four β strands and the other one of five strands, while the CDRs arrange into loops that connect the five β strands, thus these loops cluster at one side of the domain [93–97]. The 3D structure and protein domain arrangement of the anti-GFP nanobody which is the most commonly known nanobody, and for the anti-lysozyme nanobody which is the first crystalized nanobody are shown in (Figure 1.4).

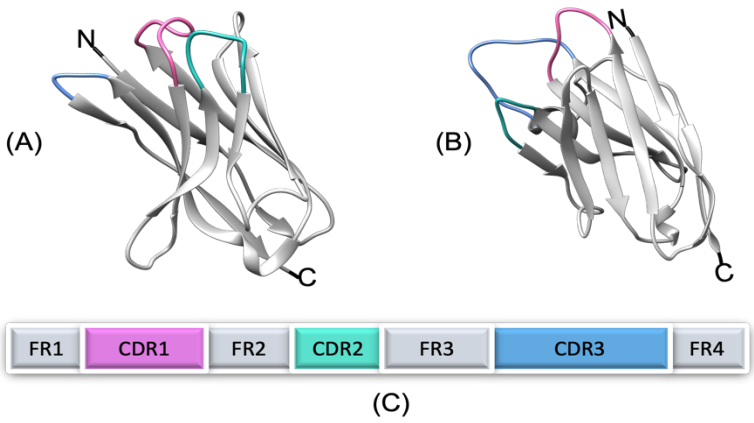

Figure 1. 4: 3D structure of common nanobodies.

(a) Anti-GFP VHH (PDB: 3OGO). (b) Anti-lysozyme VHH (PDB: 1MEL). (c) A schematic representation of VHH different protein domains. CDR1, CDR2, and CDR3 regions are shown in pink, green, and blue respectively.

The differences in this typical structure between VH and VHH are concentrated in two main areas: the framework regions that form the side of the VH that is in contact with the VL domain, and the CDRs that form the antigen-binding site. Regarding the framework regions of the VH that is in contact with the VL domain, this side is mainly formed by the FR2. In VH domains This region is highly conserved and composed of hydrophobic amino acids that provide an anchoring place for the VL domain. However, in VHH, given the absence of the VL and CH1 domains, many amino acids that were providing functional interaction with these domains are substituted with new amino acids providing new functional effects. For example, the Leu 11 structural organization in normal immunoglobulin provides a ball-and-socket joint with the hydrophobic residues Phel49 and Pro150 of the CH1 domain [98], while in VHH and since this function is no longer needed, the Leu11 was substituted with a hydrophilic polar Ser that contributes to increased solubility of VHH. More hydrophilic amino acids substitutions were found in other positions such as Gly 44 Glu, Leu 45 Arg or Cys45, and Trp47 to Gly [92,97,99]. Other substitutions are aimed to increase the exposed interaction surface to accommodate for missing VL by more bulky amino acids. For example, Val37 normally buried within the adjacent amino acids with only 6 Å² exposed surface is substituted with Tyr or Phe with 60 Å² exposed surface [92,100].

The sequence alignment of both the VH and VHH shows that the CDR1 and CD3 of the VHH are more extended than those of VH and in some instances contain substitutional Cys residues. These longer loops and the presence of Cys residues that are associated with disulfide bond formation affect the overall structure of the loop and collectively are thought to increase the Ag recognition and binding capacity of these nanobodies [92,101,102].

Form another aspect, the crystal structure of the antigen-binding loops does not follow the canonical structural restrictions, instead, many different loop architectures can be seen [92,96,97]. This is attributed to substitutions that create hotspots for somatic hypermutations. Precisely in the CDR1 region of VHH, there is a substitution of two Phe codons with two Tyr codons thereby creating two additional hotspots for somatic hypermutations [103,104].

Additionally, the VHH paratope is found to be convex in shape, in contrast to the concave or flat surface VH–VL paratope. CDRs of VHH, precisely the CDR3, are shaped into a long fingerlike polypeptide loop, the fact that increases the antigen–VHH interface area of ~1700 Å², which is as large as the interface between antigens and a VH–VL pair [92]. This convex structure also allows these nanobodies to reach buried epitopes in clefts on protein surfaces which are mostly low antigenic to the conventional antibodies [97,105].

1.3.2. Advantageous Properties of Nanobodies

Owing to the structure and properties of nanobodies that are described above, nanobodies have many advantages over conventional antibodies. As mentioned above, nanobodies are smaller in size; approximately 120 amino acids, 12–15 kDa, and 2.5 × 4 nm size [90,92,97] compared to 450–550 amino acids for each heavy chain and 211–217 amino acids for each light chain in the conventional antibodies with overall molecular size of 150 kDa and 10- 15 nm size. This small size allows them to penetrate intercellular spaces and tissues that are usually not accessible for conventional antibodies.

Additionally, due to their simple monomeric structure nanobodies are conformationally more stable even under hard conditions such as high or low temperatures, high concentration of detergents and proteases, high pressure, or different pHs [106–108]. Moreover, nanobodies are known for their higher solubility due to the structure described above [92,99,106]. Conformational stability and solubility are favorable properties for protein purification. Nanobodies are also simple to clone and synthesis in high yields in a variety of microbial systems, including bacteria and yeasts. Such microbial systems are lower in cost compared to cellular systems that are usually used for monoclonal antibodies (mAbs) production [106,109].

From another aspect, nanobodies recombinant fragments render the affinity of their original counterparts, the fact that makes them an ideal building block for multidomain constructs with various purposes such as increasing the binding avidity towards an antigen by generating bivalent monospecific nanobodies or monospecific nanobodies binding to

different epitopes on the same antigen [110]. Bivalent nanobodies binding to two different antigens are also possible [111,112]. Furthermore, different molecules can be linked to nanobodies with multiple useful applications without affecting the binding capacity of the nanobody such as fluorophores, radionuclides, nanoparticles, or viruses, which is very useful for imaging or therapeutic purposes [113–117]. Finally, nanobodies are rapidly [118] cleared from the blood and do not elicit an unwanted immune response. Indeed, no immune response was raised against injected nanobody-containing constructs in mice or humans. This is likely due to the lack of Fc regions that prevents them from undergoing Fc receptor-mediated immune recognition [118,119].

1.3.3. Generation of Nanobodies

Various techniques for nanobodies generation are currently available, but they all follow the same three steps: generation of a nanobody library, screening for the successful candidates, and finally producing these nanobodies in various expression systems for more characterization.

1.3.3.1. Generation of Nanobody Libraries

There are two main ways for generating a nanobody library, natural or synthetic. To date, natural immune libraries have been used to isolate the vast majority of known nanobodies. Camelids such as camels, dromedaries, llamas, or alpacas are injected with the specific antigen until their adaptive immune response peaks. Following that, lymphocytes from camelids are extracted and used to amplify the Nb gene sequences (360 bp). As a result, a library of VHH gene sequences is created, which may then be used in various screening systems to find the best binders [120] (Figure 1.5). Although the Nanobodies generated by this approach have a high affinity and specificity [121], it has some drawbacks. Time, cost, pathogenicity or toxicity of some antigens, and immunological tolerance to antigens found naturally in these animals are all significant constraints [122]. Furthermore, control over the

chemical environment or antigen conformation are not possible through the immunization process. This is particularly problematic for antigens with many conformations, such as membrane proteins [123]. On the other hand, naive libraries, or called non-immune libraries can overcome many of these drawbacks [124]. Since these libraries do not require an antigen immunization step, they can produce a considerably larger range of VHH sequences. This diversity reduces the cost and time required to create a new immune library for each targeted new antigen, and it is well adapted to produce nanobodies against non-immunogenic or toxic antigens [125–127]. However, the benefit of diversity is counterbalanced by the loss of affinity. As a result, there is a trade-off between naive and immune libraries when it comes to selecting between functional stability or diversity. Low affinity, on the other hand, can be a requirement for particular applications, such as affinity purification ligands and *in-vivo* imaging props, to assess elution and quick clearance [128]. Alternatively, synthetic libraries can be utilized. These libraries are based on *in-silico* techniques that fix framework regions to maintain domain fold stability while randomizing antigen-specific regions of nanobodies (CDRs). The full randomization of these sequences influenced stability and resulted in a huge amount of diversity ($>10^{30}$ clones) that could not be handled by regular screening technologies as phage display (maximum 10^{12} clones). Limiting the randomization to amino acids that are most frequently found in nature decreased library size while maintaining adequate diversity. (1.8×10^{10})[129,130].

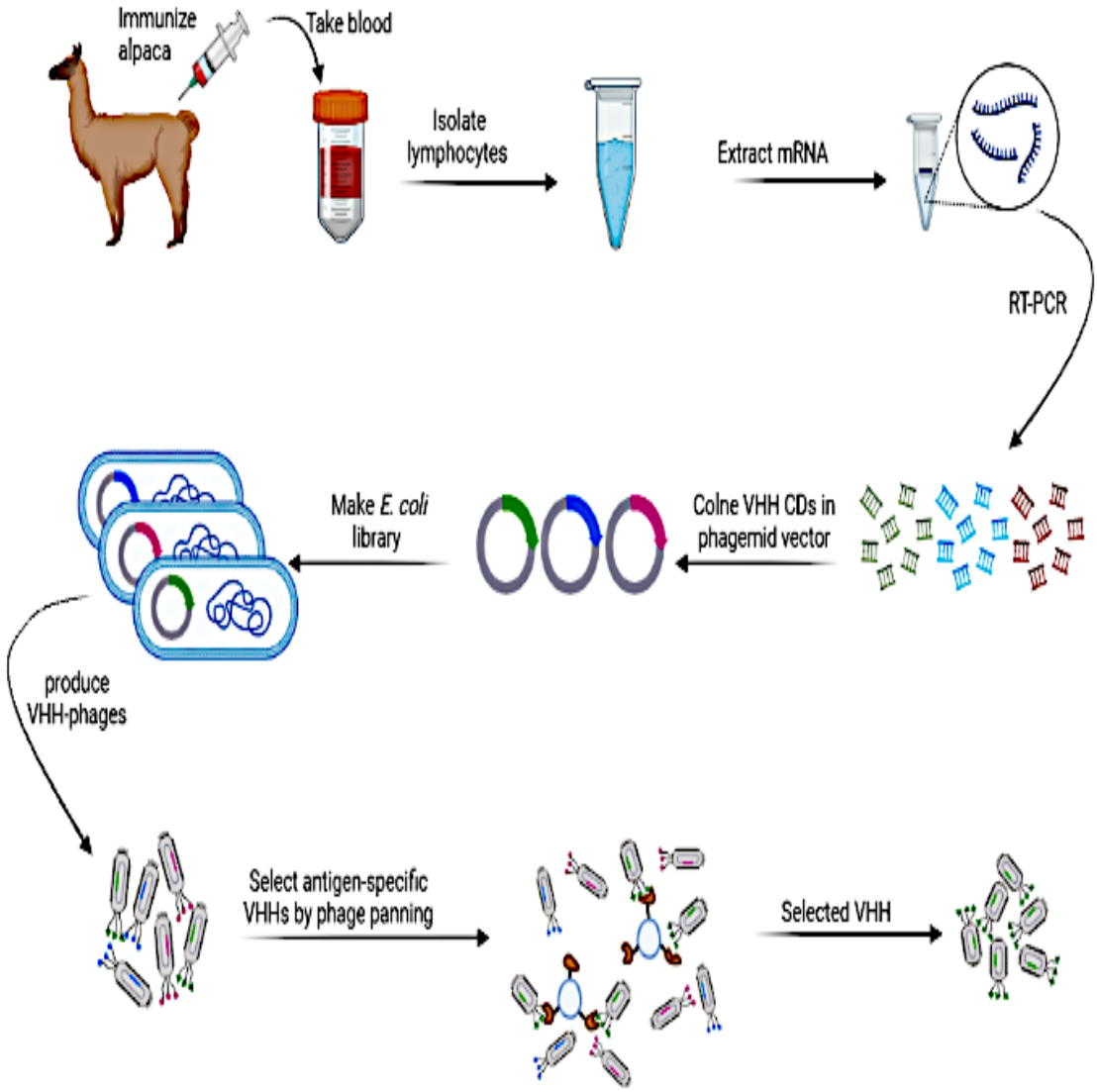

Figure 1. 5: Schematic illustration of generating a phage display immune library

1.3.3.2. Screening Methods

Following the generation of the library, different screening processes are employed to find nanobodies with specific desirable features. High affinity, stability, resistance to aggregation, ability to block or neutralize an enzyme, and the possibility of intracellular expression are some of these properties. Several techniques have been explored with varying degrees of success to efficiently select for these features in combination with high antigen

specificity. The most common method for screening nanobody libraries is phage display [131]. It is based on the expression of nanobodies fused to surface coat proteins of phages, then selecting the best binders to the antigen of interest through multiple rounds of selection [106]. The selection step is typically carried out using *in-vitro* assays such as phage ELISA, then the nucleotide sequences of ELISA-positive clones are sequenced. The method has the advantages of being simple, low in cost, efficient, fast, and can be applied to large libraries (10^6–10^{11}). This technique, on the other hand, does not permit the selection of intracellularly stable clones. Yeast surface display is another interesting approach that can overcome this issue. In this method nanobodies are linked to the yeast cell surface via an anchor to follow a secretory pathway similar to that of higher eukaryotes, thus, ensure the selection of active binders [132]. The relatively large size of yeasts simplifies the selection process by using a flow cytometer where the single yeast cells that bound the fluorescently labeled antigen of interest can be selected [133]. Another technique that allows for the selection of intracellular soluble binders is the yeast two-hybrid. It works by interacting a bait protein with a target protein, both of which are linked to proteins that must interact for a reporter gene to be transcribed [134,135]. However, because of yeasts low transformation efficiency, yeast-based methods are less common than phage display techniques. The two-hybrid system can also be used in bacteria (B2H). In addition to the simplicity and efficiency of this system, it overcomes the problem of low transformation efficiency, making it highly recommended for large libraries [136]. However, it is unclear whether such a system can be efficient in the generation of intrabodies that are meant to function in eukaryotic cytoplasm, and it is uncertain whether fusion to the bait and target proteins will affect the antigens normal folding.

Lentiviral screening is another alternative method that has been successfully used to select nanobodies that are both intracellularly stable and capable of neutralizing viruses. After immunization of the animal with the targeted virus, the collected lymphocytes were used to amplify the VHH sequences and clone them into a lentiviral plasmid rather than the more common phagemid plasmid that is used with phage display systems. The produced lentivirus particles are then transfected into human A549 cells, which are then exposed to a lethal dose of the targeted virus. Selection is done for those cells that survived. These cells have a VHH that is both stable in the cytoplasm and capable of neutralizing the virus [137]. Biotinylated

nanobody screening [138], ribosome display [139], mRNA/cDNA display [140], and others are alternative methods that have been reported but are less commonly used.

1.3.3.3. Nanobody Expression and Purification

Following the selection step, the corresponding nanobodies will be produced *in-vitro* using different expression systems. A variety of expression models for nanobody production have been used, including organisms such as bacteria, yeast, fungi, mammalian cells, and even plant hosts [141].

Escherichia coli is the cheapest, easiest, and most commonly used expression system [142]. The oxidizing periplasmic compartment of this bacteria provides an excellent environment for disulfide bond formation and the production of stable functional nanobodies [143,144]. The folded nanobodies are usually recovered from the supernatant after permeabilizing the bacterial outer membrane which is typically done by osmotic shock. However, low yield and protein aggregation as a result of limited space and overburdening of chaperone machinery are significant limitations of this system [145]. To overcome this limitation, cytoplasmic overexpression of a sulfhydryl oxidase and disulfide bond isomerase (DsbC) was used to create the required oxidizing environment [146,147] It is also worth noting that many nanobodies can gain their functional fold even in non-oxidizing conditions [148]. Bacterial secretion mechanisms, like hemolysin secretion, have also been employed to extract nanobodies from the culture medium without lysing the cells [149]. The poor yields obtained, however, limit its broad application.

Because nanobodies can be expressed in cheap and simple bacterium systems with high functional yields, their expression in other systems of higher cost, longer time, and complex handling must be justified. For example, mammalian cells such as CHO and HEK293T cells can be used when obtaining nanobodies that have undergone all the physiologically relevant post-translational modifications is required. For instance, nanobodies-Fc fusions for *in-vivo*

therapeutic proposes [150,151]. Yeast and fungi systems produce high yields, and both of which have been successfully used, but their manufacturing procedure is more complicated [152].

1.3.4. Nanobody Applications

1.3.4.1. Nanobodies as Molecular Probes for *In-Vivo* Imaging

The unique properties of nanobodies provided many distinct advantages for imaging applications. Several nanobody-based probes are now used in many nuclear imaging techniques that enable diagnosis and assessment of prognosis of many diseases in a non-invasive manner. For this, nanobodies are coupled with different radioisotopes such as ^{99}mTc for single-photon emission computed tomography (SPECT) or ^{68}Ga and ^{18}F for positron emission tomography (PET)[153]. These nanobody-bases probes provide the advantages of adequate tissue penetration and rapid clearance from circulation, the fact that ensures a high signal-to-noise ratio and better imaging quality [119,154]. Nanobodies-based probes against human epidermal growth factor receptor type 2 (HER2) [155], macrophage mannose receptor (MMR) [156], programmed death-ligand 1 (PD-L1) [157], cytotoxic T-lymphocyte-associated protein 4 (CTLA-4) [158], carcinoembryonic antigen (CEA) [159], and many others are now at different stages of clinical trials.

1.3.4.2. Nanobodies as Crystallization Chaperones

Nanobodies have been used to stabilize many proteins in different conformational states for crystallization purposes that wouldn't have been otherwise possible. Additionally, the banding of nanobodies to their targets decreases their tendency to aggregate and thus increases their solubility and improves their crystalizing chances. The chaperone function of nanobodies is attributed to their long and diverse CDR loops that improve their binding efficiency into un-accessible sites. A long list of proteins has been crystallized with the aid

of nanobodies. In this sense, nanobodies not only solved their 3D structure but in some cases revealed their different conformational states, explored their associated protein complexes, and allowed to study their intracellular functions [160,161]. Recently, Cryo-electron microscopy is being used to solve larger and more complex multi-subunit structures, and nanobodies are likely to be useful here as well. The structure of poliovirus virions is an example of nanobody-mediated cryo-electron microscopy where their complex structure was stabilized with four nanobodies that bind to the VP3 capsid protein [162].

1.3.4.3. Nanobodies for Therapeutic Applications

Nanobodies can also be used in many therapeutic applications. For example, they are well suited to deliver therapeutic drugs, radionuclides, or toxins. In a similar manner to conventional antibodies, nanobodies can bind transmembrane receptors or soluble ligands and affect their downstream signaling pathways. Furthermore, multivalent, or multi-specific nanobodies can be paired to increase their binding efficiency. However, the absence of Fc domains prevents nanobodies from initiating cell-mediated immune response or complement-dependent cytotoxicity. To overcome this limitation, nanobodies can be linked to human Fc chains to gain immune effector functions with many therapeutic applications [163]. Recent research has shown that nanobodies have the potential to be used in disease treatment. Namely, caplacizumab nanobody was recently approved for the treatment of acquired thrombotic thrombocytopenic purpura (aTTP) [164], and an increasing number of clinical trials for other nanobodies are still ongoing.

Recently, nanobodies have received special attention in CAR-T cell-mediated immune therapy. Because nanobodies can bind to multiple antigens simultaneously, they can generate chimeric antigen receptors (CARs) with higher target specificity [165]. Additionally, nanobodies have a unique ability to bind to virus cryptic epitopes. For example, nanobodies were able to fit into canyons on the HIV (human immunodeficiency virus) envelope that were not accessible to IgGs [166]. Therefore, these nanobodies have potential applications for HIV-1 diagnostics, vaccine design, or immunotherapy.

The delivery of these nanobodies into the cytoplasm as functional therapeutic agents can be in two forms, i) as intracellularly expressed nucleic acids, ii) or as purified proteins. The nucleic acid delivery of nanobodies through viral delivery was reported in mice with only minor antiviral effects [167]. However, protein delivery is thought to be a safer option for clinical development [168]. This can be done via fusion with cell-penetrating peptides [169], bioreversible esterification [170], or cationic resurfacing [171].

1.3.4.4. Nanobodies as Intracellular Imaging and Biosensing Tools

Concerning light microscopy or live-cell imaging, nanobodies have proofed superiority as a labeling tool for an intracellular antigen over conventional IgGs, which due to their large dimension (150 kDa, 10–15 nm), result in displacement of the fluorophore from the target nanobodies (linkage error). In this regard, nanobodies can be genetically fused to a vast of fluorophores for intracellular expression, these fusions are commercially known as "chromobodies". Alternatively, they can be fused to various tags for post-expression detection with fluorescent antibodies. Anti-GFP chromobody, for example, was first used to identify GFP-labeled nuclear lamin and histone H2B [172]. Following that, many chromobodies were used to observe a variety of biological activities, such as DNA damage and repair [173], DNA replication, and actin dynamics [174]. These chromobodies advantageously can be expressed in a variety of cellular systems using common transfection protocols like lipofection or electroporation. Alternatively, CRISPR technology can be used to generate stable cell lines that stably express chromobodies [175]. For example, cell lines stably expressing chromobodies against adenosine diphosphate ribose (ADP-ribose), vimentin [176], ß catenin [177], and proliferating cell nuclear antigen (PCNA) [178], have become available.

The applications of chromobodies were exploited far beyond intracellular localization of molecules to the development of biosensors that track functional changes of cellular targets in a dynamic manner. These biosensors are based on targeted nanobodies that are fused to fluorescence sensors that only operate when the target proteins are activated. For example, an anti-GFP nanobody coupled to red fluorescent Ca^{2+} sensors can be utilized as a targeting

moiety to drive the Ca^{2+} sensor into close proximity to the GFP-labeled mitochondria, allowing Ca^{2+} concentrations to be monitored and quantified [179]. A wide range of fluorescent sensors can be generated in this manner such as pH and ATP/ADP sensors [179]. In the same context, nanobody-based biosensors have also been utilized for monitoring cancer biomarkers. Poly (ADP-ribose) polymerase 1 (PARP1), for example, is a key molecule in DNA repair and cell survival that is associated with many cancer types [180]. For the first time, a PARP1 chromobody permitted live-cell detection of PARP1 recruitment to DNA damage sites. The study also demonstrated the feasibility of real-time profiling of different chemical compounds and their effect on PARP1 translocation [181].

1.3.4.5. Nanobodies as Modulators of Gene Expression

P53 is a well-known transcription factor that plays an essential role in many cellular activities such as cell cycle arrest and apoptosis. Nanobodies directly binding the p53 transcription factor were developed by Gettemans group from a lama derived phage display library. The selected nanobodies were able to distinctively target p53 and perturb the transcription of its target genes such as p21, GADD45A, PUMA, and MDM2 that were all decreased in a significant manner [182]. A recent study demonstrated the possibility of gene control via nanobodies by using these nanobodies to target chromatin regulators to specific genomic locations. For example, an anti-GFP nanobody can be used to control gene expression of GFP-tagged chromatin regulators such as GFP-HP1α and GFP- HDAC5. Other nanobodies directly targeting other chromatin regulators such as DNMT1 and HP1 were able to silence reporter gene and confer epigenetic memory [183]. On the protein level, nanobodies can form fusions with F-box proteins. These are subunits of the ubiquitin ligases Skp, Cullin, F-box containing. Such fusions can mediate protein knockout or induce selective degradation of various intracellular targets. For an instance, GFP-tagged intracellular proteins can be selectively targeted with anti-GFP/F-box fusions [184].

2. AIM OF THE STUDY

The BTB-ZF family transcription factor PATZ1 plays an important role in many distinct biological processes such as development, differentiation, fertility, pluripotency, and neurological development. This crucial role in biology is thought to be mediated through its BTB domain that is responsible for oligomerization, recruitment of multiple corepressors, and a wide range of protein -protein interactions. The multiplicity of possible combinational interactions with this domain reflects its diverse functions and explains its significance especially in tumorigenesis. PATZ1 was found to be differentially expressed in a variety human cancers and translocations involving the Patz1 gene are associated with sarcomas and glioblastomas. However, our understanding of the precise molecular mechanisms underlying these activities is still in its infancy.

In this study we targeted PATZ1 using nanobodies; the small antigen binding domains of single chain antibodies from camelids. Nanobodies have become popular biotechnological tools, due to their unique biophysical and functional properties. They launched an entire spectrum of biotechnological, basic research, and medical applications. Nanobody-based modulation of transcription factor activity is emerging as a powerful method in basic research and synthetic biology. Therefore, in this study, we aimed to utilize nanobodies to assist the characterization of the structure and function of the PATZ1-BTB domain.

Precisely, this study has three main aims, that validate the structure and function of nanobodies. The first aim was to isolate and identify nanobodies specific against the PATZ1-BTB domain. These nanobodies were retrieved from a phage display library through consecutive rounds of bio-panning. The second aim was to generate and characterize these

nanobodies in different *in-vitro* and inter-cellular systems to identify the best binders. The third aim was to assess the functionality of the selected nanobodies as modulators of the activity of the PATZ1 transcription factor through assessing the changes in the expression of the known PATZ1 target genes.

3. MATERIALS AND METHODS

3.1. Materials

3.1.1. Chemicals

All the chemicals used in this study are listed in Appendix A.

3.1.2. Equipment

All the equipment used in this study are listed in in Appendix B.

3.1.3. Solutions and Buffers

Bio-Panning Blocking Buffer: 1X PBS pH 7,4 was used to which tween20 and skim milk were added to final concentration of 0,1% and 2% respectively.

Phage Precipitation solution 30% polyethylene glycol (PEG): Dissolve 150 g of PEG (avg. mol. Wt. = 8000) and 73 g of NaCl in 500 mL of distilled water. Heat up to 500°C to dissolve and autoclave.

Calcium Chloride (CaCl2) Solution: 60 mM $CaCl_2$ (from 1 M stock), 15% glycerol and 10 mM PIPES (pH 7.0) were mixed, and the mixture was completed up to 500 mL with ddH_2O. The final solution was filter-sterilized with 0.22 µM filter and stored at 4°C.

Agarose Gel: For preparation of 100 mL of 1% w/v agarose gel, 1 g of agarose powder was dissolved in 100 mL of 0.5X Tris-Borate-EDTA (TBE) buffer by heating in a microwave. After cooling, ethidium bromide was added to a final concentration of 0.002% (v/v).

Tris-Borate-EDTA (TBE) Buffer: For preparation of 1 L 5X stock solution, 54 g Tris-Base, 27.5 g boric acid, and 20 mL 0.5 M ethylenediaminetetraacetic acid (EDTA) (pH 8.0) were dissolved in 1 L ddH_2O. The solution was stored at room temperature and diluted 1: 10 with ddH_2O to get a working solution of 0.5X concentration just before use.

Phosphate-Buffered Saline (PBS): For preparation of 1 L volume of 1X solution, 100 mL of 10X PBS were mixed with 900 mL of ddH2O. The solution was filter-sterilized with 0.22 µM filter.

Polyethyleneimine (PEI) Solution: For preparation of 1 mg/mL (w/v) working stock solution, 100 mg of PEI powder were dissolved in 100 mL of ddH_2O by heating at 80°C. The pH was then adjusted to 7.0 with 33% HCl. Finally, the solution was filter-sterilized, aliquoted into 1 mL volume, and stored at -20°C.

SDS Separating Gel: For preparation of 8 mL of 10% separation gel, 2 mL of Acrylamide (40%), 2 mL of Tris (1.5 M pH 8.8), 80 µL of 10% (w/v) sodium dodecyl sulfate (SDS), 80 µL of 10% (w/v) APS, and 8 µL of TEMED were mixed well with 3.8 mL of ddH_2O. For 14% separation gel, the volumes of Acrylamide (40%), Tris (1.5 M pH 8.8), and water are adjusted to 2.8, 2, and 3 mL respectively.

SDS Stacking Gel: For preparation of 5 mL of 6% stacking gel, 1.25 mL of Tris (0.5M pH 6.8), 0.75 mL of Acrylamide (40%), 50µL of 10% SDS (w/v), 50 µL of 10% APS (w/v), and 5 µL of TEMED were mixed well with 2.9 mL of ddH_2O.

SDS Running Buffer: Initially, 1 L of 10X Tris-Glycine stock solution was prepared by dissolving 40 g of Tris-Base and 144 g of Glycine in 1 L of ddH_2O then pH was arranging to 8.3. This stock solution was used to prepare 1X SDS running buffer, by mixing 100 mL of it with 5 mL of 20% (w/v) SDS solution and completing the volume to 1 L by adding 895 mL of ddH_2O.

Protein Loading Dye: For preparation of 10 mL of 4X protein loading dye, 2.4 mL of Tris (1 M pH 6.8), 0.8 g of SDS, 4 mL of 100% glycerol, 0.01% bromophenol blue, and 2 mL of β-mercaptoethanol were mixed, then the volume was completed up to 10 mL with ddH_2O.

Bacterial cells Lysis Buffer (for protein purification): For preparation of 50 mL of 1X lysis buffer, 50 mM HEPES, 250 mM NaCl, 10 mM imidazole, 1 tablet of EDTA-free protease inhibitor cocktail, 5µL DNase I (100U/ µL), and 50 mg of lysozyme were mixed. The volume was completed to 50 mL with ddH_2O.

Buffer IMAC-A: For preparation of 1 L of IMAC-A solution, 50 mM HEPES, 250 mM NaCl, and 10 mM imidazole were mixed then the volume was completed up to 1 L with ddH_2O. The solution was then filter-sterilized and stored at 4°C. TCEP was freshly added before using the solution at a final concentration of 0.5 mM.

Buffer IMAC-B: For preparation of 1 L of IMAC-B solution, 50 mM HEPES, 250 mM NaCl were mixed. Imidazole was added in different gradient concentrations (100,300,600 mM) according to protein elution requirements. The solution was filter-sterilized and 0.5 mM TCEP was refreshed each time before using the solution

Binding buffer (used with His Trap FF AKTA column): For preparation of 1 L of binding buffer, 20 mM sodium phosphate, 0.5 M NaCl, 20 mM imidazole, pH 7.4 were mixed then the volume was completed up to 1 L with ddH_2O. The buffer was then filtered and degassed.

Elution buffer (used with His Trap FF AKTA column): For preparation of 1 L of elution buffer 20 mM sodium phosphate, 0.5 M NaCl, 100 mM imidazole, pH 7.4 were mixed then the volume was completed up to 1 L with ddH_2O. The buffer was then filtered and degassed.

FACS Buffer: For preparation of 500 mL 1X solution, 0.5 g bovine serum albumin (BSA) were mixed 0.5 g sodium-azide in 500 mL 1X HBSS and stored at 4°C.

3.1.4. Growth Media

Luria Broth (LB): For preparation of 1 L of 1X LB medium, 20 g of LB powder were dissolved in 1 L of ddH_2O then the medium was autoclaved for 15 min at 121°C. For antibiotic selection, the medium was cooled then Amp, Kan, or Chl were added at the following final concentrations 100 µg/mL, 50 µg/mL, and 34 µg/mL respectively.

LB-Agar: For preparation of 1 L of 1X agar medium, 35 g of LB-Agar powder were dissolved in 1 L of ddH_2O then the medium was autoclaved for 15 min at 121°C. For antibiotic selection, the medium was cooled to 50°C and the appropriate antibiotics were added into the final concentrations mentioned in Luria Broth (LB) section. The solution was then poured into sterile petri dish, solidified, para-filmed, and stored at 4°C.

2xYT Broth: For preparation of 1 L of 1X 2xYT medium, 17 g bacto-tryptone, 10 g bacto-yeast extract, 5 g NaCl were mixed in ddH_2O to a total volume of 1 liter. If necessary, adjust pH to 7.0 with 5N NaOH. The medium was then autoclaved for 15 min at 121°C. the medium was cooled then Amp, Kan, glucose were added at the following final concentrations 50 µg/mL, 50 µg/mL and 2% respectively.

2xYT Agar: For preparation of 1 L of 1X 2xYT agar medium, prepare 2xYT broth as above, then add bacto-agar (18 g/L) before autoclaving. For antibiotic selection, the medium was cooled to 50°C and the appropriate antibiotics were added into the final concentrations mentioned in 2xYT Broth section. The solution was then poured into sterile petri dish, solidified, para-filmed, and stored at 4°C.

Minimal Medium (MM): For preparation of 50 mL of MM, 10 mL M9 medium (5x), 100 µL MgSO4 1M, 2.5 mL glucose 20%, and 100 µL Thiamine 1%, were added to mqH2O to volume. The medium is sterilized by filtration only.

DMEM: BHK and HCT116 cells were cultured in DMEM growth medium supplemented with heat-inactivated fetal bovine serum (FBS) 10% and Pen-Strep 1% (Penicillium 100 U/mL and Streptomycin100 µg/mL).

Freezing Medium: Cells were frozen suing heat-inactivated fetal bovine serum to which 10% DMSO (v/v) was added.

3.1.5. Molecular Biology Kits

All the commercially supplied kits for molecular biology purposes that were used in this study are listed in Appendix C.

3.1.6. Enzymes

All restriction enzymes, DNA modifying enzymes, polymerizing enzymes, and their appropriate buffers were supplied from New England Bioblabs (NEB) or Fermentas.

3.1.7. Bacterial Strains

Escherichia coli (E. coli) DH-5α was used for general transformation purposes. *E. coli* TG1 cells were used for all phage bio-panning work. For cytoplasmic expression of nanobodies and purification *E. coli* BL21 DE3 SOX strain was used. This strain was kindly offered by Prof. Ario de Marco, University of Nova Gorica, Slovenia.

3.1.8. Mammalian Cell Lines

BHK-2: Baby Hamster Kidney cells-2 commercially supplied from ChromoTek ®.

HCT116: Human colorectal carcinoma cell line (ATCC CCL-247™).

3.1.9. Plasmid and Oligonucleotides

All the plasmids used in this thesis are listed in Table 3.1.1 while all the oligonucleotides used in this thesis are listed in Table 3.1.2.

Table 3.1. 1: List of plasmids

The list of the plasmids used in this study. Plasmid names, their purpose of use, and sources are listed.

PLASMID NAME	PURPOSE OF USE	SOURCE
pHEN4-Nb plasmid (41 plasmids, one for each selected nanobody clone)	Phage expression plasmid for expression of nanobodies in phages.	Kindly offered by Prof. Ario de Marco University of Nova Gorica, Slovenia.
pET-mCherry-800	Bacterial expression plasmid.	Kindly offered by Prof. Ario de Marco University of Nova Gorica, Slovenia,
pET-Nb- mCherry (37 plasmids, one for each selected nanobody clone)	Bacterial expression plasmid for the expression of	Lab construct

	nanobodies with a C-terminus mCherry tag.	
pET-28a (+)	Bacterial expression plasmid.	Novagen (69864)
pET-28a (+)-Nb (5 plasmids, one for each selected nanobody clone)	Bacterial expression plasmid for the expression of solitary nanobodies.	Lab construct
pCDNA3.1/ myc- His (-) B	Mammalian expression plasmid with CMV promoter.	Thermo Fischer Scientific (V85520)
pCDNA3.1/ myc- His (-) B- Nb-mCherry (5 plasmids, one for each selected nanobody clone)	Mammalian expression plasmid for expression of nanobodies with a C-terminus mCherry tag used in F2H assay.	Lab construct
pcDNA3.1/myc-His (-) B-TagGFP-PATZ1-BTB	Mammalian expression plasmid for the expression of PATZ1-BTB domain with an N-terminal tag GFP used in F2H assay.	Lab construct
pcDNA3.1/myc-His (-) B-TagGFP-PATZ2-BTB	Mammalian expression plasmid for the expression of PATZ2-BTB domain with an N-terminal Tag GFP used in F2H assay.	Lab construct
pcDNA3.1/myc-His (-) B-GBP-LacI	Mammalian expression plasmid for expression of GBP-LacI fusion protein for F2H assay	Lab construct
pEGFP-N2- ccdc124-mCherry	Mammalian expression plasmid for expression of mCherry as a negative control used in F2H assay.	Kindly offered by Prof. Uygar TAZEBAY, Gebze Technical University, Turkey

Table 3.1. 2: List of oligonucleotides

The list of the oligonucleotides used in this study. Oligonucleotides names, their sequence, and purpose of use are listed.

OLIGONUCLEO-TIDE NAME	SEQUENCE	PURPOSE OF USE
pHEN4-Nb-NcoI (Forward)	TAACCCAGCCGGCCATGG CT	Cloning Nbs from pHEN4_Nb plasmid to pET-mCherry-800 and to pET-28a (+)

pHEN4-Nb-NotI (Reverse)	ATGTGCGGCCGCGCTGGAGACGAC	Cloning Nbs from pHEN4_Nb plasmid to pET-mCherry-800 and to pET-28a (+)
pET-Nb-mCherry EcoRI(Forward)	GCGAATTCGAAGGAGATATACCATG	Cloning Nbs from pET-Nb-mCherry plasmid to pCDNA3.1 myc- His (-) B
pET-Nb- mCherry-T7 terminator-BamHI (Reverse)	CCGTTTAGAGGCCCCAAG	Cloning Nbs from pET-Nb-mCherry plasmid to pCDNA3.1 myc- His (-) B
ETV1 (Forward)	TCACTTCAGCTCTGGCAGTT	Real-time qPCR
ETV1(Reverse)	GCGGAGTGAACGGCTAAGT	Real-time qPCR
CTH (Forward)	GCACTCGGGTTTTGAATATAG	Real-time qPCR
CTH (Reverse)	CAGATGCCACTTGCCTGAAG	Real-time qPCR

3.1.10. DNA and Protein Molecular Weight Markers

DNA ladders and molecular weight markers of proteins that were used in this study are listed in Appendix D.

3.1.11. DNA Sequencing

DNA sequencing was provided commercially by MCLAB, CA, USA. (https://www.mclab.com/home.php).

3.1.12. Software, Computer-Based Programs, and Websites

Software, computer-based programs, and websites that were used in this study are listed in Table 3.1.3.

Table 3.1. 3: List of software and computer-based programs and websites

The list of software and computer-based programs and websites used in this study. Their names, source, and purpose of uses are listed.

SOFTWARE, PROGRAM, WEBSITE NAME	COMPANY/WEBSITE	PURPOSE OF USE
CLC Main Workbench v7.9.4	QIAGEN Bioinformatics	Design molecular cloning strategies including vector maps constructing, restriction sites analysis, sequence analysis and alignment, etc.
Addgene	https://www.addgene.org/	Source of basic information about plasmids.
Tecan i-control	https://www.tecan.com/	Analyzing ELISA results
ExPASy	https://www.expasy.org/	Assessment in protein translation and properties analysis.
UNICORN 7.1	https://www.cytivalifesciences.com/en/us	Chromatographical experiments and data evaluation and processing.
BIACORE T200 software v3.0	https://www.cytivalifesciences.com/en/us	SPR experiments and data evaluation and processing.
ZEN 2.3 (blue edition)	https://www.zeiss.com/microscopy/int/products/microscope-software/zen-lite.htmL	View, analyze, process microscope Images.
FlowJo V10	Tree Star Inc.	Viewing and analyzing flow cytometry data.
LightCycler 480 SW 1.5	ROCHE	Analyzing qPCR results.
Prism	GraphPad https://www.graphpad.com/scientific-software/prism/	Statical analysis of qPCR results.

3.2. Methods

3.2.1. Vector Construction

Polymerase Chain Reaction (PCR): The optimized PCR conditions are shown in Table 3.2.1. The thermal cycler conditions shown in Table 3.2.2.

Table 3.2. 1: Optimized PCR conditions

Component	Volume Used	Final Concentration
Template DNA	2 µL	<10 ng
5X Q5 Reaction Buffer	5 µL	1X
10 mM dNTPs	0.5 µL	200 µM
10 µM Forward Primer	1.25 µL	0.5 µM
10 µM Reverse Primer	1.25 µL	0.5 µM
Q5 High-Fidelity DNA polymerase	0.25 µL	0.02 U/µL
ddH_2O	Up to 25µL	-
Total	25µL	-

Table 3.2. 2: Optimized thermo-cycler conditions

Steps	Temperature	Time	
initial denaturation	98ºC	30 s	
denaturation	98ºC	5-10 s	30-35 cycles
annealing	According to primers	10-30 s	
extension	72ºC	20-30 s/ kb	
final extension	72ºC	2 min	

Restriction enzyme digestion: For enzymatic digestion reactions, the desired amount of DNA was mixed with the selected enzymes and their appropriate buffers in a PCR tube according to the manufacturer recommended protocols. The mixture was then incubated in a Thermal Cycler for 2 hs at the optimum temperature for the used enzymes. Variable amounts of DNA were digested depending on the subsequent experimental requirements. For diagnostic digestions, 1µg of DNA was generally used. When the digested plasmid was to be used for subsequent ligation reaction, then the linear plasmid obtained after enzymatic

digestion was dephosphorylated by the alkaline phosphatase enzyme CIAP (calf intestinal alkaline phosphatase) to prevent self-ligation. For that, CIAP enzyme with its appropriate buffer was added to the digested plasmid according to the manufacturer recommended protocols, then the mixture was incubated at 37 ºC for 30 min followed by inactivation of the enzyme at 65 ºC for 5 min.

Agarose gel electrophoresis and DNA gel extraction: 1% agarose gels were used to visualize or extracted DNA fragment. For that, 1 g of agarose powder was dissolved in 100 mL of 0.5X TBE in a glass flask. The powder was dissolved completely by heating the flask in a microwave oven for 2 min. The liquid mixture was then cooled down before adding 2 µL of ethidium bromide (0.0002% v/v). The mix was then casted in a gel apparatus and allowed to solidify. When the gel was ready, DNA samples were loaded after mixing them with the loading dye. Electroporation was carried out for 45-60 min, at 100 V, in a 0.5X TBE buffer, and the bands were visualized using Biorad Imager. When DNA fragments were to be retrieved from the gel, the corresponding DNA band was cut from the gel under minimum UV light and the DNA was purified with the aid of the commercially supplied NucleoSpin Gel and PCR Clean-up kit (Macherey-Nagel) following the manufacturer's instructions.

Ligation: For all ligation experiments, T4 DNA Ligase from NEB was used with its appropriate buffer. Optimal ligation results were achieved using 1:3 vector to insert ratio. The ligation reaction was carried out by mixing 100 ng vector DNA with the required amount of inserted DNA in a PCR tube then the mixture was incubated at room temperature for 2 hs. In each cloning experiment, vector-only (with no insert) was ligated as a control of vector self-ligation. Finally, the whole ligation product was used for transformation into *E. coli* DH5α competent cells for subsequent plasmid isolation.

3.2.2. Bacterial Cell Culture

3.2.2.1. Bacterial Cultures

The bacterial strains that were used in this study were cultured by incubating them in suitable medium with the appropriate antibiotics for selection. Cultures were maintained at 37 °C with vigorous shaking (221rpm) for 12-16 h. For long term storage, glycerol stocks were made by mixing bacterial cultures with 10% (v/v) glycerol under the fume hood then aliquoted in 1 mL volume in cryovial and stored at -80 °C. For obtaining single bacterial colony, small portion of the culture or glycerol stock was spread with the aid of autoclaved wood sticks on an agar petri dish provided with appropriate antibiotics. Plates were incubated overnight at 37°C.

3.2.2.2. Preparation of Competent Bacteria

Previous lab stocks of competent cells were used as a reservoir for preparing new patches. A single colony of competent bacteria from an agar petri dish was inoculated into 40 mL of fresh bacterial medium provided with the appropriate selection antibiotics. The culture was incubated in 200 mL flask at 37°C with 221 rpm shaking for overnight. The next day, 4 mL of this culture was used to prepare a 1:100 diluted new culture in 2 L flask with the same selection antibiotics. The culture was incubated at the same conditions until the optical density (OD) of 0.375 was reached at 590 nm. The culture was then transferred into 50 mL falcon tubes and incubated for 10 min on ice. Following centrifugation for 10 min at 1600 g and 4°C, the supernatant was discarded, and the bacterial pellets were resuspended in 10 mL of ice-cold $CaCl_2$ solution for each tube. A second centrifugation was then done for 5 min at 1100 g and 4°C, the supernatant was discarded, and the pellets were resuspended in 10 mL of fresh ice-cold $CaCl_2$ solution for each tube. The cells were then left on ice for an additional 30 min, then they were subjected to a final centrifugation for 5 min and at 1100 g and 4 °C. After discarding the supernatants, the pellet in each tube was resuspended in 2 mL of fresh ice-cold $CaCl_2$ solution. Finally, all the tube contents were combined in a single 50 mL tube, mixed well, and aliquoted into ice-cold microcentrifuge tube in a 200 µL volume. Freshly prepared cells were immediately flash-frozen in liquid nitrogen and stored at -80 °C.

The transformation efficiency of each new patch of competent cells was calculated by transforming them with standard pUC19 plasmid at different concentrations (efficiency was mostly between 10^7-10^8 cfu/μg).

3.2.2.3. Transformation into Competent Bacteria

Heat-shock method of bacterial transformation was used for all bacterial transformations carried out in this study. For that, one aliquot of competent bacteria was thawed on ice. A 100 pg of pure plasmid was added to these cells, or in case of ligation product, the whole ligation product (20 μL) was added. The mixture was kept on ice for 30 min before it was subjected to heat-shock at 42 °C for 90 s. Immediately after heat-shock, the cells were placed on ice for 1 min. After that, 800 μL bacterial medium was added, and the culture was incubated for 45 min at 37°C. Following that, the cells were centrifuged for 30 s at 13200 rpm, then the supernatant was discarded leaving only 100 μL of it for the bacterial pellet to be resuspended in. Finally, the cells were spread on agar petri dishes of appropriate antibiotic with the aid of autoclaved glass beads and the plates were incubated at 37 °C overnight.

3.2.2.4. Plasmid DNA Isolation

For isolating plasmid DNA, alkaline lysis protocol was used following the protocols of Molecular Cloning described in the Laboratory Manual of Sambrook et at. Alternatively, a commercially supplied Macherey Nagel Midiprep kit was used for midipreps according to the manufacturer's instructions. The obtained DNA concentration and purity were measured by using NanoDrop spectrophotometer.

3.2.3. Mammalian Cell Culture

3.2.3.1. Maintenance of Cell Lines

BHK and HCT116 cells were grown in 10 cm sterile tissue culture plates using complete DMEM medium. The plates were maintained in an incubator of fixed temperature at 37 °C and CO_2 level at 5%. For passaging the cells, confluent cells were first washed with serum-free DMEM, then trypsinized for 5 min in the incubator, then, they were resuspended in pre-warmed fresh medium. Finally, cells were split into a new DMEM containing plate at 1:10 ratio. Passaging was repeated every 2-3 days.

3.2.3.2. Cryopreservation of Cells

For long term storage, freshly passaged cells (1day before freezing) were first counted then centrifuged for 5 min at 300 g. Pelleted cells were resuspended in freezing medium in a density of 1-5x10^6 cells/mL. Using cryovials, 1 mL aliquots were made then put into a freezing container at -80 °C for at least 24 h. These containers are regularly refilled with isopropanol for gradual decrease in temperature. Finally, the cells were stored in liquid nitrogen tanks.

3.2.3.3. Thawing Frozen Mammalian Cells

In a 15 mL centrifuge tube, frozen cells (1 mL aliquot) were immediately thawed by adding 9 mL of fresh DMEM medium. The cells were centrifuged for 5 min at 300 g. This insures removal of any residual DMSO from freezing medium. Finally, pelleted cells were resuspended in 10 mL of fresh DMEM medium and transferred into 10 cm tissue culture plate. Plates were maintained at 37°C and 5% CO_2 incubator.

3.2.3.4. PEI Transient Transfection of Mammalian Cell Lines

Transfections were done on 70-80 % confluent cells. For this, 2.5 X 10^5 cells were split onto each well of 6-well tissue culture plate one day prior to transfection. On the day of transfection, a sterile microcentrifuge tube was used to make the following mixture: 200 µL serum-free phenol-free DMEM, 3 µg of DNA, and 9 µg of polyethyleneimine **(**PEI) solution. The total mixture was then vortexed thoroughly and after incubation for 15 min at room temperature, it was added drop wise onto the cell.

3.2.4. Bio-Panning

3.2.4.1. Selection of Phage Displayed VHHs

Two separate bio-pannings were performed. For each one, 50 µg of His-tagged soluble antigens were captured on 50 µL of anti-His magnetic beads (10103D; Invitrogen) prewashed three times with PBS 1X. The mixture is incubated under rotation overnight. Next day, the beads are washed from access antigen three times with PBS 1X then blocked in 2% skim milk in PBS 1X for 30 min then washed again once with PBS 1X. Panning was performed by using a pre-immune phage library (10^9 cfu- described in Monegal et al., 2009) kindly offered by Prof. Ario de Marco, University of Nova Gorica, Slovenia. The library was first blocked with 2% skim milk in PBS 1X for 30 min then incubated with blocked beads for 1 h. All incubations were performed at 4 ºC and under rotation and a magnetic stand was used to recover the beads after each step. In the first bio-panning (I) phages underwent three rounds of depletion against spy catcher protein (a small protein with His-tag used for depletion of His-tag binders), MIZ-BTB and PATZ2-BTB antigens. In the second bio-panning (II), phages underwent just one rounds of depletion against spy catcher protein. After that, positive selection with mouse (m)PATZ1-BTB domain was performed in the same manner.

After 10 washing steps of positively selected beads using PBS 1X, the bound phages were eluted by incubating the sample for 10 min in 900 µL of glycine 0,1M pH 2,2, with gentle shaking at 4 ºC and finally recovering them from the supernatant by using a magnetic stand. After neutralization in the presence of 250 µL of neutralization solution (Tris-HCl 1M pH 9,1), phages were amplified by using 750 µL of neutralized eluate to infect 9,25 mL of pre-cultured TG1 bacterial cells in 2xYT medium. The bacterial culture was then pelleted and plated on 2xYT Amp, glucose large plates which were then used for monoclonal screening. After that, 93 clones were selected form each bio-panning and grown at 37 ºC in 2xYT Amp, glucose medium in 96 well plate (three wells were used for control). Phages were then produced in wells by infecting bacteria with helper phages. The recovered phages from the culture supernatant were then used for ELISA screening. A detailed bio-panning protocol is provided in appendix E.

3.2.4.2. Screening of VHHs by ELISA

Three 96-well plates were separately coated with 1µg of antigen/well of our antigens of interest; mPATZ1-BTB, PATZ2-BTB, or MIZ1-BTB, in PBS 1X for overnight and at 4 ºC. Next day the plates were blocked with 2% BSA in in PBS 1X for 45 min, then incubated 2 h with 100 µL of blocked phages.

Plates were washed four times with PBS 1X and treated with α-M13HRP conjugate (sigma, GE27-9421-01) at 4 ºC. After 1 h the plates were washed four times with PBS 1X then the reaction was developed by adding 50 µl/well of TMB solution (sigma, T0440). The reaction was then stopped by adding 100 µL of H_2SO_4 1N and the absorbance at 405 nm was measured. Empty wells blocked with PBS 1X were used as a negative control. Clones that had absorbance value on mPATZ1-BTB at least ten-fold higher than that of background and at least two-fold higher than that of PATZ2-BTB and MIZ-BTB controls were selected for confirmative ELISA in triplicate. Clones with the highest absorbance value were then considered positives and their sequences was analyzed to identify unique binders. A detailed protocol for ELISA screening is provided in appendix F.

3.2.5. Protein Purification

3.2.5.1. Vector Construction of Bacterial Expression Plasmid

To obtain a C-terminus mCherry-His-tagged recombinant nanobody proteins, all nanobody sequences that were selected after the alignment of the first and second bio-panning (37 clones) were first cloned into the pET-mcherry-800 bacterial expression vector. All nanobody sequences were PCR amplified from the pHEN4-Nb phage plasmid using a forward primer with NcoI and a reverse primer with NotI restriction sites. Two additional base pairs (GC) were added to the 3' end of the reverse primer to preserve the reading frame with the mCherry tag. The PCR products were then evaluated on an agarose gel for the presence of bands that correspond to the expected size of nanobody-mCherry insert (~ 1100 bp). Correct bands were then gel extracted and digested with NcoI-HF and NotI-HF restriction enzymes. On the other hand, the pET-mCherry-800 plasmid was prepared by digestion with same restriction enzymes and dephosphorylation of cut ends to prevent any chances of self-ligation. After running on an agarose gel, the desired bands were extracted and used for ligation with nanobody-mCherry insert. The generated plasmids were then transformed into DH5α competent cells which were then used for making DNA midi-preps. Successful cloning was confirmed by diagnostic digestion with suitable restriction enzymes and by sequencing (details of vectors construction are given in section 3.2.1).

For solitary nanobodies production, the selected nanobody clones (IG1, IF9, IIA3, IIC10, IIE1) were first clones into pET 28 a (+) bacterial expression vector to obtain a C-terminus His-tagged nanobodies. Nanobody fragments were PCR amplified from the pHEN4-Nb phage plasmid using the same NcoI and NotI tailed primers. The two additional base pairs (GC) in the 3' end of the reverse primer preserved the reading frame with the His-tag. The PCR products were then evaluated on an agarose gel for the presence of bands that correspond to the expected size of nanobodies (~ 400 bp). Correct bands were then gel extracted and digested with NcoI-HF and NotI-HF restriction enzymes. On the other hand, the pET 28 a (+) plasmid was prepared by digestion with same restriction enzymes and

dephosphorylation of cut ends to prevent any chances of self-ligation. After running on an agarose gel, the desired bands were extracted and used for ligation with nanobody inserts. The generated plasmids were then transformed into DH5α competent cells which were then used for making DNA midi-preps. Successful cloning was confirmed by diagnostic digestion with suitable restriction enzymes and by sequencing (details of vectors construction are given in section 3.2.1).

3.2.5.2. Protein Expression

The bacterial expression strain *E. Coli* BL21 DE3 SOX was used for the cytoplasmic expression of all nanobodies whether in solitary form or as mCherry fusions. This strain is stably transformed with SOX plasmid for the expression of the recombinant sulfhydryl oxidase enzyme to allow the formation of the disulfide bond of nanobodies in the reducing environment of the bacterial cytoplasm. The constructed plasmids for bacterial expression of nanobodies (see section 3.2.5.1) were transformed into this bacterial strain under Amp/ Kan antibiotic selection for pET-Nb- mCherry and pET 28 a (+)-Nb plasmids respectively. Additionally, Chl antibiotic was used for bacterial selection.

After transformation, a single colony was randomly picked and inoculated into 3 mL of LB medium with appropriate antibiotics. This preculture was incubated at 37 °C for 6-12 hs with vigorous shaking (221 rpm). For small scale protein purification this culture was directly used for induction and affinity purification (see section 3.2.5.3). For large scale purification, this culture was transferred into 50 mL of LB supplemented with appropriate antibiotics and incubated overnight under the same conditions. The next day, the culture was transferred into 1 L of LB medium supplemented with appropriate antibiotics and incubated under the same conditions until the OD_{600nm} reached 0.4-0.6. The culture was then kept on ice for 1 h to cool down. For induction, the expression of SOX plasmid was first induced with arabinose at a final concentration of 0.2% (w/v) for 30 min. The expression of nanobodies was then induced by adding isopropyl β- d- 1- thiogalactopyranoside (IPTG) at a final concentration of 0.1 mM. The cultures were incubated under induction for overnight

at 18 °C in a shaker incubator (180 rpm). Un-induced culture was prepared in the same manner but at a small scale of 50 mL for control.

3.2.5.3. Affinity Chromatography

After induction, the bacterial cells were harvested by centrifugation at 4000 rpm for 10 min and the supernatant was discarded. For small scale culture, the pellet was dissolved in 350 µL of freshly prepared lysis buffer (see section 3.1.3), then sonicated at 4 °C using Bioruptor ® Pico sonication device (10 min, 30 s on, 30 s off). The lysate was then centrifuged at 4 °C for 5 min at 13000 rpm and the supernatant containing the soluble proteins was saved in a separate eppendorf. HisPur™ Cobalt Superflow Agarose beads (25228; Thermo Scientific) were used to capture His-tagged nanobodies. For that, 20 µL of beads were washed three times with 500 µL of IMAC-A buffer (see section 3.1.3) and centrifuged at 6000 rpm for 2 min. The beads were then ready for mixing with the nanobody supernatant. The mixture was incubated rotating at 30 rpm for 30 min at 4 °C. After that, beads were collected by centrifugation and washed three times with IMAC-A buffer. Finally, beads were resuspended in 20 µL of water, and 5 µL of protein loading dye (see section 3.1.3) was added. The mixture was then boiled at 95 °C for 5 min and the total 25 µL were loaded on 14% SDS-PAGE (see section 3.1.3). Additionally, fractions from each purification step: un-induced sample, induced sample, pellet, supernatant, non-retained proteins after incubation with beads, and wash flowthrough were also loaded onto the SDS-PAGE.

For large scale cutlers, the cells were resuspended in 30 mL of freshly prepared lysis buffer (see section 3.1.3), then sonicated at 4 °C using Sonics-VibraCell™ (standard probe 1.5 min, 5 s on,10 s off, 40% amplitude). The lysate was then centrifuged at 4 °C for 45 min at 15000 rpm. During this time, the CrystalCruz® chromatography column was prepared by first washing it with 10 mL of ddH2O, then loading it with 3 mL of the same agarose resin beds, then washing the beads three times with 10 mL of ddH2O, and finally equilibrating with 10 mL of IMAC-A buffer (see section 3.1.3). After completion of centrifugation, the supernatant containing the soluble proteins was loaded onto the prepared column and the

whole mixture was incubated for 30 min in an end-to-end rotation at 4 °C. After incubation, the flowthrough containing the non-retained proteins was allowed to flow out of the column. The retained beads in the column together with bound proteins were washed with 10 mL of IMAC-A for three times. Finally, the His-tagged protein was eluted with 2 mL of serial concentrations of IMAC-B buffer (100, 300,600 mM) (see section 3.1.3) and repeated when necessary. The best concentration of elution buffer was used for subsequent purifications. Samples from elution together with samples from different purification step were then prepared by adding 1X protein loading dye, boiling at 95 °C for 5 min then loaded onto the SDS-PAGE.

His Trap FF 1 ml affinity column (Cytiva) was used for large scale affinity chromatography of solitary nanobodies. For that, the same steps were followed to prepare the lysate and to collect the supernatant. Following the manufacturer recommendations, the column was then connected to the AKTA Pure system (Cytiva), washed with five column volumes of distilled water, and equilibrated with five column volumes of binding buffer (see section 3.1.3). The supernatant was then applied onto the column using repeated syringe injections to the connected injection loop. Following fifteen column volume washes of the column with binding buffer, the protein was eluted by the addition of twenty column volumes of elution buffer (see section 3.1.3) in a linear gradient of imidazole.

When protein concentration was low, Vivaspin® 20 concentrators were used according to manufacturer's instructions (Sartorius; VS2001**)**. Protein concentration was measured by NanoDrop and aliquots of purified samples were flash frozen in liquid nitrogen and saved at -80 °C.

3.2.5.4. SDS-PAGE and Coomassie Blue Staining

First 14% separating gel (see section 3.1.3) was prepared and poured into the casting apparatus then left to solidify. Next, 6% stacking gels (see section 3.1.3) was prepared and loaded on top of the separating gel with placement of appropriate size comb. When the

stacking gel was solid, the comb was removed, and the cast was mounted on electrophoresis chamber and merged with 1X running buffer (see section 3.1.3). Samples that were obtained from each step of protein purification were mixed with protein loading dye (see section 3.1.3) to a 1X dilution then denatured by boiling at 95 °C for 5 min. When the samples were ready, they were loaded into the wells and the proteins molecular weight marker (appendix D) was loaded into the first well. Electroporation was carried out at 80 v and 15 amp for the first 30 min then the v was increase up to 120 v for 2 h. When the bands are well separated and electroporation is finished, the gel was removed from the glasses carefully and placed into the staining solution for 2 hs followed by overnight de-staining.

3.2.5.5. Size-Exclusion Chromatography

As a second level of purification, size exclusion chromatography was carried out using an AKTA pure system (Cytiva) to remove any non-specific proteins after affinity chromatography. The samples were injected to the system using a sample injection loop at a total volume of 500 µL. A Superdex ™ 200 Increase 10/300 GL size exclusion column (column volume of 24 mL, flow 0.75 mL/min) equilibrated with the PBS 1X at 4 ºC was used. Samples absorbance at 280 nm was analyzed and peak fractions relevant to the proteins expected size were analyzed on an SDS–PAGE (see section 3.2.5.4).

3.2.6. Size Exclusion Chromatography (SEC) Co- Elution

Solitary purified nanobodies IF9, IG1, and IIE1 were used for this experiment. Purified proteins of mPATZ1-BTB, zebrafish (zf)PATZ1-BTB, and PATZ2-BTB were taken from lab stocks. The mPATZ1-BTB protein (70 µM) was mixed with (70 µM) of each nanobody separately in 1:3 molar ratio in 1X PBS and incubated for 1 h at 4 ºC. The mixture was then analyzed on an AKTA pure system (Cytiva) by injecting a total volume of 50 µL to a Superdex ™ 200 Increase 5/150 GL size exclusion column (column volume of 3 mL, flow 0.35 mL/min) equilibrated with the same buffer. As a control, all proteins were run separately

on the same column in the same manner. To demonstrate specificity of binding, all selected nanobodies against mPATZ1-BTB domain were also analyzed for complex formation with the PATZ2-BTB and zfPATZ1-BTB domains.

3.2.7. Surface Plasmon Resonance (SPR)

For these experiments, solitary purified nanobodies IF9, IG1, and IIE1 were used and purified proteins of mPATZ1-BTB, zfPATZ1-BTB, and PATZ2-BTB were taken from lab stocks. The experimental setup was based on immobilizing anti-His antibody on the reference and active flow-cells then capturing His-tagged nanobodies on the active flow cells and flowing different concentrations of un-His-tagged BTB domains sequentially. To match this experimental setup, His-tags were first removed from BTB domains using lab produced 3c pre-scission protease. For this, 5 µg of protease was incubated over night at 4 ºC with 2 mg of His-tagged proteins in a total volume of 1 mL. The next day, the protease enzyme was cleared from the sample using 200 µL of Glutathione Sepharose TM 4 Fast Flow beads (GE Healthcare) for each sample. The beads were washed twice in 1X PBS before being incubated for 30 min with the samples. After 5 min of centrifugation at 300 g, the cleared supernatant was collected. Next, each sample was incubated with 60 µL HisPur ™ Cobalt Superflow Agarose beads (Thermo Scientific) for removal of His-tags. The beads were washed three times with 500 µL of water before being incubated with the samples for 30 min. The cleared samples were then recovered by centrifugation for 2 min at 6000 rpm. For confirmation of efficient His-tag removal, 50 µL of each sample (100 µg) from cleaved and un-cleaved proteins were loaded on a calibrated Superdex ™ 200 Increase 5/150 GL size exclusion analytical column equilibrated with the 1X PBS and applied to AKTA pure chromatography system (Cytiva).

For SPR experiments, all measurements were performed on a BIACore T200 system at 12 °C using a CM5 chip. The running buffer was commercially supplied HBS-EP buffer (Cytiva). Following the manufacturer instructions, a His Capture Kit (Cytiva) was used to

immobilize the anti-His antibody on the sensor surface of the reference and active flow cells by standard amine coupling to a level of approximately 7000 response unit (RU).

For affinity measurements, single cycle kinetics were performed. In summary, the method comprises three main stages starting with the capture of the first His-tagged nanobody on the generated anti-His surface of active flow cell, followed by sequential injections of increasing concentrations of BTB domains over both reference and active flow cells, and finally the whole surface was regenerated, and the entire method is repeated for the second and third nanobodies.

For nanobody capture, 1300-1400 RU were achieved by injecting 5 µg/mL of each nanobody for 60 s in 30 µL/min flow rate. Three-fold serially diluted BTB domain (6,18,54,162 nM) were injected in duplicates for 60 s in 10 µL/min flow rate followed by 2 min of dissociation in running buffer. Surface was regenerated with a quick pulse (60 s) of 10 mM glycine-HCl, pH 2.5 commercially supplied (Cytiva). All raw data were processed using BIACORE^{TM} T200 Software Set V3.0 (Cytiva). The replicates of two were used to calculate the experimental standard errors. Sensorgrams were corrected from reference cell and blank buffer cycles and the data were fitted into a 1:1 binding model. The affinity constant (K_D) was calculated from the ratio of k_d/k_a. PATZ2- BTB and zfPATZ1-BTB domains were used for comparison.

3.2.8. Fluorescent Two- Hybrid (F2H) Assay

The aim of this assay is to assess the interaction between nanobodies and PATZ1-BTB domain in normal cellular environment. For this we used the fluorescent two - hybrid (F2H) assay. In this system a lac operator/repressor system is used to generate a stable nuclear interaction platform in single living cells. Then, a fluorescent bait protein is derived to the interaction platform and assayed for co-localization with a fluorescent prey fusion protein using live cell microscopy. For this, the genetically modified BHK cells were used. These cells have multiple lac operator sequences randomly integrated into their genome. Nuclear

localization of Tag-GFP PATZ1-BTB plasmid is achieved by co-transfection with a LacI-GBP (GFP binding protein) plasmid. Protein-protein interaction is then assessed by co-localization with fluorescent spots of Nb-mCherry plasmid in live cell microscopy. The following sections describe the generation of bait, prey, and nuclear localization plasmids, transfection of these plasmids in BHK cells, and live cell imaging steps of this assay.

3.2.8.1. Vector Construction

Three main plasmids were used for this assay which are the F2H-bait (pcDNA3.1/myc-His (-) B-TagGFP-PATZ1-BTB), the F2H-prey (pCDNA3.1/ myc- His (-) B- Nb-mCherry), and the nuclear localizing plasmid (pcDNA3.1/myc-His (-) B- GBP-LacI). These vectors are all based on the mammalian expression vector - pcDNA 3.1/ myc-His (-) B - as a backbone plasmid. The F2H-bait and the nuclear localizing plasmid were taken from lab stocks. The F2H-prey vectors were generated for 5 nanobodies (IF9, IG1, IIA3, IIC10, IIE1). For that, the nanobody-mCherry sequences were PCR amplified from the pET-Nb- mCherry plasmid using designed primers with EcoRI and BamHI restriction sites. The PCR products were evaluated on an agarose gel for the presence of bands that correspond to the expected size of nanobody-mCherry insert (~ 1100 bp). Correct bands were then gel extracted and digested with EcoRI and BamHI restriction enzymes. On the other hand, the pcDNA 3.1/ myc-His (-) B plasmid was prepared by digestion with same restriction enzymes and dephosphorylation of cut ends to prevent any chances of self-ligation. Desired bands were then extracted from an agarose gel and used for ligation with nanobody-mCherry insert. The generated plasmids were then transformed into DH5α competent cells which were then used for making DNA midi-preps. Successful cloning was confirmed by diagnostic digestion with suitable restriction enzymes and by sequencing (details of vectors construction are given in section 3.2.1).

For control experiments, pcDNA3.1/myc-His (-) B-TagGFP-PATZ2-BTB plasmid was also taken from lab stocks while pEGFP-N2- ccdc124-mCherry plasmid was kindly offered by Prof. Uygar TAZEBAY, Gebze Technical University, Turkey.

3.2.8.2. Transfection and Live Cell Imaging

The BHK cells were used for transfection with equal amounts of the above-mentioned plasmids (refer to section 3.2.3.4.). After 24 hs, the transfected cells were visualized using live cell imaging microscope (ZEISS Axio Observer Z1) with suitable laser wavelength and intensity for GFP and mCherry fluorophores. Each well was scanned for the presence of green, fluorescent spots in the nucleus in the green channel. The positive cells were then checked for the presence or absence of co-localizing red fluorescent spots in the red channel. The Ziess Zen 2010 software was used to acquire images for positive and negative cells.

3.2.8.3. Image Processing and Quantification

ZEN 2.3 (blue edition) software was used to analyze images. In each image, cells showing nuclear green foci in the green channel were numbered. In these cells, the availability of co-localizing red foci in the red channel was scored 1 while the absence was scored 0. MS Excel was then used for quantification of the total percentage of cells showing positive interaction.

3.2.9. Generation of Stable Cell Lines

Human colon cancer cells (HCT116) stably expressing nanobodies were generated by PEI transfection of these cells with nanobody- mCherry constructs cloned into pcDNA 3.1/ myc-His (-) B (see section 3.2.8.1). Cells were then subjected to neomycin selection of for 10 days. Expression of nanobodies was assessed with live cell imaging microscope (ZEISS Axio Observer Z1) with suitable laser wavelength and intensity for mCherry fluorophores. Fluorescence-activated cell sorting (FACS) was used for sorting cells that are stably expressing nanobodies.

3.2.10. Flow Cytometry

Around 50 x10^6 HCT116 stably expressing nanobodies were counted and washed twice with FACS buffer before resuspending them in final 5 mL of FACS buffer. Cells were then sorted by BD Influx Cell Sorter until at least 5 x 10^5 positive cells were collected. Data analysis was performed using FlowJo Software. The sorted cells were then expanded, and aliquots were stored in liquid nitrogen.

3.2.11. Quantitative (real-time) PCR

To evaluate the nanobody-related alterations in the expression of the known PATZ1 target genes (CTH, ETV1), specific primers were designed for these two genes and used for quantitative PCR. The PATZ1 wild type HCT116 stably expressing nanobodies were used for total RNA isolation using Trizol reagent then cDNA was generated using Thermo Scientific's RevertAid First Strand cDNA Synthesis Kit according to the manufacturer's instructions. A Thermo Pikoreal system was used to assess gene expression using the Luna Universal qPCR Master Mix Protocol (Biolabs). The $2^{-\Delta\Delta CP}$ method was used to determine relative expression levels with data normalized to the expression level of the glyceraldehyde 3-phosphate dehydrogenase gene (Gapdh). Statistical data analysis and significance of fold change was determined using unpaired t-test in GraphPad Prism software

4. RESULTS

4.1. Selection of PATZ1-BTB-Specific Nanobodies

In this study, we aimed to isolate nanobodies that are specific against the BTB domain of the PATZ1 transcription factor. Two separate bio-panning rounds were performed. The first bio-panning had a stricter criterion for the selection of specific PATZ1-BTB binders. For this, MIZ-BTB and PATZ2-BTB antigens were used first for negative selection followed by positive selection using the PATZ1-BTB domain. In the second bio-panning, the criterion was less strict to ensure that all possible PATZ1-BTB binders were selected. For this, the PATZ1-BTB domain was used directly for the selection of positive binders without a preliminary step of negative selection. A total of 93 clones were picked for each round of bio-panning and their binding specificity was tested by ELISA (single samples) followed by a second round (triplicate samples) for the selected clones. Figure 4.1 shows a schematic illustration of bio-panning procedure.

In the ELISA of the first and second bio-panning, both PATZ2-BTB and MIZ1-BTB antigens were used for coating the wells separately (as controls), in addition to three empty wells (no nanobodies) for background subtraction. A total of 68 clones (41from the first and 27 from the second bio-panning) were selected. Three clones (ID9, IF9, IG1) from the first bio-panning, and 15 clones (IIA3, IIA5, IIC3, IIC8, IIC10, IIE1, IIE2, IIE6, IIE7, IIF2, IIF3, IIF8, IIF9, IIG9, IIH3) from the second revealed PATZ1-BTB specific binding activity, defined as VHHs of which the binding signal on PATZ1-BTB was at least ten-fold higher than that of background and at least two-fold higher than that of PATZ2-BTB and MIZ-BTB

controls. The rest of the clones (38 from the first bio-panning and 12 from the second bio-panning) also showed specificity against PATZ2-BTB, MIZ1-BTB, or no specificity at all. All of these samples were nevertheless tested in the second ELISA using triplicate samples. In the confirmatory ELISA of the first bio-panning, only MIZ1-BTB Ag was used as a negative antigen and PATZ1 BTB as a positive antigen for coating the wells, since a negative selection step was already performed during the bio-panning. The second bio-panning was a direct bio-panning with no negative selection step, therefore both PATZ2-BTB and MIZ1-BTB antigens were used as controls for confirmatory ELISA. Additionally, at least three empty wells (no nanobodies) were used for subtraction of background. Five clones (IC9, ID9, IF9, IG1, IG2) from the first bio-panning, and 3 clones (IIA3, IIC10, IIE1) from the second revealed PATZ1-BTB specific binding activity, using the same criteria as in the first ELISA. Nine other clones from the first bio-panning and the rest of the clones from the second bio-panning (24), were also selected since they showed PATZ2-BTB, MIZ1-BTB, or no specificity. In summary, a total of 41 clones were selected for further characterization. The results of the confirmatory ELISA analysis of the first and second bio-panning are shown in (Figure 4.2) and (Figure 4.3) respectively. The raw data of ELISA experiments of the first and second bio-panning are shown in Appendix G and H respectively.

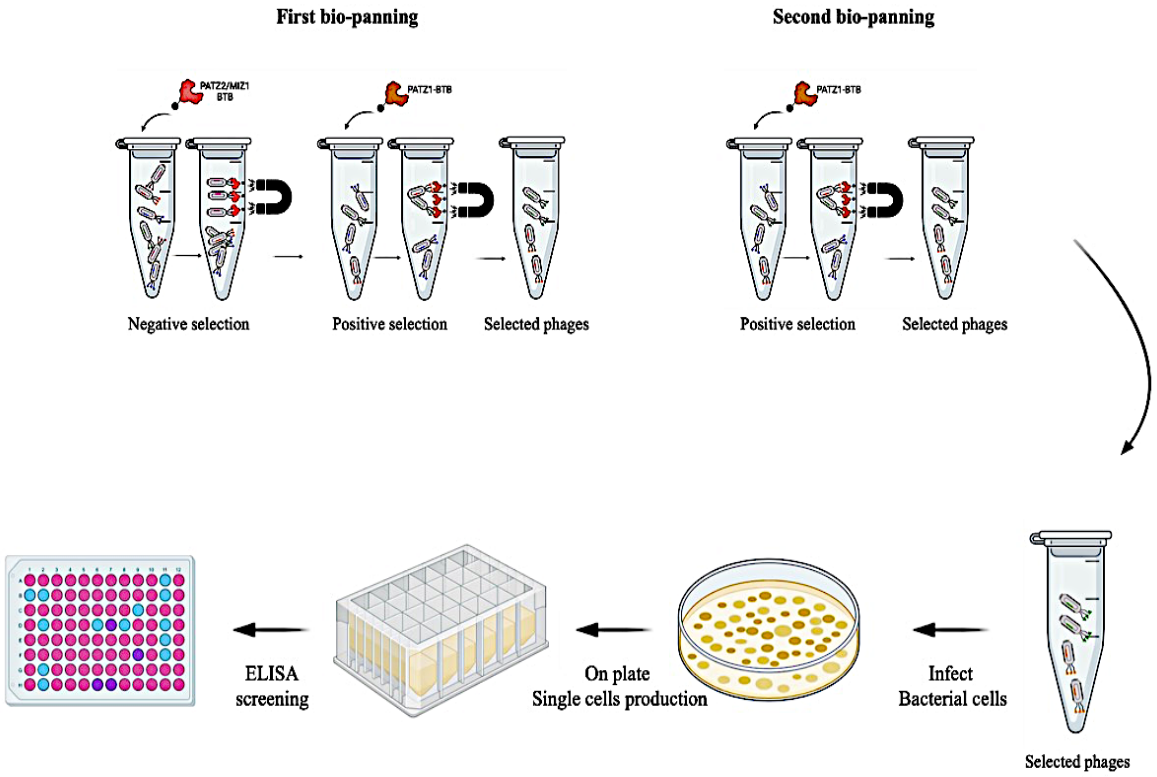

Figure 4. 1: Schematic illustration of bio-panning procedure.

Top left side shows first bio-panning using negative and positive selection steps, while the right side shows the second bio-panning using only positive selection.

These 41 ELISA selected nanobody encoding phagemids were sequenced using the M13-Rev primer. Sequence alignment revealed two similar groups of VHHs. IIF8 had the same sequence as IIE7 and IIE6 had the same sequence as IIA5, IIF3, and IIH3, therefore, only IIE6 and IIF8 were selected. Clones that had amber stop codons (TAG) were also excluded. These include (IA3, IG6, IH5, and IH6) from the first bio-panning and (IID10, IID2, and IIC2) from the second bio-panning. These clones can only be expressed in amber suppressor bacterial strains like TG1 cells, which were used for phage production. The tRNA of these cells enables read through translation of the amber codon and results in the production of a full-length protein encoding the nanobody and the phage protein XX. The deduced amino acid alignment of the selected 30 clones (10 from the first bio-panning and 20 from the second bio-panning) are shown in (Figure 4.4). The DNA sequencing results of these clones are given in Appendix J.

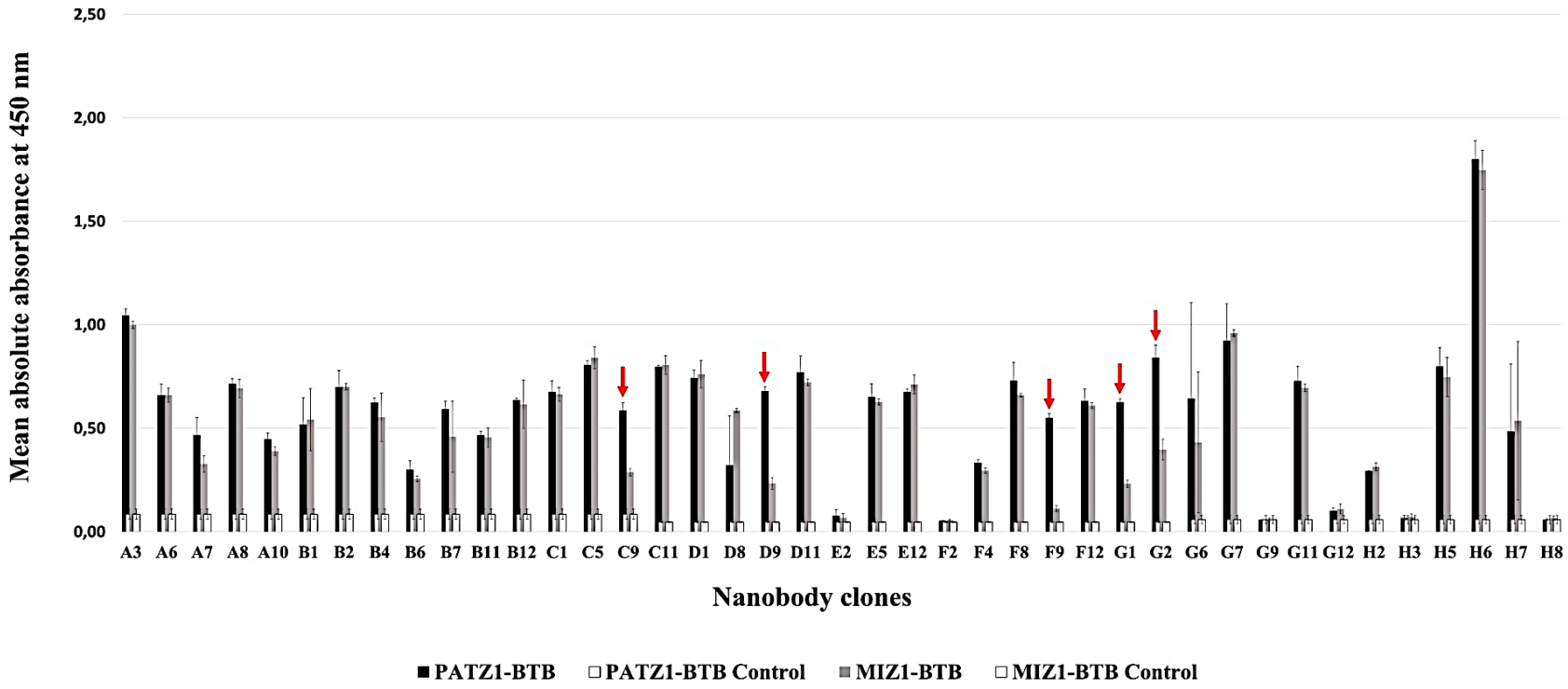

Figure 4. 2: Confirmatory ELISA results of the selected nanobodies from first bio-panning.

Absolute values of absorbance at 450 nm – as a measure of the concentration of converted TMB substrate – obtained with a Tecan microplate reader. Color legend: reactivity of the nanobodies to the PATZ1-BTB-coated wells is shown in black bars, reactivity to the MIZ1-BTB-coated wells in grey bars, and background reactivity in white bars. Red arrows indicate PATZ1-BTB specific clones. The results show the mean of three measurements for each nanobody

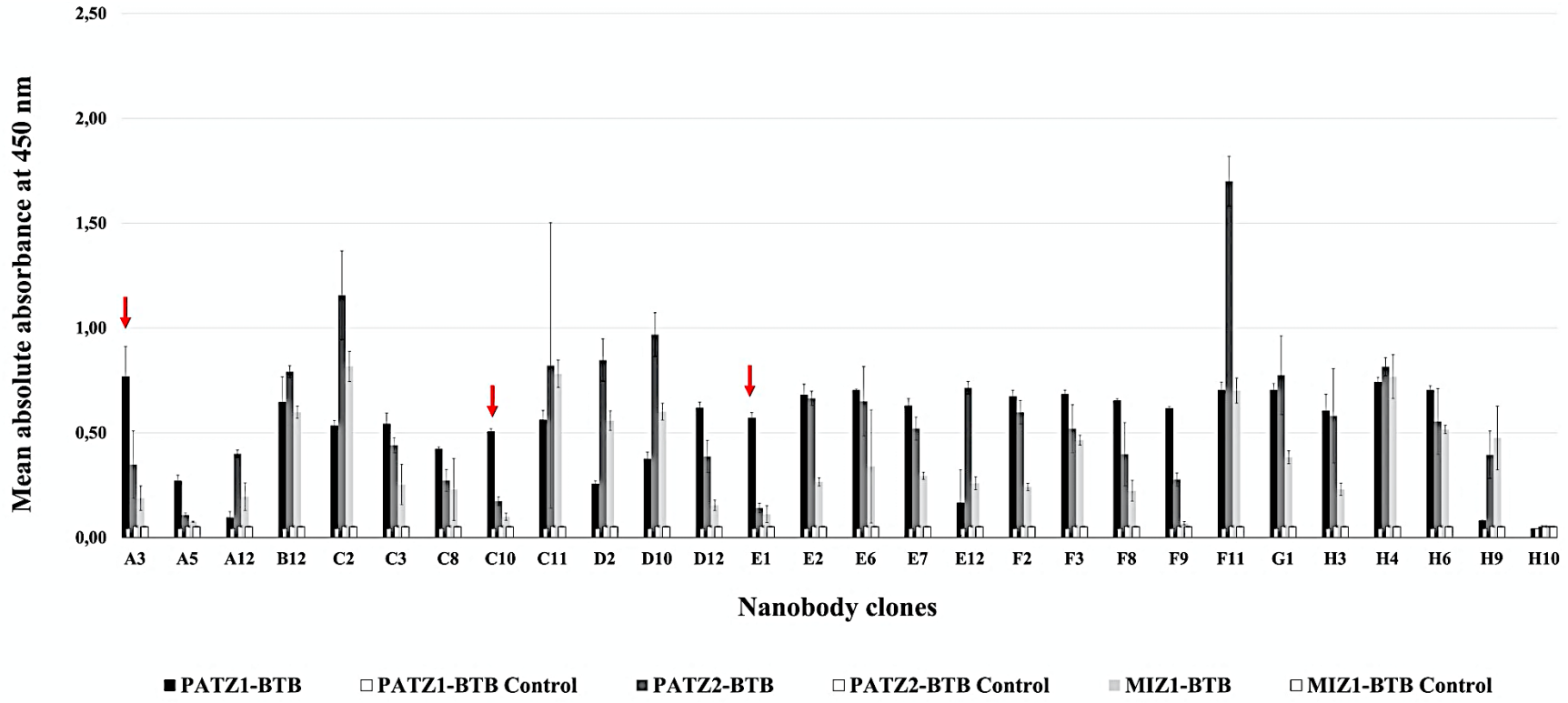

Figure 4. 3: Confirmatory ELISA results of the selected nanobodies from second bio-panning.

Absolute values of absorbance at 450 nm - as a measure of the concentration of converted TMB substrate - obtained with the Tecan microplate reader. Color legend: binding of the nanobodies to the PATZ1-BTB-coated wells is shown in Black, to PATZ2-BTB-coated wells in Dark Gray, to MIZ1-BTB-coated wells in light Gray, and background in white. Red arrows indicate PATZ1-BTB specific clones. The results show the mean of three readings for each nanobody

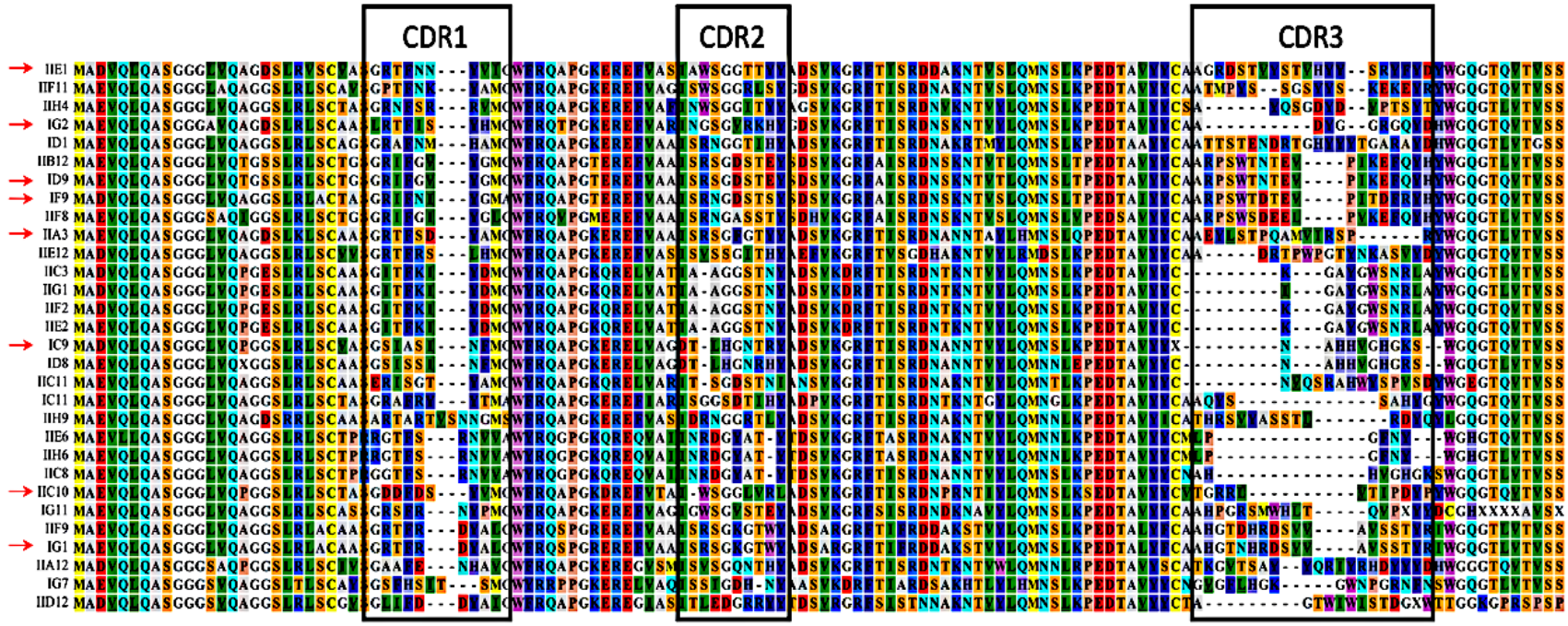

Figure 4. 4: Sequence alignment and analysis of selected nanobodies from the first and second bio-panning.

CDR regions (CDR1, CDR2, and CDR3) are shown in black boxes. Red arrows indicate PATZ1-BTB specific clones.

4.2. Production and Characterization of Selected Nanobodies

4.2.1. Bacterial Expression and Purification

4.2.1.1. Recombinant Nanobody Production

All (37) clones with a unique sequence were PCR amplified with appropriate primers and cloned from the phage plasmid (pHEN4) into a bacterial expression vector. Clones that had an amber stop codon in their sequences were also included. The pET-800 mCherry bacterial expression vector was selected to obtain C-terminally mCherry and hexahistidine-tagged recombinant VHH for ease of purification and for subsequent applications. The plasmids were then transformed into BL21(DE3) SOX competent cells for cytoplasmic expression of nanobodies. These cells express a recombinant sulfhydryl oxidase enzyme required for cytoplasmic disulfide bond formation and resulting in the confirmational stability of nanobodies in the reducing environment of the bacterial cytoplasm. Clones (IA3, IG6, IH5, IH6, IID10, IID2, and IIC2) that contain internal amber codons are expected to result in premature termination as only the TG1 strain and not the BL21 strain contains the tRNA necessary for readthrough translation.

4.2.1.1.1 Small Scale Bacterial Expression and Purification

First, we attempted to scan for optimal expression levels of nanobodies using small scale (3 ml) cultures. After lysis of the cells, we captured soluble proteins on anti-His cobalt agarose beads and analyzed the total bound (TB) protein by SDS-PAGE followed by Coomassie staining. We also loaded fractions from induced lysate (I), pellet (P), supernatant (S), non-retained proteins after incubation with beads (NR) as well as after washing the beads (W). This scanning process was done in batches and for each batch, a control sample of un-

induced culture was included for comparison. The expected molecular weight of the nanobody-mCherry construct was calculated to be ~ 41 kDa.

Different clones of nanobodies showed different levels of expression ranging from strong to mild. Some clones failed to be expressed such as IC9, IC11, IIE12, IIF2, IIF9, IIF11, and IIG1. Clones IG6 and IID2 were expected not to be expressed due to the presence of an amber stop codon. However other clones with amber stop codons including IA3, IH5, IH6, IID10, and IIC2 were fairly expressed. This could be attributed to the presence of a second start codon and an alternative open reading frame or simply due to sequencing errors (Figures 4.5 and 4.6).

At this point we decided to continue with the clones that showed PATZ1-BTB specificity in the first and second ELISA screening and were successfully expressed and purified in small scale. Accordingly, clones IG1, IF9, IIA3, IIC10, IIE1 were selected for large scale expression and purification.

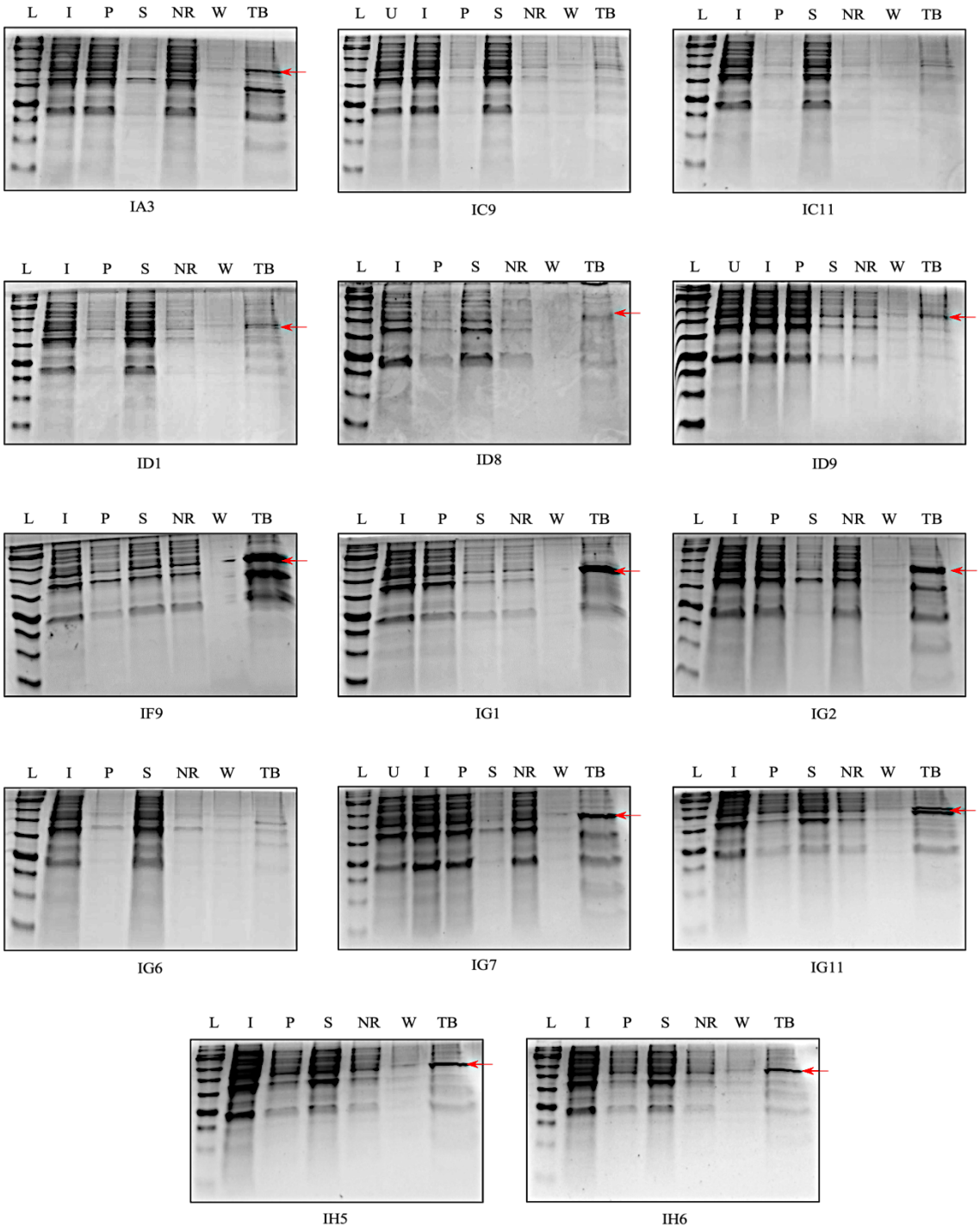

Figure 4. 5: Small scale purification of nanobodies selected from the first bio-panning

Nanobody-mCherry constructs of all clones selected from the first bio-panning were expressed and purified in a small scale of 3 ml culture. 14% coomassie-stained SDS-PAGE was used to analyze fractions from each purification step. Legend: U: un-induced sample, I: induced, P: pellet, S: supernatant, NR: non retained, W: wash, and TB: total bound. Red arrows indicate expressed nanobodies with an expected band size of ~ 41 kDa.

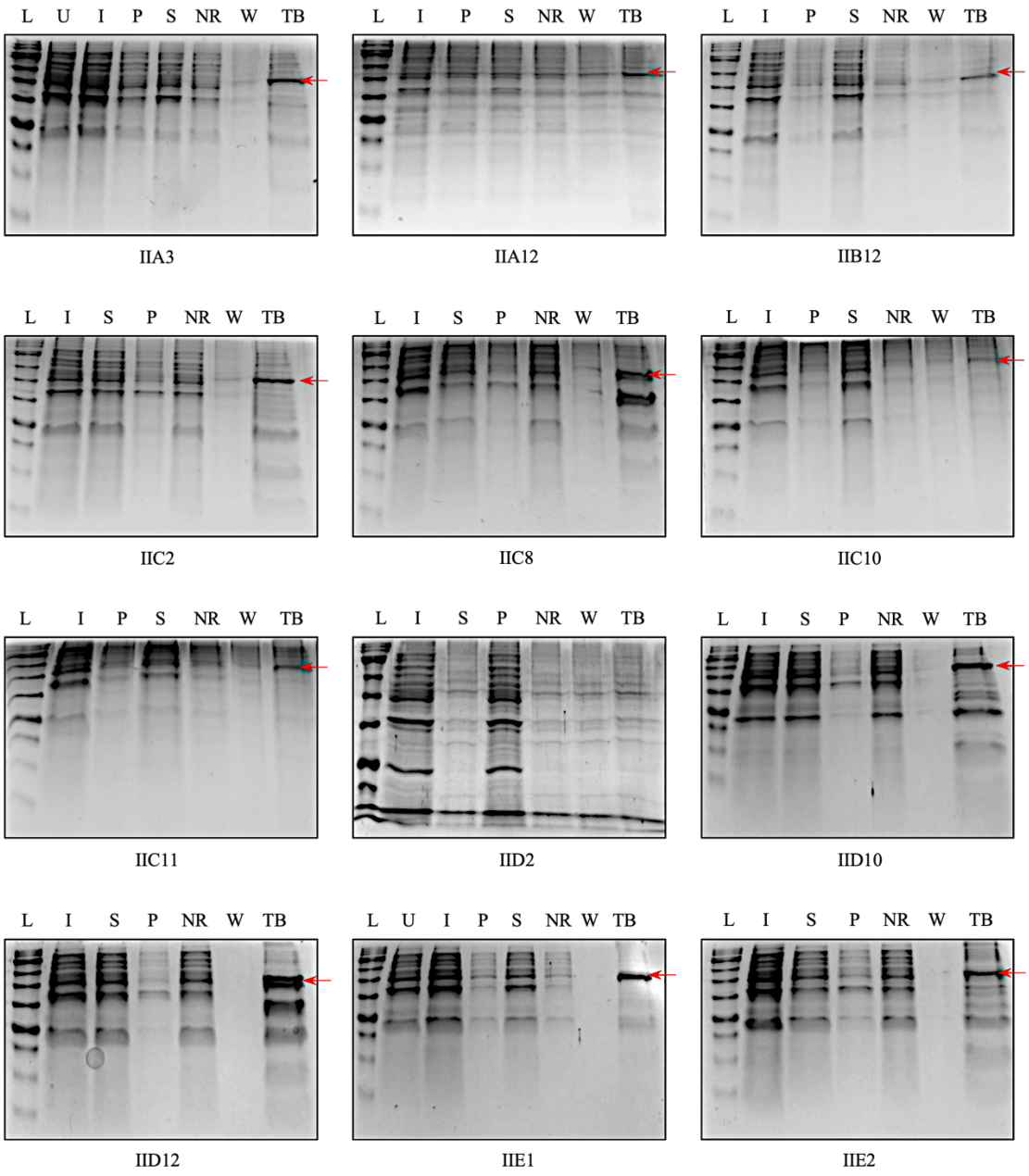

Figure 4. 6: Small scale purification of nanobodies selected from the second bio-panning.

Nanobody-mCherry constructs of all clones selected from the second bio-panning were expressed and purified in a small scale of 3 ml culture. 14% coomassie-stained SDS-PAGE was used to analyze fractions from each purification step. Legend: U: un-induced sample, I: induced, P: pellet, S: supernatant, NR: non retained, W: wash, and TB: total bond. Red arrows indicate expressed nanobodies with an expected band size of ~ 41 kDa.

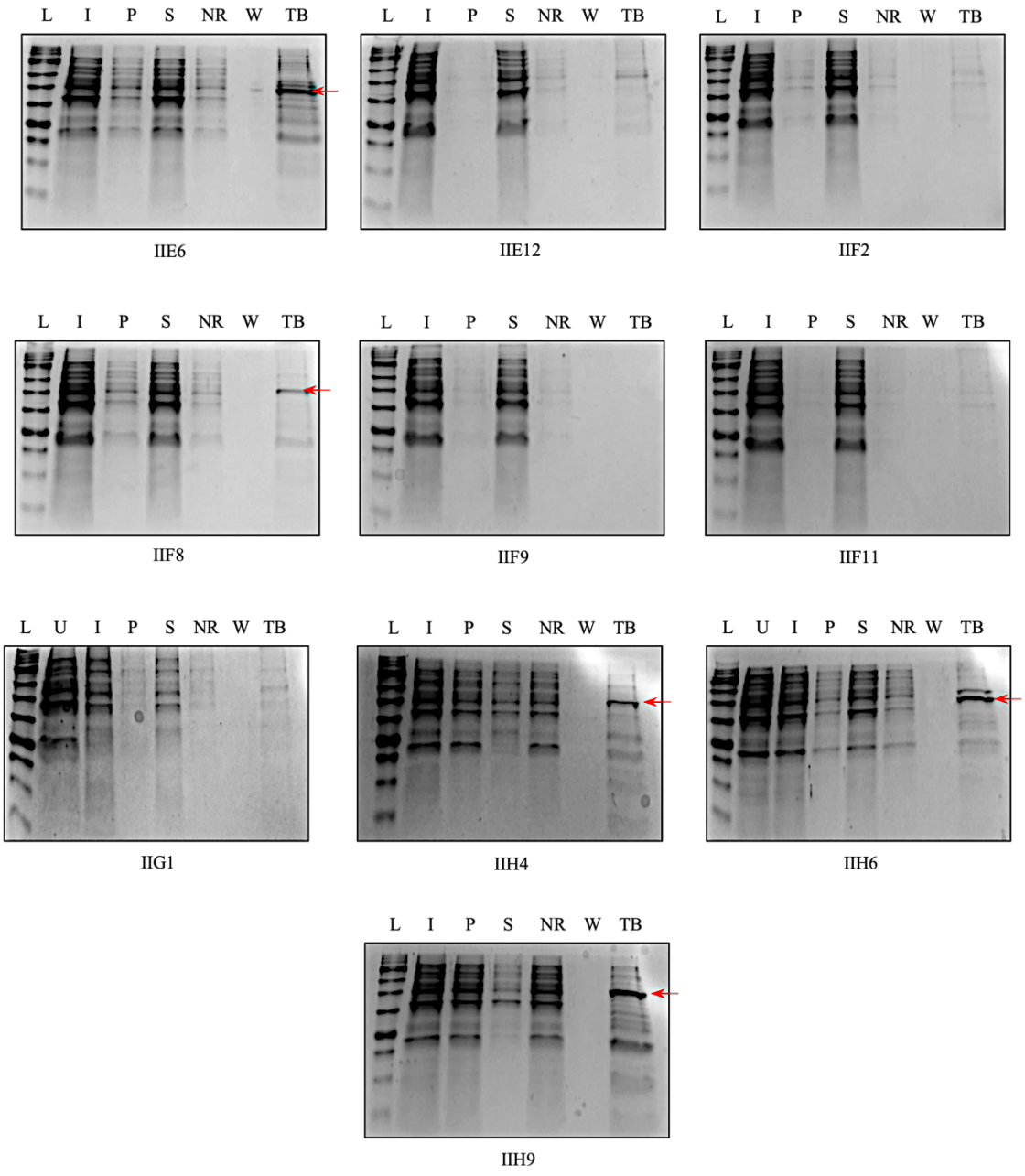

Figure 4. 6 (continued): Small scale purification of nanobodies selected from the second bio-panning

Nanobodies-mCherry constructs of all clones selected from second bio-panning were expressed and purifies in small scale of 3 ml. 14% coomassie-stained SDS-PAGE was used to analyze fractions from each purification step. Legend: U: un-induced sample, I: induced, P: pellet, S: supernatant, NR: non retained, W: wash, and TB: total bond. Red arrows indicate expressed nanobodies with expected band size of ~ 41 kDa.

4.2.1.1.2 Large Scale Bacterial Expression and Purification

For large scale protein expression and purification, we continued with five clones (IG1, IF9, IIA3, IIC10, IIE1). We used the same bacterial expression stocks that were previously used for small scale expression. Cultures were grown in 1 L, lysed, and affinity chromatography was performed on lysates using anti-His cobalt agarose beads. Fractions from each step of purification were analyzed by SDS-PAGE (Figure 4.7). The concentrations of purified proteins were determined by measuring absorbance at 280 nm (table 4.1.).

Bands equivalent to the size of the nanobody-mCherry construct (~ 41 kDa) were seen for all samples. When several elutions were performed, thicker bands were evident in earlier elutions. Smaller bands (~ 27 kDa) were also seen in all samples. The size of these small bands corresponds to the size of mCherry protein alone, which might suggest degradation of a fraction of our purified proteins. The IIA3 sample showed bands corresponding to nanobody-mCherry and mCherry only, but additionally there were two extra bands just below these bands. After referring to the sequence of this clone we found two cut sites for the restriction enzyme NcoI, which was used for cloning these nanobodies into the pET mCherry vector. The second cut site produces a truncated gene encoding a protein that is missing 35 amino acids in the N-terminus. This observation indicates that clone IIA3 is a mixed clone of both full and truncated versions. SDS-PAGE also showed impurities in the eluted factions; therefore, we decided to run size exclusion chromatography for all samples.

# Elution	IG1 mg/ml	IF9 mg/ml	IIA3 mg/ml	IIE1 mg/ml	IIC10 mg/ml
1st elution	5.76	0.80	1.16	3.42	1.04
2nd elution	13.99	1.85	3.07	6.73	3.57
3rd elution	5.11	0.37	0.84	1.17	0.90
4th elution	1.11			0.5	
Combined		1.06	0.93		1.24

Table 4. 1: Concentrations of purified recombinant nanobodies.

Protein concentration was determined by measuring absorption at 280 nm after affinity chromatography for each purified recombinant nanobody. Elution was repeated if necessary. Samples with low concentrations (IF9, IIA3, IIC10) were combined and the total concentration was measured.

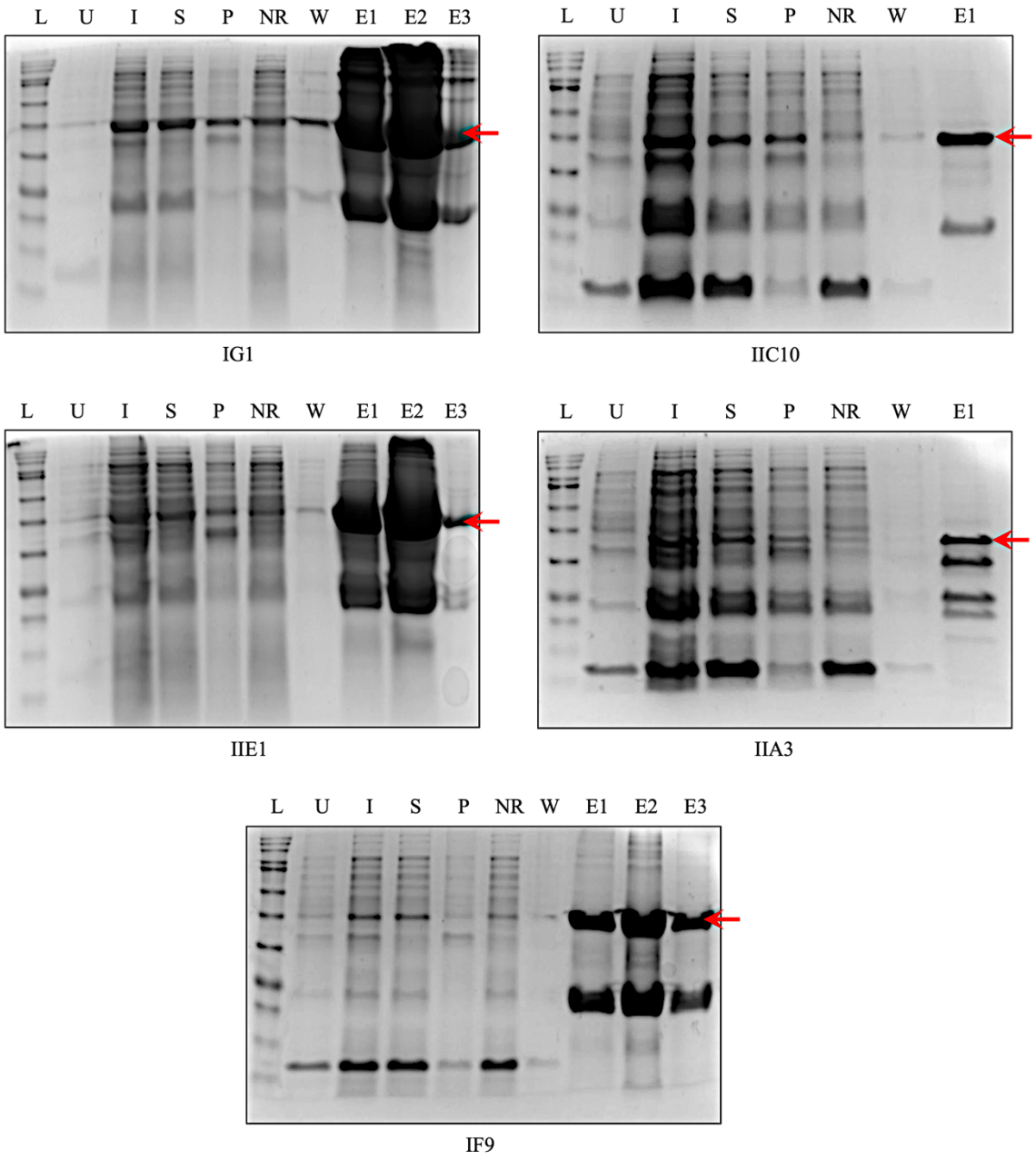

Figure 4. 7: Large scale purification of selected nanobodies.

Affinity chromatography of selected nanobodies expressed in large scale of 1 L. 14% coomassie-stained SDS-PAGE was used to analyze fractions from each step of purification. Legend: U: un-induced sample, I: induced, P: pellet, S: supernatant, NR: non retained, W: wash, and E: elution. Red arrows indicate expressed nanobodies with an expected band size of ~ 41 kDa.

For size exclusion chromatography, samples that had high concentration (IG1, IIE1) were directly used, while samples that had low concentrations (IIA3, IIC10, IIF9) were first concentrated using a 10 kDa molecular weight cut-off concentrator in order to obtain a final concentration of at least 2 mg/ml. We used a superdex 200 Increase 10/300 GL column with an AKTA Pure chromatography system (Cytiva). Chromatographs showed a single peak corresponding to the molecular mass of nanobody-mCherry (~ 41 kDa) with reference to peaks of a calibration run that was performed previously for this column (Figure 4.8 left panel). Exceptionally, the IIA3 sample showed two distinct peaks, which is in line with our previous results for this sample. A confirmative SDS–PAGE was run for fractions relevant to the SEC peaks (Figure 4.8 right panel). Bands corresponding to the size of nanobody-mCherry were clearly seen in all samples, however, bands corresponding to the size of mCherry only were also seen, which might be attributed to the denaturing nature of this gel and possible proteolysis after the SEC purification. Other larger bands that were observed might possibly be due to aggregate formation after SEC.

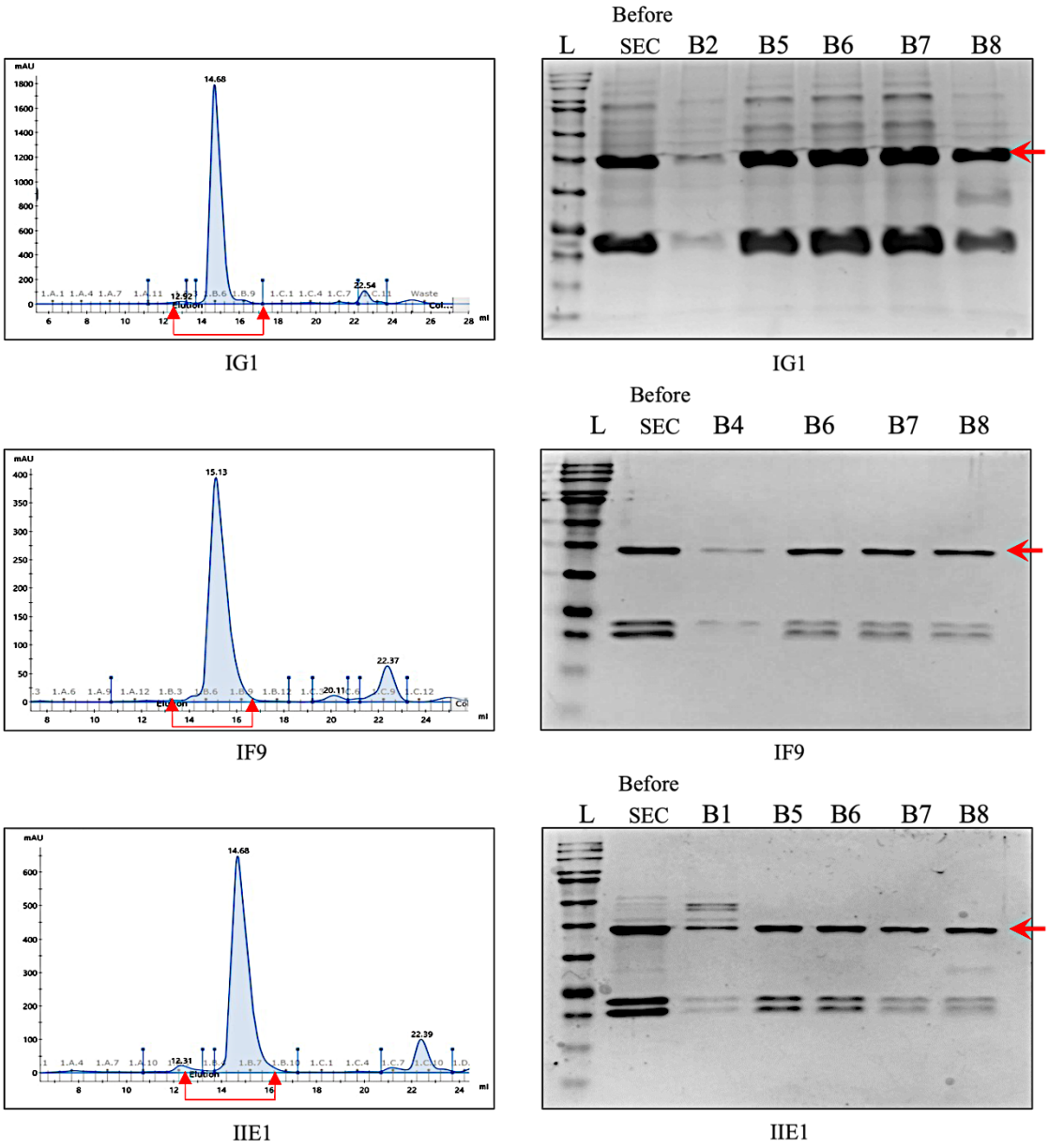

Figure 4. 8: Size exclusion chromatography of selected nanobodies.

Size exclusion chromatograms of nanobodies IG1, IF9, and IIE1 are shown on the left panel. A superdex 200 Increase 10/300 GL column was used with an AKTA Pure system (Cytiva). The blue graph displays absorbance at 280 nm. The main peak elutes at ~15 ml with only minor contaminants. Fractions enclosed between the red arrows were analyzed on 14% coomassie-stained SDS-PAGE shown on the right panel. Red arrows indicate purified nanobodies with an expected band size of ~ 41 kDa.

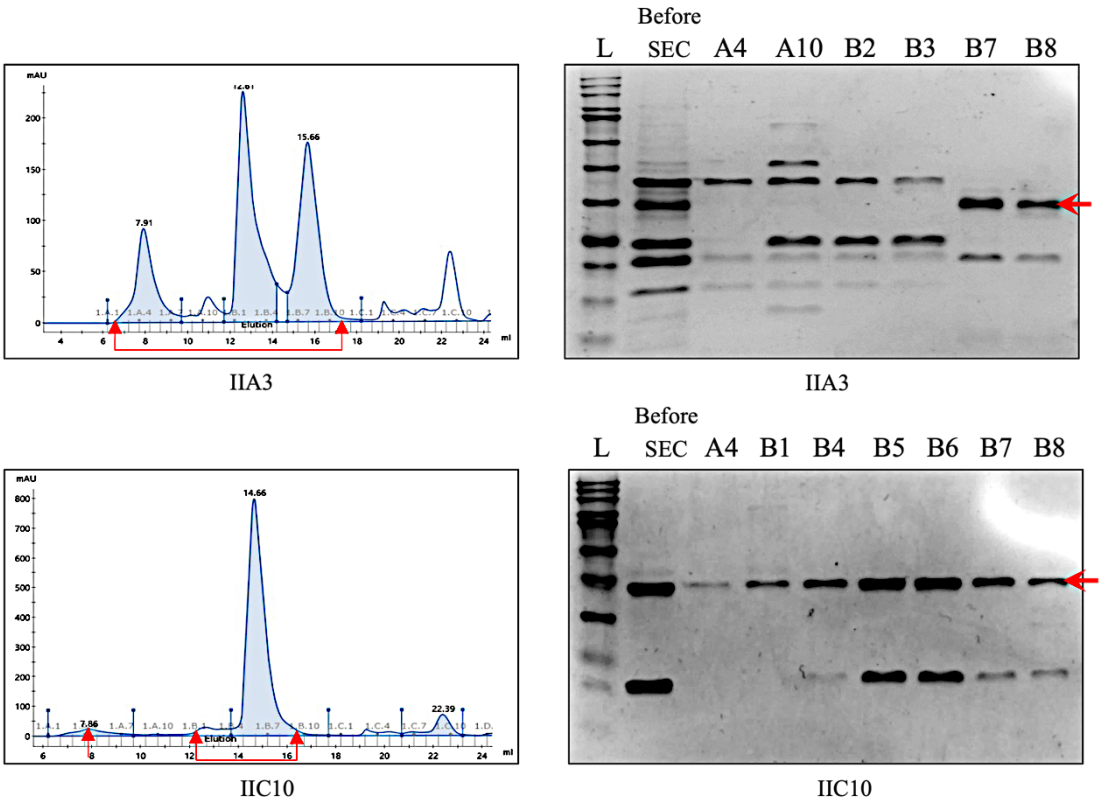

Figure 4.8 (continued): Size exclusion chromatography of selected nanobodies.

Size exclusion chromatograms of nanobodies IIA3, and IIC10 are shown on the left panel. A superdex 200 Increase 10/300 GL column was used with AKTA Pure system (Cytiva). The blue graph absorbance at 280 nm. The main peak elutes at ~15 ml with only minor contaminants. Fractions enclosed between red arrow were analyzed on 14% coomassie-stained SDS-PAGE shown on the right panel. Red arrows indicate purified nanobodies with expected band size of ~ 41 kDa.

4.2.1.2. Solitary Nanobody Production

Selected nanobody clones (IG1, IF9, IIA3, IIC10, IIE1) were also produced as solitary nanobodies without the mCherry moiety for subsequent experiments. For this, the selected five clones were cloned into the pET 28a (+) bacterial expression plasmid o obtain their N terminus His-tagged versions which were then transformed into *E. coli* BL21 DE3 SOX expression strain for cytoplasmic expression. Single colonies of transformed bacteria were grown in 1 L culture and cells were harvested and lysed by sonication. A HisPur Cobalt Resin column was used for affinity chromatography using an AKTA pure chromatography system

(Cytiva) and yields were determined by measuring the absorbance at 280 nm. Monodispersity of purified nanobodies was confirmed by size-exclusion chromatography. We used a Superdex 200 Increase 10/300 GL column connected to an AKTA pure chromatography system (Cytiva). Fractions from affinity and size exclusion chromatography were analyzed on a 10% coomassie-stained polyacrylamide gels.

Affinity chromatography of nanobodies IF9, IG1, and IIE2 was successful, and yields were in the range of 3-7 mg/ml (table 4.2.); however, concentrations of IIA3 and IIC10 were drastically low. When compared to other clones, these two clones also had a lower concentration when expressed as fusions to mCherry (refer to table 4.1.) This suggests a possible toxic effect of these proteins on bacterial cells. Elution with gradient concentration of imidazole of successfully purified nanobodies (IF9, IG1, and IIE2) showed single peaks in affinity chromatograms. Size exclusion chromatograms of the same nanobodies showed single peaks relevant to the nanobodies' molecular mass (~ 15 kDa) with reference to peaks of calibration runs that were performed previously for the column that was used (Figure 4.9 left panel). SDS–PAGE analysis of fractions collected from affinity and size exclusion chromatography showed single bands corresponding to the size of nanobodies, indicating a high level of purity (Figure 4.9 right panel).

	IG1	IF9	IIE1
Concentration mg/ml	5.76	0.80	3.42

Table 4. 2: Concentrations of purified solitary nanobodies.

Protein concentration measured at 280 nm after affinity chromatography for each purified recombinant nanobody. Elution fractions were combined, and total concentration was measured.

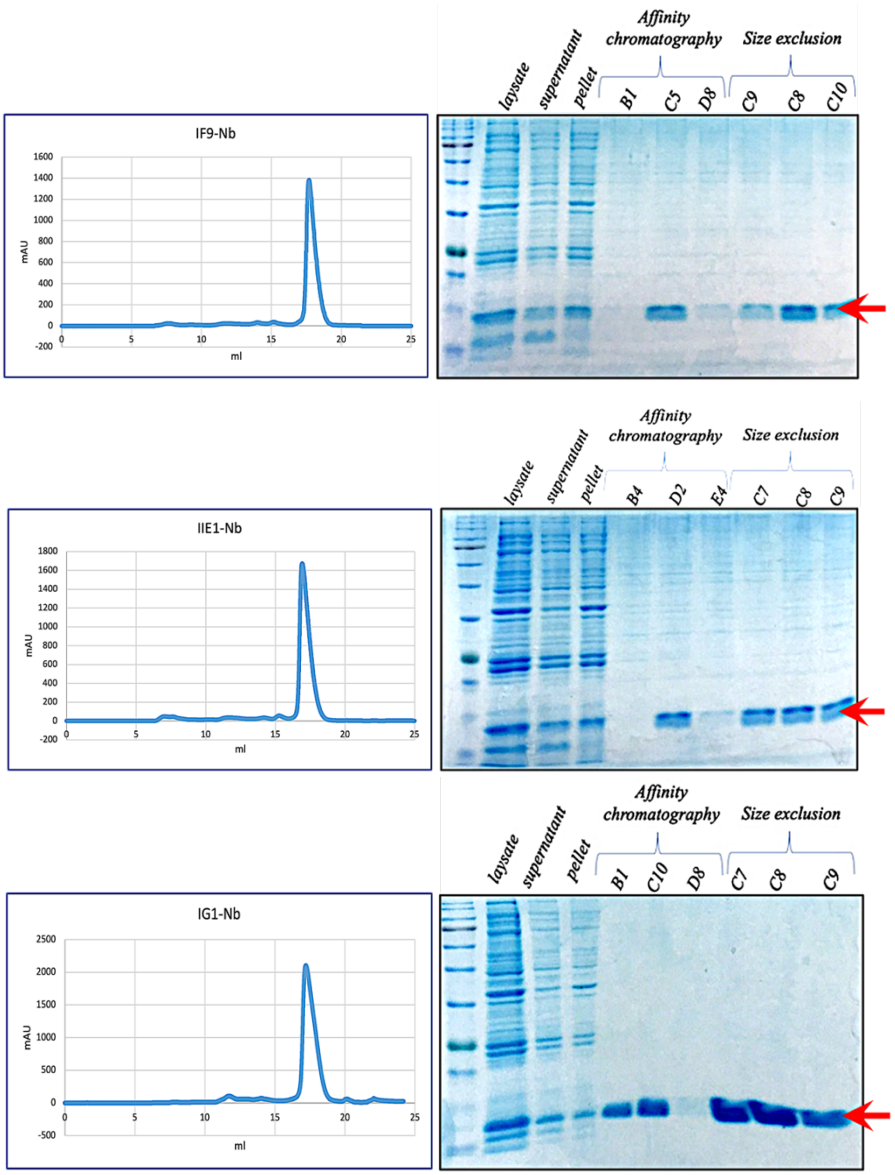

Figure 4. 9: Purification of solitary nanobodies.

Size exclusion chromatograms of nanobodies IF9, IG1, and IIE1 are shown on the left panel. Superdex 200 Increase 10/300 GL column was used with an AKTA Pure system (Cytiva). The blue graph displays absorbance at 280 nm, which corresponds to the nanobody peak. The main peak elutes at ~17 ml with almost no contaminants. Fractions from affinity and size exclusion chromatography were analyzed on 10% coomassie-stained SDS-PAGE shown on the right panel. Red arrows indicate purified nanobodies with an expected band size of ~ 15 kDa.

4.2.2. Analysis of Binding

4.2.2.1. SEC Co- Elution

Characterization of binding specificity and affinity was first performed using a SEC co-elution experiment in order to determine the possibility of complex formation between nanobodies and different BTB domains. For this experiment, we used solitary purified nanobodies IF9, IG1, and IIE1. Purified proteins of mPATZ1-BTB, zfPATZ1-BTB, and PATZ2-BTB were taken from lab stocks. The mPATZ1-BTB protein was incubated separately with different nanobodies and subsequently the mixture was analyzed in a Superdex 200 5/150 GL analytical size exclusion column connected to an AKTA Pure chromatography system (Cytiva). As a control, both proteins were also run individually on the same column. To demonstrate specificity of binding, all selected nanobodies against mPATZ1-BTB domain were also analyzed for complex formation with the PATZ2-BTB and zfPATZ1-BTB domains.

In this experiment, peaks corresponding to the size of all BTB domain homodimers (~38 kDa) were obtained. Similarly, peaks corresponding to the size and nanobodies (~15 kDa) were also obtained. Complex formation after incubation of nanobodies with BTB domains was then clearly demonstrated by a shift of the BTB domain peak to a lower retention volume. The increased absorbance of this peak was also associated with a decrease or total loss in absorbance of the nanobody peak. The nanobodies IF9 and IIE1 showed a clear tendency towards complex formation with the mPATZ1-BTB domain, while IG1 demonstrated a slight decrease in absorbance intensity of the nanobody peak without any effect on the BTB domain peak. Specificity of binding to mPATZ1-BTB domain was clearly observed by weaker complex formation after incubation of nanobodies with PATZ2-BTB domain. Complex formation of nanobodies IF9 and IIE1 with zfPATZ1-BTB was less pronounced than with mPATZ1-BTB. This is clearly visible when comparing the level of decrease in the nanobody peak and the shift of the BTB domain peak. Interestingly, IG1 was

the only nanobody which totally failed to form a complex with zfPATZ1-BTB, indicating specificity of IG1 nanobody towards mPATZ1-BTB (Figure 4.10).

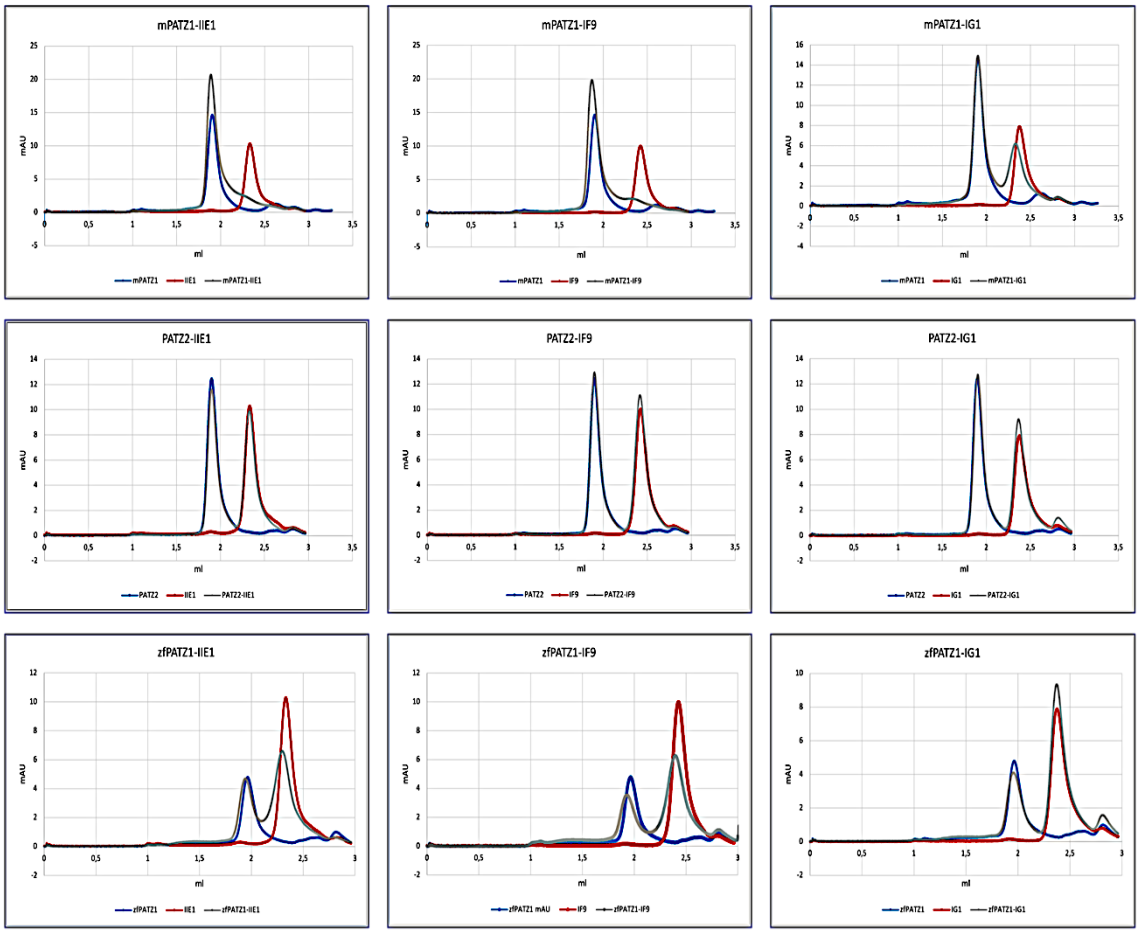

Figure 4. 10: SEC analysis of BTB-Nanobody complex.

BTB-nanobody complex formation was assessed using a SD 200-5/150 GL analytical size exclusion column connected to an AKTA pure chromatography system (Cytiva). Blue line: chromatogram of BTB domains, red line: chromatogram of nanobodies, grey line: chromatogram of BTB-Nb complex. Peaks at 1.9 ml represent the unbound BTB/BTB-nanobody complex, while peaks at 2.4 ml represent unbound nanobodies. Top panel represent profiles of the binding analysis of IIE1, IF9, and IG1 nanobodies against mPATZ1-BTB domain, middle panel display the same experiments but using the PATZ2-BTB domain, while bottom panel display the results against zfPATZ1-BTB domain.

4.2.2.2. Competition Assay of Nanobodies

The same assay that was described in section (4.2.2.1) was used to assess the binding of nanobodies to different binding sites on mPATZ1- BTB by using nanobodies of different molecular sizes. For this, large molecular size nanobodies (fused to mCherry tag ~ 41 kDa), and a small molecular size nanobodies (without the mCherry tag ~ 15 kDa) were both incubated with mPATZ1- BTB (~38 kDa) at the same time. Binding to different sites was then clearly demonstrated by formation of a single peak representing the three bound proteins, associated with loss of small and large nanobody peaks. The nanobodies IF9 and IG1 demonstrated formation of a single peak when incubated together with PATZ1-BTB indicating binding to different binding sites. On the other hand, the IIE1nanobody seems to compete with the binding of IF9 and IG1 nanobodies. This was demonstrated by the formation of two peaks (Figure 4.11).

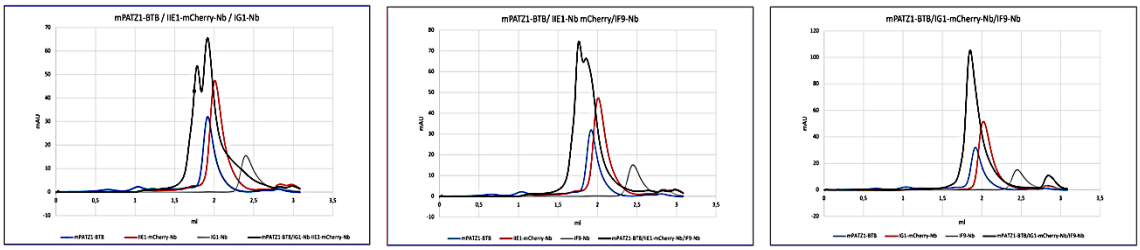

Figure 4. 11: Competition assay of nanobodies.

Competition between nanobodies to bind mPATZ1-BTB was assessed using a SD 200-5/150 GL analytical size exclusion column connected to an AKTA pure chromatography system (Cytiva). Blue line: chromatogram of BTB domains, red line: chromatogram of large nanobodies (fused to mCherry tag), grey line: chromatogram of small nanobodies (without mCherry tag), black line: chromatogram of BTB-nanobodies complex. Peaks at 2.4 ml contain unbound small nanobodies, peaks at 2 ml contain unbound large nanobodies, peaks at 1.9 ml contain the mPATZ1-BTB/ mPATZ1-BTB-small nanobodies complex, peaks at 1.7 ml contain mPATZ1-BTB- large nanobodies complex.

4.2.2.3. Measuring Binding Affinity with Surface Plasmon Resonance

For this experiment, we also used solitary, purified IF9, IG1, and IIE1 nanobodies and purified proteins of mPATZ1-BTB, zfPATZ1-BTB, and PATZ2-BTB from lab stocks. To match our experimental setup, His-tag removal from mPATZ1-BTB, zfPATZ1-BTB, and PATZ2-BTB protein was first performed using 3C protease. For confirmation of efficient His tag removal, samples from cleaved and un-cleaved proteins were loaded on calibrated Superdex 200 5/150 GL size exclusion analytical column applied to AKTA pure chromatography system (Cytiva). Chromatograms of these samples showed a clear shift of cleaved sample towards higher retention volumes, indicating smaller size and efficient removal of His-tag (Figure 4.12).

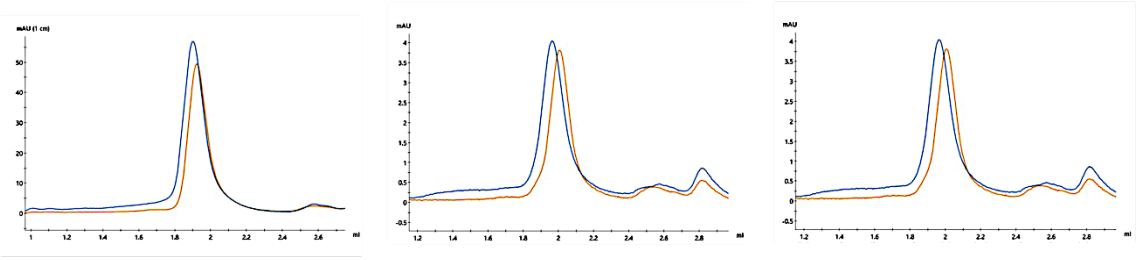

Figure 4. 12: His-tag cleavage of BTB domains.

Size exclusion chromatographs of mPATZ1-BTB, zfPATZ1-BTB, and PATZ2-BTB. A Superdex 200 5/150 GL size exclusion analytical column was connected to an AKTA pure chromatography system (Cytiva). The blue and orange graphs represent absorbance at 280 nm for cleaved and un-cleaved proteins, respectively.

Binding affinities were determined using surface plasmon resonance with CM5 chips on a BIACore T200 system. The His tagged nanobodies were immobilized on the chip using anti-his antibody. Our experimental setup was based on having anti-his antibody only on the first flow cell as a reference and the same antibody followed by his-tagged nanobodies on the next flow cell. Single cycle kinetics were recorded with the flow of mPATZ1 BTB, zfPATZ1-BTB, or PATZ2-BTB proteins with removed His-tags at different concentrations

(6,18,54,162 nM). Replicates of two were used to calculate the experimental standard errors. Sensorgrams were corrected using reference cell and blank buffer cycles and the data was fitted to a 1:1 binding model. The affinity constant (K_D) was calculated from the ratio of k_d/k_a. PATZ2- BTB and zfPATZ1-BTB domains were used for comparison.

All three nanobodies showed high binding affinity towards mPATZ1 BTB domain with K_D values in the nanomolar range. A sequential increase in response units (RU) with increased concentration can be observed. Remarkably, the sensorgram of IIE1 nanobody showed a very rapid on rate with high Chi^2 values (more than 10% of R_{max}); therefore, the K_D value could not be determined accurately. Such sensorgrams could be explained by the effect of differences in liquid composition between the running buffer and the samples, which is seen as a change in surface refractive index. This kind of effect is known as bulk effect. However, since all samples were run in the same buffers this is unlikely to be the cause. More reasonably, such sensorgrams might be suggestive of a rapid interaction event between ligand and analyte. As for the control, interactions with PATZ2-BTB domain were weak and could not be fitted into any binding model. As for zfPATZ1-BTB, IF9 and IIE showed binding patterns close to those seen in mPATZ1-BTB. Interestingly, only IG1 nanobody did not show any binding affinity towards zfPATZ1-BTB, indicating specificity of this nanobody towards the mPATZ1-BTB domain and confirming our SEC co-elution results (Figure 4.13). Resulting on and off rates and dissociation constants are summarized in (Table 4.3.).

Interestingly, during running of the first concentration of all analytes over the IG1 nanobody, a drop in the binding response was always observed. This might be due to binding of this nanobody to the reference flow-cell. Subtracting the signal of this cell from the active binding-cell, results in a sensorgram with a negative response as seen in (Figure 4.13). Nanobody binding to the reference cell might be a carry-over from the immediate previous nanobody injection during immobilization of this nanobody on the active cell.

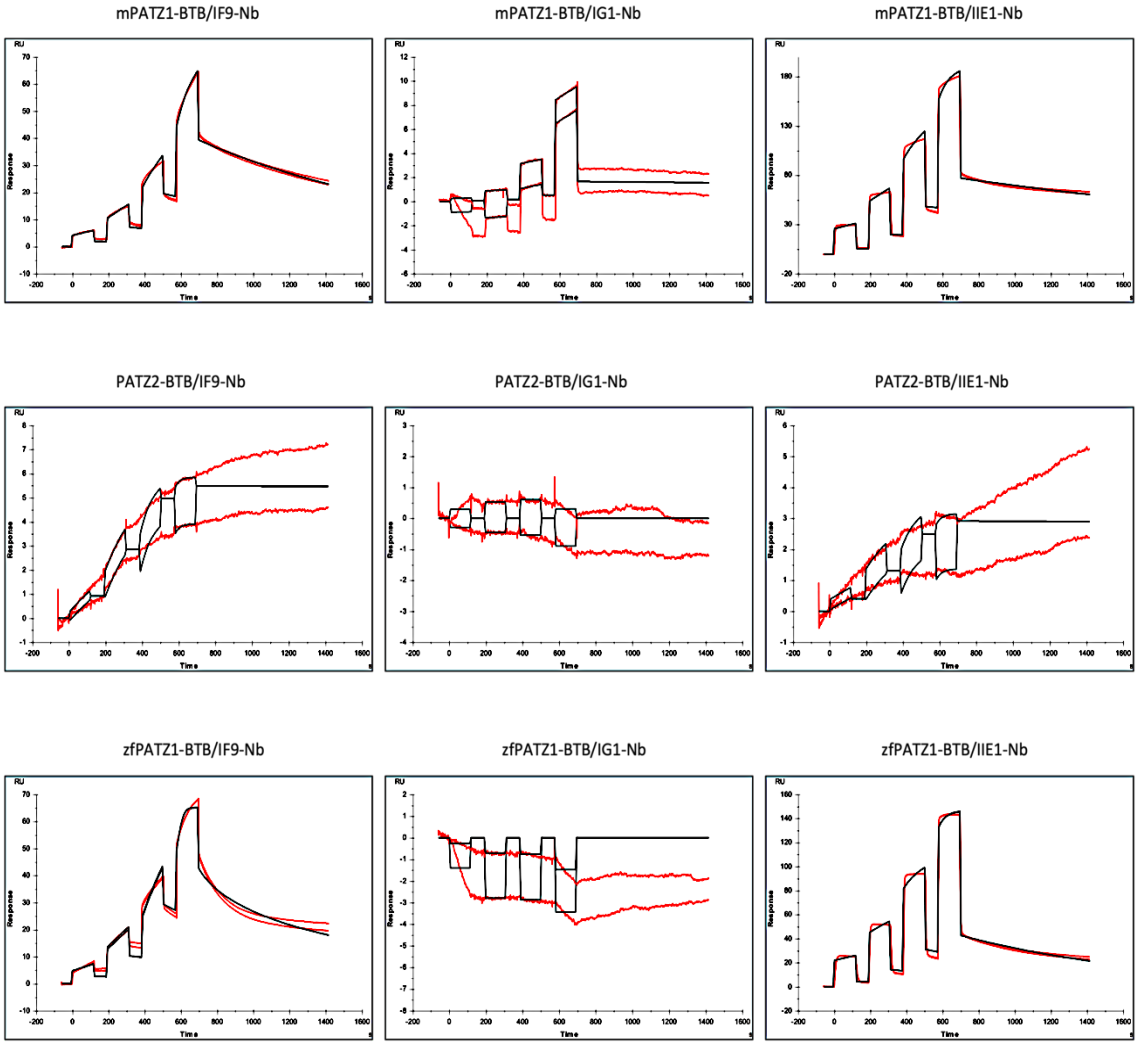

Figure 4. 13: Surface plasmon resonance analyses of nanobody affinities to different BTB domains.

Different concentrations of purified BTB domains (6,18,54,162 nM) were injected across a surface coated with purified nanobodies (IF9, IG1, and IIE1). Sensorgrams with blank buffer injections were subtracted. The top panels represent sensorgrams of single cycle kinetics for nanobodies IF9, IG1, and IIE1 against mPATZ1-BTB domain. The middle panels display the same experiments but using the PATZ2-BTB domain, while bottom panels display the results using zfPATZ1-BTB domain. Sequential peaks represent response units (RU) relative to the concentration of injected BTB domains. Experimental curves are plotted in black; red lines denote the corresponding 1:1 interaction model fit to the experimental data.

Table 4. 3: Single cycle kinetic constants of the selected VHH binders.

Association rate K_{on} (1/Ms), disassociation rate K_{off} (1/s) Affinity (K_D), Rmax, and Chi^2 values are shown for selected VHH clones (IF9, IG1, IIE1) against mPATZ1-BTB, zfPATZ1-BTB, and PATZ2-BTB antigens.

Antigen	VHH clone	K_{on} (1/Ms)	K_{off} (1/s)	K_D (nM)	R_{max}	Chi^2
mPATZ1-BTB	IF9	5.40 e^{+4}	7.46 e^{-4}	13	53.46	0.95
	IG1	406.4	9.27 e^{-5}	56	144.80	0.96
	IIE1	9.57 e^{+4}	3.42 e^{-4}	3.5	84.22	21.40
zfPATZ1-BTB	IF9	5.27 e^{+5}	0.00	6.2	44.61	4.69
	IG1	8.44 e^{+5}	0.54	650	0.04	4.16
	IIE1	1.45 e^{+5}	9.61 e^{-4}	6.6	45.49	29.40
PATZ2-BTB	IF9	2.54 e^{+5}	1.50 e^{-6}	-	5.48	0.85
	IG1	5.75 e^{+5}	0.03	-	0.00	0.39
	IIE1	2.06 e^{+5}	8.29 e^{-6}	-	2.91	0.93

4.2.2.4. Fluorescent Two Hybrid (F2H) Assay

For assessment of intracellular binding of nanobodies to the PATZ1-BTB domain, recombinant nanobody-mCherry sequences (IF9, IG1, IIA3, IIC10, IIE1) were cloned from pET mCherry plasmids into pcDNA 3.1/ myc-His (-) B mammalian expression vector. Other plasmids used for this experiment were taken from lab stocks. We used BHK-2 cells genetically modified for use in F2H assays. In this system, nanobodies were overexpressed intracellularly as mCherry fusions, while PATZ1-BTB domain was overexpressed as a GFP fusion protein. Intracellular localization is achieved by co-transfection with a GBP-LacI plasmid which enabled the binding of GFP-tagged BTB domains to specific LacI foci in the nucleus. Intracellular binding of nanobodies to PATZ1-BTB domain is evaluated by assessing co-localization of GFP and mCherry fluorescent spots in live cell microscopy (ZEISS Axio Observer Z1). To demonstrate specificity of binding, all selected nanobodies

were also co-transfected with the PATZ2-BTB. Figure 4.14 provides a schematic illustration of this assay.

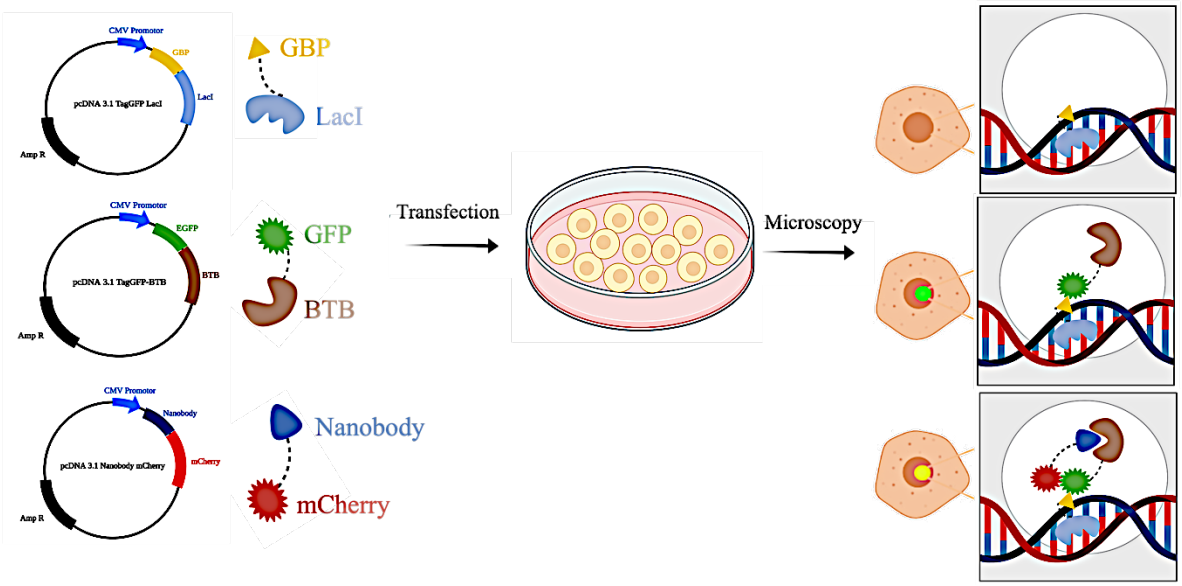

Figure 4. 14: Schematic representation of the F2H assay.

The left side panel represent the bait and prey expression vectors coding for GFP labeled BTB domain and mCherry labeled nanobodies respectively, in addition to the LacI-BGP protein. The right-side panel demonstrates the LacI domain of the bait protein mediating the binding of the GFP labeled BTB domain to the integrated lac operator array in the nucleus, which is visible as a green fluorescent spot in the nuclei of the transfected cells. In case of interaction with the nanobody protein, the prey is enriched at the same spot resulting in co-localization of green and red fluorescent spots.

In this system, nanobodies IG1 and IIE1 showed colocalization with PATZ1-BTB domain. This colocalization was not observed with the other nanobodies (IF9, IIA3, IIC10) (Figure 4.15). Quantification of this co-localization was performed by counting cells showing nuclear green foci in the green channel. In these cells, co-localization of red foci in the red channel was scored 1 while its absence was scored 0. Total positive and negative percentages were then calculated and demonstrated in Figure 4.16.

Previously, in SPR, nanobody IF9 had demonstrated a high affinity for PATZ1-BTB. SEC co-elution experiments also confirmed this affinity. However, these are *in-vitro*

experiments, and the intracellular environment is a more complex environment with more effector and interacting proteins, so protein behavior is expected to differ, which could explain the lack of IF9-PATZ1-BTB interactions. Also, the presence of GFP tag with mPATZ1-BTB protein in this experiment might be masking the binding epitope of the IF9 nanobody. None of the nanobodies colocalized with PATZ2-BTB, which is in line with our previous results and confirms the specificity of these nanobodies towards PATZ1-BTB domain (Figure 4.17).

Failure of some nanobodies to co-localize with the PATZ1-BTB domain confirms that the successful co-localization of the others is confined to nanobodies and PATZ1-BTB domain rather than their fluorescent moieties or LacI-GBP. To corroborate this, we performed control experiments with LacI-GBP, PATZ2-BTB GFP, or mCherry plasmids to exclude that co-localization is due to LacI-GBP, GFP, or mCherry, respectively (Figure 4.17, 4.18, 4.19).

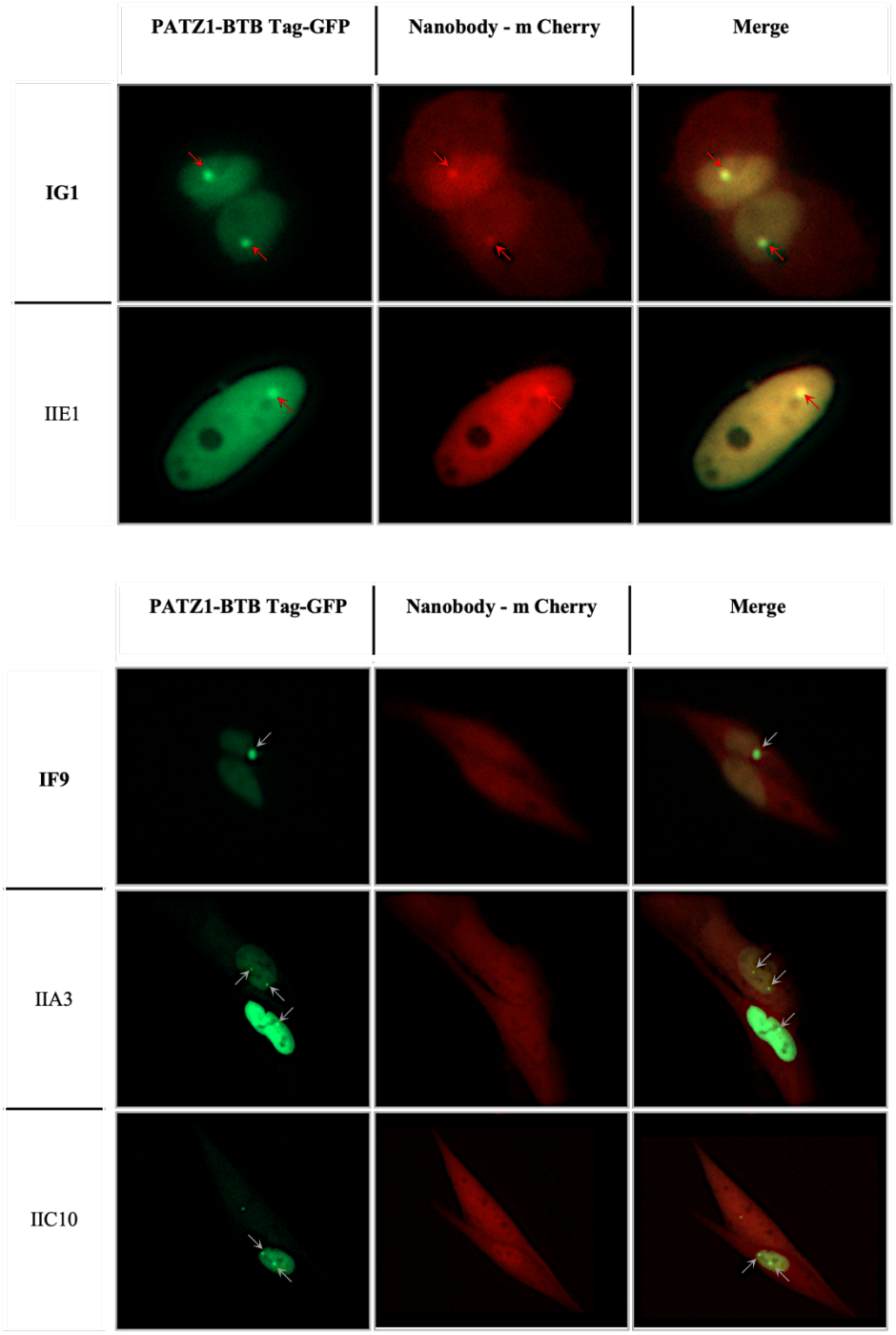

Figure 4. 15: Nanobody interaction with PATZ1-BTB in F2H assay.

Representative images of BHK-2 cells co-transfected with the respective expression vectors shown at the top panel. Arrows show specific fluorescent foci. Positive co-localization was observed for PATZ1-BTB with nanobodies IG1 and IIE1 (top group), while absent for IF9, IIA3, and IIC10 (bottom group).

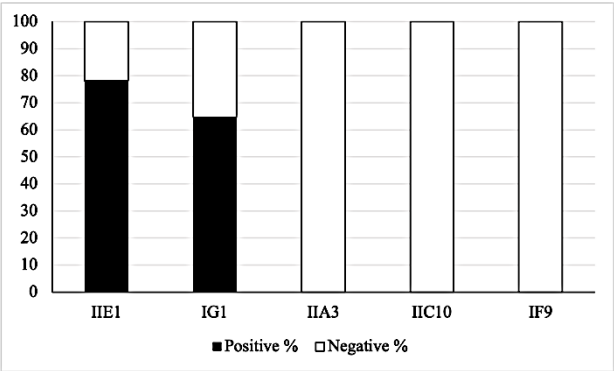

Figure 4. 16: Percentage of positive nanobody interactions in F2H assay.

Cells showing nuclear green foci in the green channel were counted. In these cells, co-localization of red foci in the red channel was scored 1 while its absence was scored 0. Total positive and negative percentages were then calculated. Black: positive co-localization, White: no colocalization of green and red foci.

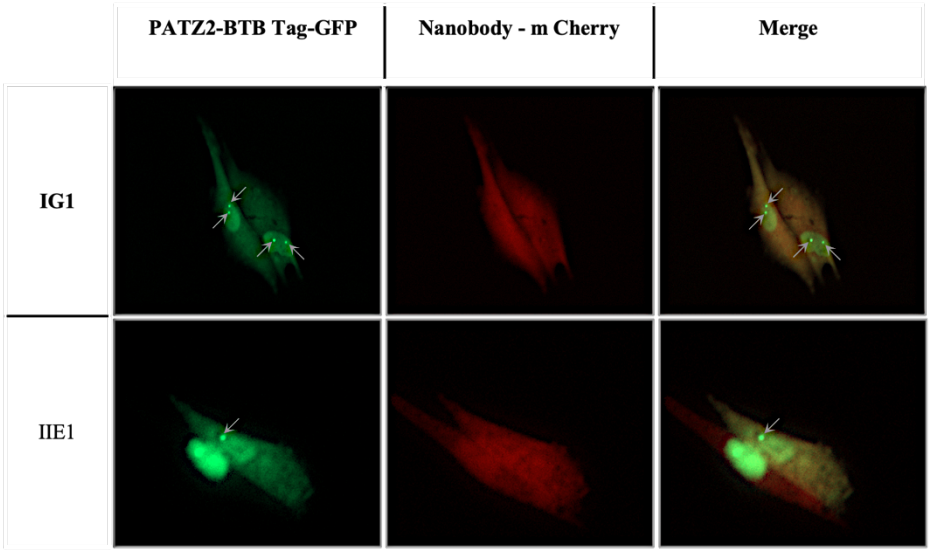

Figure 4. 17: Negative nanobody interaction with PATZ2-BTB in F2H assay.

Representative images of BHK-2 cells co-transfected with the respective expression vectors shown at the top panel. Arrows show specific fluorescent foci. Nanobodies IG1 and IIE1 failed to co-localize with PATZ2-BTB.

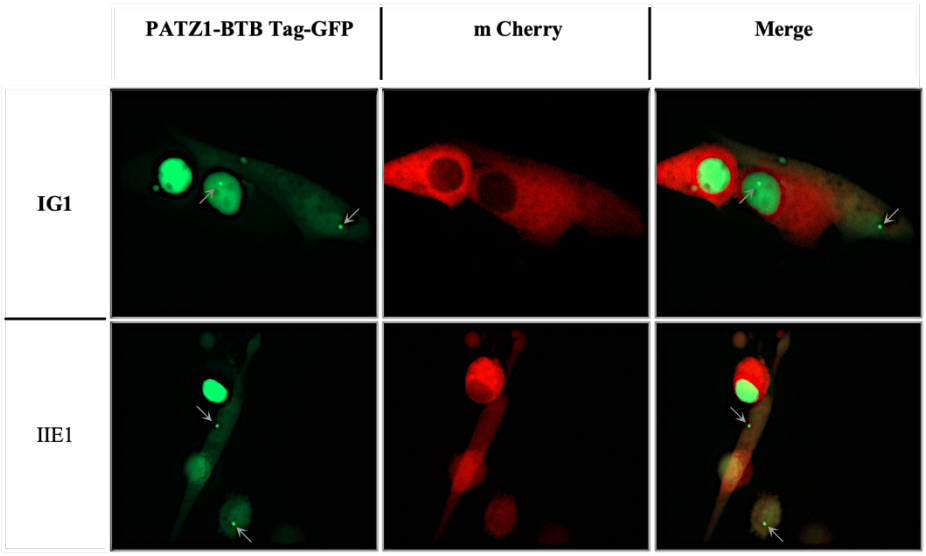

Figure 4. 18: Negative nanobody interactions with mCherry-tag in F2H assay.

Representative images of BHK-2 cells co-transfected with the respective expression vectors shown at the top panel. Arrows show specific fluorescent foci. Fluorescent mCherry protein failed to co-localize with PATZ1-BTB.

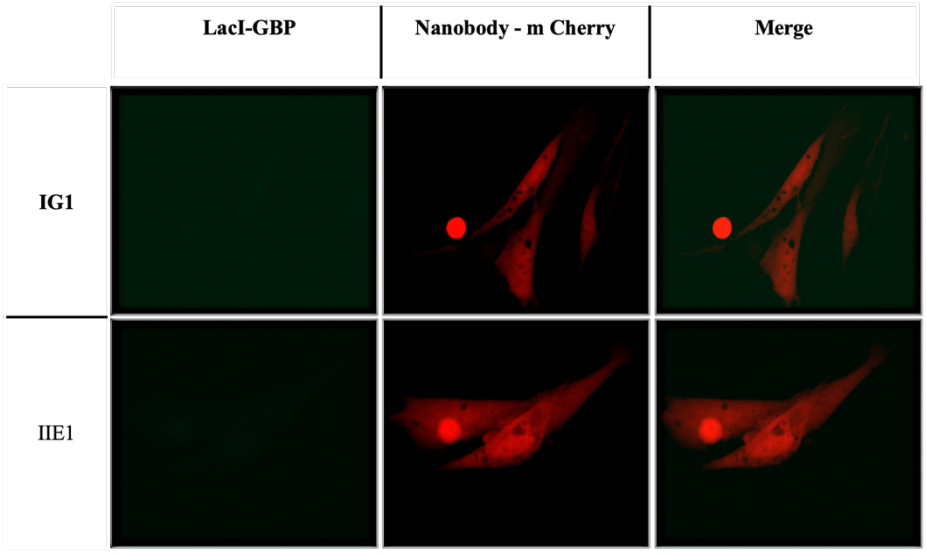

Figure 4. 19: Negative nanobody interactions with Lac-GBP in F2H assay.

Representative images of BHK-2 cells co-transfected with the respective expression vectors shown at the top panel. No fluorescent foci were formed confirming that nanobodies IG1 and IIE1 failed to co-localize with LacI-GBP in the absence of PATZ1-BTB tag-GFP.

4.3. Functionality Assays of Selected Nanobodies

4.3.1. Generation of Nanobody Stable Cell Lines

Human colon cancer cells (HCT116) stably expressing nanobodies (IIE1, IF9, IG1) were generated by PEI transfection of these cells with nanobody- mCherry constructs cloned into pcDNA 3.1/ myc-His (-) B. Cells were then subjected to neomycin selection for 10 days. Expression of nanobodies was assessed with microscopy and fluorescence-activated cell sorting (FACS) was used for sorting cells that are stably expressing nanobodies. HCT116 cells stably expressing IG1 and IF9 mCherry nanobodies were successfully generated (Figure 4.20). However, the expression of IIE1 mCherry nanobody was strikingly low, therefore we decided to continue with IG1 and IF9 nanobody cell lines for further experiments.

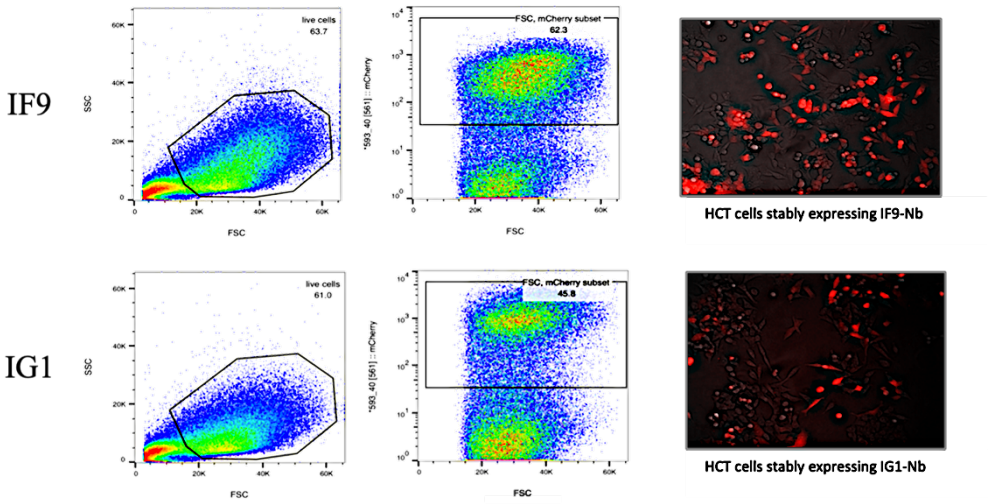

Figure 4. 20: Generation of stable nanobody cell lines.

The right panel shows fluorescent microscope images of HCT116 cells stably expressing IF9 mCherry Nb (Top) and IG1 mCherry Nb (bottom) The Left panel shows FACS profiles after sorting and culturing these cells.

4.3.2. Effect of Nanobodies on The Transcriptional Activity of PATZ1

Based on previous lab work, we found that the PATZ1 transcription factor has a significant effect on two target genes, namely cystathionine gamma-lyase (CTH), and ETS translocation variant 1 (ETV1). The CTH gene encodes for an enzyme that plays an important role in hydrogen sulfide synthesis, a major regulator of cell signaling. On the other hand, the ETV1 gene codes for a transcription factor that belongs to the ETS (E twenty-six) family and regulates a number of target genes that modulate significant biological processes such cell growth, migration, proliferation, and differentiation. Total RNA sequencing as well as real-time quantitative PCR (RT-qPCR) revealed up-regulation of the CTH gene, and down-regulation of the ETV1 gene, in HCT116 Patz1-/- cells as compared to WT cells. Therefore, we investigated the changes in the expression of these two targets in our generated stable nanobody cell lines.

HCT cells stably expressing IF9 and IG1 mCherry nanobodies were used for total RNA isolation using and cDNA synthesized. Specific primers were designed for the evaluation of gene expression using qPCR. Two biological samples were used in triplicates for each qPCR experiment. The mean value of gene expression was calculated relative to un-transfected cells. An unpaired t-test was performed to assess significance of gene expression fold change. In comparison to control conditions, intracellular stable expression of IF9 and IG1 nanobodies resulted in significant increases and decreases in mRNA levels of ETV1 and CTH target genes, respectively (Figure 4.21)

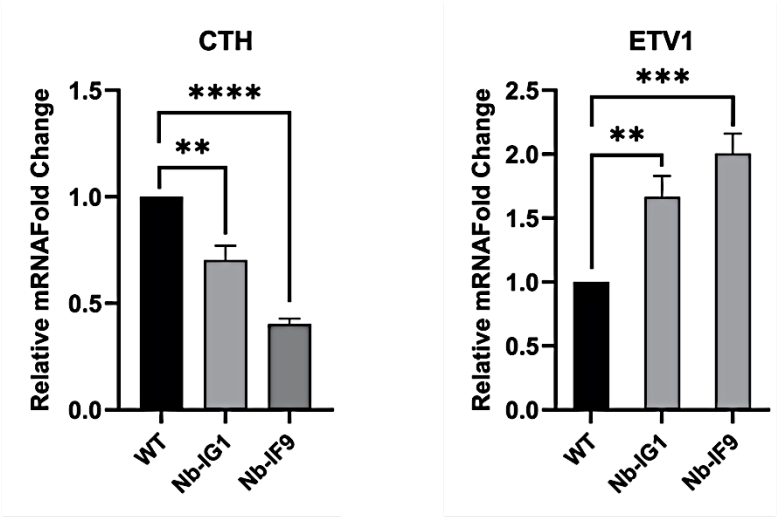

Figure 4. 21: Effect of nanobodies on the expression level on PATZ1 target genes.

HCT116 cells stably expressing IF9 and IG1 mCherry nanobodies were used to assess the level of expression of CTH and ETV1 genes using real-time qPCR. Expression levels of CTH and ETV1 genes is shown in grey in nanobody stably expressing cells while in black in WT cells. An unpaired t-test was performed, P value = ** < 0.01, *** < 0.001, **** < 0.0001).

5. DISCUSSION

In this study we screened a pre-immune phage display nanobody library for nanobodies targeting the PATZ1-BTB domain. A total of 41 initial nanobody hits were selected and sequence analysis refined the number to 30 clones with distinct sequences. After characterizing these clones, we identified three nanobodies (IIE1, IF9, IG1) as specific PATZ1-BTB targeting nanobodies. These three nanobodies bind PATZ1-BTB in high affinity whether they are *in-vitro* or intracellular. Functional assessment of these nanobodies intracellularly revealed significant effect on PATZ1 target genes. Our data presents these nanobodies as potential modulators of PATZ1 function that requires further investigation.

Selecting PATZ1 as a target in this study was based on the known significance of this transcription factor and the crucial role that it plays whether in healthy or disease conditions. Furthermore, our laboratory's extensive work on PATZ1 over the years, has increased our knowledge about the importance of this transcription factor and its potential oncogenic role. This role is mainly detected in colon cancer, sarcomas, and gliomas. The BTB domain of PATZ1 is a primary candidate to play this oncogenic role as it is responsible for oligomerization, recruitment of corepressors, and other protein-protein interaction. For example, the BTB domain was found to recruit co-repressor proteins such as SMRT and NCOR. It was also found to oligomerization in a multiplicity of functional combination of homo or heterodimers. Recently the BTB domain of PATZ1 was shown to interact with the BTB domain of PATZ2, which is another member of the same ZBTB transcription factor family [185]. Based on this accumulated knowledge on the PATZ1-BTB domain we thought that targeting this domain with selective nanobodies could increase our understanding of the

precise molecular mechanisms underlying its functional activities and provide a beginning point for the generation of nanobody-based modulators, tuning its transcriptional activity.

Two separate rounds of bio-panning were carried out in this study to retrieve potential PATZ1-BTB selective nanobodies from a naive nanobody library. For this, we used lab stocks of purified mPATZ1 protein. The human and the mouse PATZ1-BTB domain sequences are 98.9% identical and diverge at only one residue (T91A). The isolated nanobodies against mPATZ1-BTB were therefore expected to effectively target human PATZ1-BTB. The first bio-panning had a preclearing round of negative selection using MIZ-BTB and PATZ2-BTB antigens while the second bio-panning lacked this step to ensure that all possible PATZ1-BTB binders were selected. PATZ2 and MIZ1 are members of the same BTB-ZF family, and their BTB domains show high structural similarity to PATZ1-BTB. Therefore, using them for negative selection is expected to increase the PATZ1 specificity of the selected nanobodies.

In terms of quantity, the number of clones that were selected from the elementary ELISA screening of the first and second bio-panning was 41 and 27 respectively. These numbers were reduced to 5 and 3 respectively after the confirmatory ELISA of the PATZ1-BTB specific clones. Furthermore, two of our final nanobodies (IF9, IG1) were from the first bio-panning and only one (IIE1) was from the second bio-panning. These numbers indicate that the chances of retrieving more potential candidates did not actually increase by bypassing the preclearing steps of negative selection. In terms of quality, subjecting the library to preclearing steps might increase the specificity of the retrieved nanobodies, but it has no direct impact on the quality of selected nanobodies. Affinity of binding for example, can be enhanced by applying more stringent washing and eluting steps[186] rather than preclearing steps. Our results show that the nanobody IF9 which was selected from the first bio-panning had a four folds higher affinity then the IG1nanobody selected from the same bio-panning (13nM and 56 nM respectively), while IIE1 showed a better affinity (3.5 nM) regardless of being selected without a preclearing step.

The selected clones were first expressed and purified in small scale by affinity chromatography. Among the selected 37 nanobody clones, 28 clones were successfully expressed. Three of these were produced at high concentration (IIE1, IF9, IG1) in our large-scale expression system. Nine clones could not be purified (IID2, IC9, IC11, IIE12, IIF2, IIF9, IIF11, IIG, and IG6). Two of these clones (IG6, IID2) had amber stop codons (TAG) and therefore were anticipated not to be expressed. These clones were selected by screening a phage display library where nanobodies were expressed as part of the phage coating protein. For such expression, phages were infected into the TG1 strain of *E.coli* bacterial cells. This strain is an amber suppressor bacterial strains expressing tRNA that allows translation to read through the amber stop codon. Therefore, when such clones are expressed in different bacterial systems that lack this tRNA such as BL21, that were used for cytoplasmic expression of the selected nanobodies, these amber stop codons are not suppressed, and translation is terminated. Nevertheless, several other clones (IA3, IH5, IH6, IID10, and IIC2) were unexpectedly produced despite having amber stop codons in their sequence. This could be explained by the presence of a second start codon or simply by the amber stop codon being a sequencing error. Failure of expression of other clones that had no amber stop codon (IC9, IC11, IIE12, IIF2, IIF9, IIF11, and IIG) might be due to formation of inclusion bodies which is a major problem associated high cytoplasmic expression levels. In such situations, using weaker promoters and low copy number plasmids, lowering growth temperature, and co-expression of anti-aggregation chaperones can increase the efficiency of expression[187]. Such optimizations were not carried out in this study since many other clones were sufficiently expressed, so we decided to proceed with them.

The *in-vitro* interaction between the selected nanobodies (IIE1, IF9, IG1) and PATZ1-BTB was assessed using SEC co-elution which is a reported method for such analysis [111,188,189]. In such experiments, complex formation is indicated by a shift towards lower retention volume with increased absorbance intensity upon binding as compared to unbound proteins. Due to a size estimation of 15 kDa for nanobodies, only a very small shift was detectable upon nanobody binding. However, the presence of an interaction event was inferred by the obvious increase of absorbance intensity for the PATZ1-BTB peak with the striking disappearance of the nanobody peak upon binding. This profile was clearly

demonstrated with IF9 and IIE1 nanobodies while less pronounced with IG1 nanobody suggesting a lower tendency towards complex formation with PATZ1-BTB. Our SPR results confirm these findings. The calculated affinity of IG1 nanobody towards mPATZ1-BTB was 56 nM as compared to higher affinities of IF9 and IIE1nanobodies (13 and 3.5 nM respectively).

The sequence of zfPATZ1-BTB domains is 69% identical to its mouse orthologues, however mice contain a core loop structure at A2/B3 that is likely an intrinsically disordered region and is thought to serve an unknown function [190]. Therefore, using zfPATZ1-BTB in SEC co-elution experiment we aimed to investigate for nanobodies specific to this central loop in the mPATZ1-BTB domain, thereby exploring more about its function. Only the IG1 nanobody demonstrated a clear negative binding to zfPATZ1-BTB suggesting its specificity towards mPATZ1-BTB. This was also confirmed by SPR analysis were only IG1 nanobody failed to demonstrate any affinity towards zfPATZ1-BTB, as compared to 6.2 and 6.6 nM affinities for IF9 and IIE1nanobodies respectively.

The PATZ2-BTB domain protein was used as negative control in these experiments. This is due to the fact that our phage display library was precleared from PATZ2-BTB binders during the nanobody selection stage therefore the demonstrated negative interaction of all nanobodies towards it in SEC co-elution or SPR analysis was anticipated.

Bivalent and bispecific nanobodies are common combinational forms of nanobodies that have great potential for many practical applications. Bivalent nanobodies are capable of recognizing the same epitope of two antigen molecules, the matter that was found to increase their binding affinity by the avidity effect [141,191] Such constructs are also useful when increased circulation time is a prerequisite due to the resultant increase in molecular size [150]. On the other hand, a bispecific nanobody is engineered to simultaneously recognize two different antigens. Such nanobodies have great potential in immune therapeutic applications as they can bridge immune cell antigens with target antigens [192]. Based on this understanding we aimed to assess whether our selected nanobodies (IIE1, IF9, IG1) bind to different sites on the mPATZ1-BTB protein. Non-competing epitopes would identify candidate nanobodies

that could be synthesized as bivalent or bispecific constructs for future applications. For this, two nanobodies of different molecular sizes were incubated at the same time with the mPATZ1- BTB and SEC was used to assess their competitive behavior. Formation of a single peak means binding to different binding site, which was the case for nanobodies IF9 and IG1, while formation of two peaks, in an elementary interpretation, reflects competitive tendency which was the case for IIE1 nanobody with IF9 and IG1. However, the evaluation of this experiment outcome is complicated by the dimeric nature of mPATZ1-BTB that creates more combinational possibilities of the competing nanobodies which cannot be distinguished by this method of analysis. The results of this experiment represent a starting point for assessing the possible synergistic functionalization of our nanobodies. More precise epitope mapping methods needs to be conducted to achieve this goal.

In this study, the F2H assay was utilized to demonstrate the intracellular interaction of nanobodies with the PATZ1-BTB domain. This assay is reported for assessing more than 50 different protein-protein interactions not only in static endpoint assays but also in living cells in real time [193,194]. A recent publication of our group demonstrated the utility of this method for screening eight pairs of BTB-containing proteins for homo and heterodimer formation [185]. Our results showed that two nanobodies (IIE1, IG1) positively interact with the PATZ1-BTB domain in this assay. However, in contrast to our previous FPLC and SPR results, where IF9 nanobody had interacted positively with PATZ1-BTB, this nanobody failed to show such interaction in F2H assay. This experiment is performed on BHK cells using mammalian expression vectors. Proteins expressed in such eukaryotic systems are exposed to their native cellular biomolecular environment and subjected to a variety of post-translational modifications, which may change their molecular dynamics and alter their interaction behavior. Such an environment is absent in mobile/stationary-phase-based systems such as FPLC and SPR, which may have resulted in this in vitro interaction. Moreover, the presence of the GFP tag in fusion with the PATZ1-BTB protein in this assay may have masked the targeted epitope by IF9-Nb.

To assess the effect of our nanobodies on the transcriptional activity of PATZ1, we generated new cell lines stably expressing our nanobodies (IF9, IG1). As compared to

transient transfection protocols, stable cell lines provide more reliable results by ensuring sustainable gene expression over prolonged periods of time. In this study, we used PEI chemical transfection to generate nanobody stable cell lines. This is a feasible and efficient method for the generation of stable cell lines that is reported in many studies [195–197]. In such methods, upon delivery, the plasmid DNA gets linearized in the nucleus by endo- and exonucleases. Nuclear ligases and recombination enzymes then aid the random integration of the delivered DNA into the host genome via nonhomologous recombination [198.] Stability of the delivered DNA is limited and often undergoes gradual loss in amount and in expression. Therefore, we tried to eliminate cells that had lost their plasmid by sustained antibiotic selection for 1 month before qPCR was performed.

Viral transduction is an alternative method for DNA delivery that is widely used due to its high transfection efficiency, however it requires more complicated protocols [199]. Despite being widely used, both viral and nonviral methods of DNA delivery have several drawbacks. Random integration makes the expression rate more dependent on the site of integration. Low expression is usually associated with integration into inactive chromatin sites[200]. Integrated genes are also often silenced upon long term cell culture unless directed to genomic safe harboring site [201]. Additionally, cells also tend to eliminate randomly inserted foreign genetic material that alter their genome integrity, therefore they are maintained under selection pressure for prolonged time periods which increases their chance of accumulating mutations [202]. Furthermore, the copy number of the integrated DNA can vary from cell to another, which creates a heterogeneous cell population. This requires single cell cloning to identify clones that uniformly express the target protein. Finally, the common use of strong promoters, such as the CMV promoter, often drives elevated expression levels beyond the physiological level [203]. Such problems are overcome with more efficient methods such as CRISPR/Cas9-mediated knock-in. This method ensures consistent and controllable expression of the target gene by integration into specific genomic loci however such methods are more complicated and time consuming [204].

The selection of CTH and ETV1 genes as proposed PATZ1 targets for functional assessment of our nanobodies was based on previous collected data by our group. Total RNA

sequencing of PATZ1 WT and KO MEFs and HCT116 was performed, and results identified these two genes as top differentially expressed target genes of PATZ1. The CTH gene was found to be up-regulated in HCT116 Patz1KO cells as compared to WT cells, while the ETV1 gene was found to be down-regulated [205].

The CTH gene encodes for an essential enzyme for hydrogen sulfide synthesis which was found to promote tumor growth through a variety of ways including promotion of angiogenesis, acceleration of cell cycle, and inhibition of anti-apoptosis [206]. In this regard, the CTH gene can be considered as a tumor promoter. This is consistent with the reported CTH-dependent enhancement of cell growth in breast cancer cells [207]and astrocytoma cells [208], and the upregulated expression of CTH in colon cancer initiating cells (CD133+)[209]. The fact that CTH expression in our HCT116 PATZ1 KO cells is upregulated suggests a tumor suppressor role of PATZ1 in this context. Our nanobodies, on the other hand, caused CTH downregulation. One explanation of this finding could be that PATZ1 might be controlled by a repression machinery that is potentially disrupted with our nanobodies (Figure 5.1).

On the other hand, the ETV1 gene encodes a transcription factor from the ETS (E twenty-six) family that controls a number of target genes influencing many important biological processes such proliferation, differentiation, cell growth, and migration. It is considered as a tumor promoter as it was found to be upregulated in many cancer types such prostate cancer, melanoma, and Ewing sarcoma, and gastrointestinal tumors [210,211]. ETV1down-regulation in our HCT116 PATZ1 knockout cells suggests that PATZ1 plays an oncogenic role in such context, whereas its up-regulation in response to our nanobodies can be explained by blockage of the proposed PATZ1 inhibitory machinery (Figure 5.2).

In this study, we generated potent nanobodies targeting the BTB domain of PATZ1 which is mainly associated with protein-protein interactions. NCOR and SMRT are examples of reported co-repressor proteins interacting with another ZBTB protein called BCL6 [12,13]. We recently reported PATZ1-PATZ2 interaction through their BTB domains[185]. However, such interactions and their detailed mechanisms and mode of action are poorly understood.

Therefore, understanding the exact effect of our nanobodies on the functional activity of PATZ1 requires more investigation.

In conclusion, our results suggest that the specific binding of nanobodies to the BTB domain of PATZ1 might regulate its gene transcriptional activity. Further investigation will clarify if these nanobodies might be used as PATZ1 modulators.

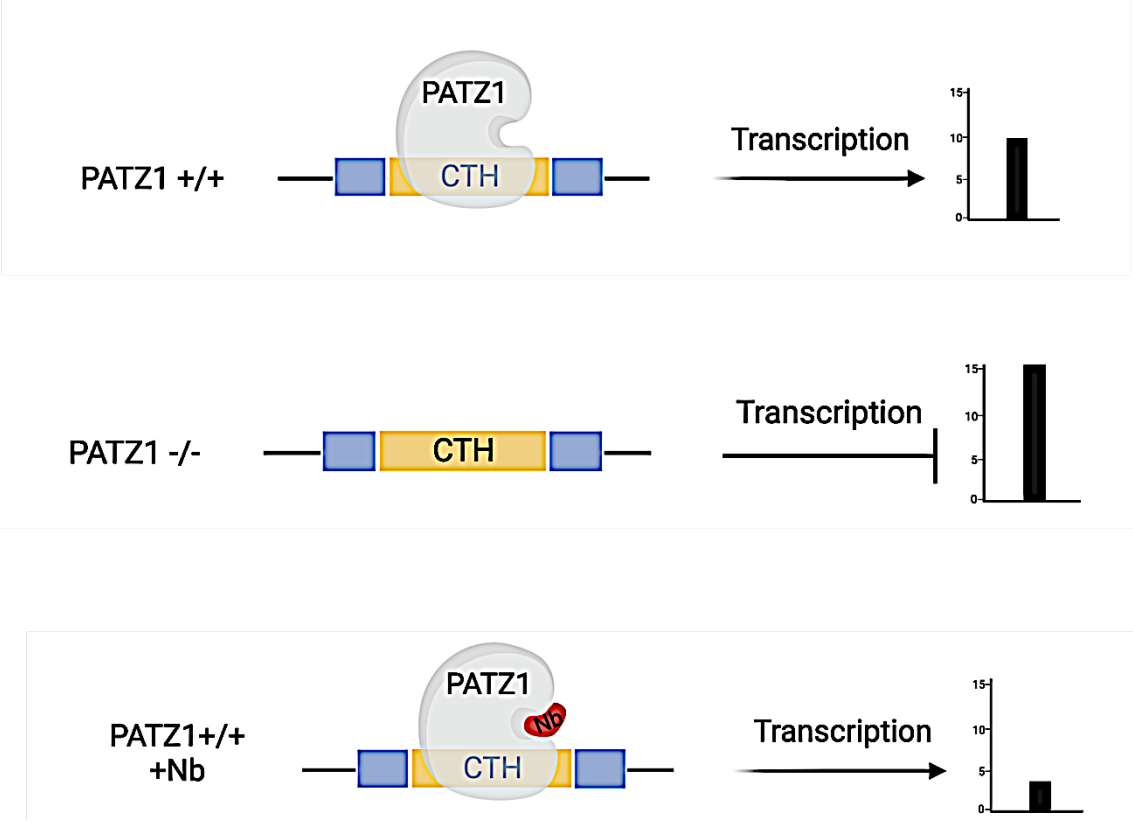

Figure 5. 1: An illustration of how nanobodies modulate PATZ1 activity and affect the transcriptional level of CTH gene

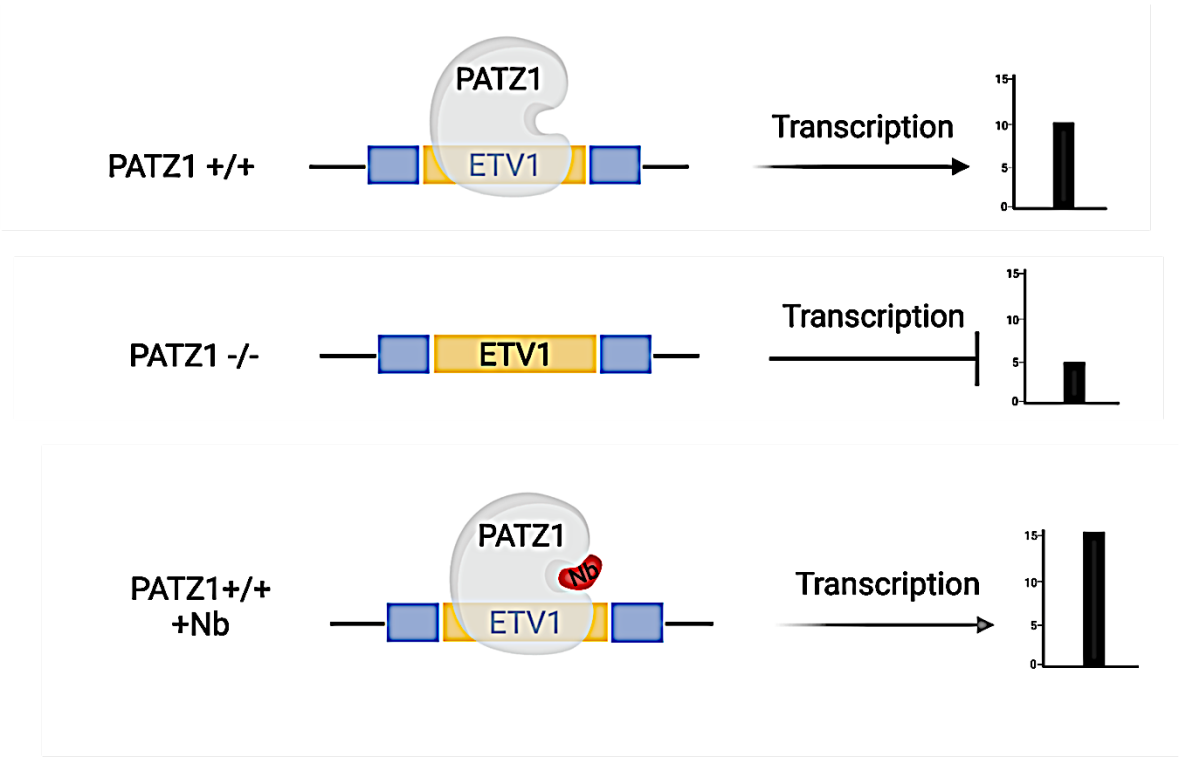

Figure 5. 2: An illustration of how nanobodies modulate PATZ1 activity and affect the transcriptional level of the ETV1 gene.

6. REFERENCES

1. Godt D, Couderc JL, Cramton SE, Laski FA. Pattern formation in the limbs of Drosophila: bric a brac is expressed in both a gradient and a wave-like pattern and is required for specification and proper segmentation of the tarsus. *Development*. 1993;119(3):799-812. doi:10.1242/dev.119.3.799
2. Harrison SDD, Travers AAA. The tramtrack gene encodes a Drosophila finger protein that interacts with the ftz transcriptional regulatory region and shows a novel embryonic expression pattern. *EMBO J*. 1990;9(1):207-216. doi:10.1002/j.1460-2075.1990.tb08097.x
3. DiBello PR, Withers DA, Bayer CA, Fristrom JW, Guild GM. The Drosophila Broad-Complex encodes a family of related proteins containing zinc fingers. *Genetics*. 1991;129(2):385-397. doi:10.1093/genetics/129.2.385
4. Zollman S, Godt D, Prive GG, Couderc JL, Laski FA. The BTB domain, found primarily in zinc finger proteins, defines an evolutionarily conserved family that includes several developmentally regulated genes in Drosophila. *Proc Natl Acad Sci*. 1994;91(22):10717-10721. doi:10.1073/pnas.91.22.10717
5. Miller J, McLachlan AD, Klug A. Repetitive zinc-binding domains in the protein transcription factor IIIA from Xenopus oocytes. *EMBO J*. 1985;4(6):1609-1614. doi:10.1002/j.1460-2075.1985.tb03825.x
6. Koonin E V., Senkevich TG, Chernos VI. A family of DNA virus genes that consists of fused portions of unrelated cellular genes. *Trends Biochem Sci*. 1992;17(6):213-214. doi:10.1016/0968-0004(92)90379-N
7. Bardwell VJ, Treisman R. The POZ domain: A conserved protein-protein interaction motif. *Genes Dev*. 1994;8(14):1664-1677. doi:10.1101/gad.8.14.1664
8. Wieschaus E, Nusslein-Volhard C, Kluding H. Krüppel, a gene whose activity is required early in the zygotic genome for normal embryonic segmentation. *Dev Biol*. 1984;104(1):172-186. doi:10.1016/0012-1606(84)90046-0
9. Siggs OM, Beutler B, Siggs OM. The BTB-ZF transcription factors. *Cell Cycle*. 2012;11:3358-3369. doi:10.4161/cc.21277
10. Klug A. The discovery of zinc fingers and their development for practical applications in gene regulation and genome manipulation. *Q Rev Biophys*. 2010;43(1):1–21. doi:10.1017/S0033583510000089
11. Beaulieu AM, Sant'Angelo DB. The BTB-ZF Family of Transcription Factors: Key Regulators of Lineage Commitment and Effector Function Development in the Immune System. *J Immunol*. 2011;187(6):2841-2847. doi:10.4049/jimmunol.1004006
12. Huynh KD, Bardwell VJ. The BCL-6 POZ domain and other POZ domains interact with the co-repressors N-CoR and SMRT. *Oncogene*. 1998;17(19):2473-2484. doi:10.1038/sj.onc.1202197
13. Staller P, Peukert K, Kiermaier A, et al. Repression of p15INK4b expression by Myc

through association with Miz-1. *Nat Cell Biol*. 2001;3(4):392-399. doi:10.1038/35070076

14. Piazza F, Costoya A, Merghoub T, Hobbs RM, Pandolfi PP. Disruption of PLZP in Mice Leads to Increased T-Lymphocyte Proliferation , Cytokine Production , and Altered Hematopoietic Stem Cell Homeostasis. 2004;24(23):10456-10469. doi:10.1128/MCB.24.23.10456
15. Takamori M, Hatano M, Arima M, et al. BAZF is required for activation of naive CD4 T cells by TCR triggering. 2004;16(10):1439-1449. doi:10.1093/intimm/dxh144
16. Mackler SA, Korutla L, Cha X, et al. NAC-1 Is a Brain POZ/BTB Protein That Can Prevent Cocaine-Induced Sensitization in the Rat. *J Neurosci*. 2000;20(16):6210-6217. doi:10.1523/JNEUROSCI.20-16-06210.2000
17. Korutla L, Neustadter JH, Fournier KM. NAC1 , a POZ / BTB protein present in the adult mammalian brain , triggers apoptosis after adeno v irus-mediated o v erexpression in PC-12 cells. 2003;46:33-39. doi:10.1016/S0168-0102(03)00024-5
18. Cattoretti G, Pasqualucci L, Ballon G, et al. Deregulated BCL6 expression recapitulates the pathogenesis of human diffuse large B cell lymphomas in mice. *Cancer Cell*. 2005;7(5):445-455. doi:10.1016/j.ccr.2005.03.037
19. Niu H. The proto-oncogene BCL-6 in normal and malignant B cell development. *Hematol Oncol*. 2002;20(4):155-166. doi:10.1002/hon.689
20. Alcalay M, Meani N, Gelmetti V, et al. Acute myeloid leukemia fusion proteins deregulate genes involved in stem cell maintenance and DNA repair. *J Clin Invest*. 2003;112(11):1751-1761. doi:10.1172/JCI17595
21. Calame KL, Lin K-I, Tunyaplin C. R Egulatory M Echanisms That D Etermine the D Evelopment and F Unction of P Lasma C Ells . *Annu Rev Immunol*. 2003;21(1):205-230. doi:10.1146/annurev.immunol.21.120601.141138
22. Kojima S, Hatano M, Okada S, et al. Testicular germ cell apoptosis in Bcl6-deficient mice. *Development*. 2001;128(1):57-65. doi:10.1242/dev.128.1.57
23. Reuter S, Bartelmann M, Vogt M, et al. APM-1, a novel human gene, identified by aberrant co-transcription with papillomavirus oncogenes in a cervical carcinoma cell line, encodes a BTB/POZ-zinc finger protein with growth inhibitory activity. *EMBO J*. 1998;17(1):215-222. doi:10.1093/emboj/17.1.215
24. Bellefroid EJ, Poncelet DA, Lecocq PJ, Revelant O, Martial JA. The evolutionarily conserved Kruppel-associated box domain defines a subfamily of eukaryotic multifingered proteins. *Proc Natl Acad Sci U S A*. 1991;88(9):3608-3612. doi:10.1073/pnas.88.9.3608
25. Bellefroid EJ, Marine JC, Ried T, et al. Clustered organization of homologous KRAB zinc-finger genes with enhanced expression in human T lymphoid cells. *EMBO J*. 1993;12(4):1363-1374. doi:10.1002/j.1460-2075.1993.tb05781.x
26. Williams AJ, Blacklow SC, Collins T. The Zinc Finger-Associated SCAN Box Is a Conserved Oligomerization Domain. *Mol Cell Biol*. 1999;19(12):8526-8535. doi:10.1128/mcb.19.12.8526
27. Klug A, Schwabe JWR. Protein motifs 5. Zinc fingers. *FASEB J*. 1995;9(8):597-604.

doi:10.1096/fasebj.9.8.7768350

28. Moore M, Klug A, Choo Y. Improved DNA binding specificity from polyzinc finger peptides by using strings of two-finger units. *Proc Natl Acad Sci*. 2001;98(4):1437-1441. doi:10.1073/pnas.98.4.1437

29. Tapia-Ramirez J, Eggen BJL, Peral-Rubio MJ, Toledo-Aral JJ, Mandel G. A single zinc finger motif in the silencing factor REST represses the neural-specific type II sodium channel promoter. *Proc Natl Acad Sci*. 1997;94(4):1177-1182. doi:10.1073/pnas.94.4.1177

30. Chaganti SR, Chen W, Parsa N, et al. Involvement ofBCL6 in chromosomal aberrations affecting band 3q27 in B-cell non-Hodgkin lymphoma. *Genes, Chromosom Cancer*. 1998;23(4):323-327. doi:10.1002/(SICI)1098-2264(199812)23:4<323::AID-GCC7>3.0.CO;2-3

31. Chen Z, Guidez F, Rousselot P, et al. PLZF-RARα fusion proteins generated from the variant t(11;17)(q23;q21) translocation in acute promyelocytic leukemia inhibit ligand-dependent transactivation of wild-type retinoic acid receptors. *Proc Natl Acad Sci U S A*. 1994;91(3):1178-1182. doi:10.1073/pnas.91.3.1178

32. Perez-Torrado R, Yamada D, Defossez PA. Born to bind: The BTB protein-protein interaction domain. *BioEssays*. 2006;28(12):1194-1202. doi:10.1002/bies.20500

33. Stogios PJ, Downs GS, Jauhal JJS, Nandra SK, Privé GG. Sequence and structural analysis of BTB domain proteins. *Genome Biol*. 2005;6(10):R82. doi:10.1186/gb-2005-6-10-r82

34. Aravind L, Koonin E V. Fold prediction and evolutionary analysis of the POZ domain: Structural and evolutionary relationship with the potassium channel tetramerization domain. *J Mol Biol*. 1999;285(4):1353-1361. doi:10.1006/jmbi.1998.2394

35. Ahmad KF, Engel CK, Privé GG, Prive GG, Privé GG. Crystal structure of the BTB domain from PLZF. *Proc Natl Acad Sci U S A*. 1998;95(21):12123-12128. doi:10.1073/pnas.95.21.12123

36. Ahmad KF, Melnick A, Lax S, et al. Mechanism of SMRT Corepressor Recruitment by the BCL6 BTB Domain. *Mol Cell*. 2003;12(6):1551-1564. doi:10.1016/S1097-2765(03)00454-4

37. Li X, Peng H, Schultz DC, Lopez-Guisa JM, Rauscher FJ, Marmorstein R. Structure-function studies of the BTB/POZ transcriptional repression domain from the promyelocytic leukemia zinc finger oncoprotein. *Cancer Res*. 1999;59(20):5275-5282. doi:10.2210/pdb1cs3/pdb

38. Kreusch A, Pfaffinger PJ, Stevens CF, Choe S. Crystal structure of the tetramerization domain of the Shaker potassium channel. *Nature*. 1998;392(6679):945-948. doi:10.1038/31978

39. Willems AR, Schwab M, Tyers M. A hitchhiker's guide to the cullin ubiquitin ligases: SCF and its kin. *Biochim Biophys Acta - Mol Cell Res*. 2004;1695(1-3):133-170. doi:10.1016/j.bbamcr.2004.09.027

40. Zheng N, Schulman BA, Song L, et al. Structure of the Cul1–Rbx1–Skp1–F boxSkp2 SCF ubiquitin ligase complex. *Nature*. 2002;416(6882):703-709.

doi:10.1038/416703a

41. Valentino T, Palmieri D, Vitiello M, et al. Embryonic defects and growth alteration in mice with homozygous disruption of the Patz1 gene. *J Cell Physiol*. 2013;228(3):646-653. doi:10.1002/jcp.24174

42. Ow JR, Ma H, Jean A, et al. Patz1 Regulates Embryonic Stem Cell Identity. *Stem Cells Dev*. 2014;23(10):1062-1073. doi:10.1089/scd.2013.0430

43. Mastrangelo T, Modena P, Tornielli S, et al. A novel zinc finger gene is fused to EWS in small round cell tumor. *Oncogene*. 2000;19(33):3799-3804. doi:10.1038/sj.onc.1203762

44. Fedele M, Benvenuto G, Pero R, et al. A Novel Member of the BTB/POZ Family, PATZ, Associates with the RNF4 RING Finger Protein and Acts as a Transcriptional Repressor. *J Biol Chem*. 2000;275(11):7894-7901. doi:10.1074/jbc.275.11.7894

45. Kobayashi A, Yamagiwa H, Hoshino H, et al. A Combinatorial Code for Gene Expression Generated by Transcription Factor Bach2 and MAZR (MAZ-Related Factor) through the BTB/POZ Domain. *Mol Cell Biol*. 2000;20(5):1733-1746. doi:10.1128/MCB.20.5.1733-1746.2000

46. Costoya JA. Functional analysis of the role of POK transcriptional repressors. *Briefings Funct Genomics Proteomics*. 2007;6(1):8-18. doi:10.1093/bfgp/elm002

47. De Ruijter AJM, Van Gennip AH, Caron HN, Kemp S, Van Kuilenburg ABP. Histone deacetylases (HDACs): Characterization of the classical HDAC family. *Biochem J*. 2003;370(3):737-749. doi:10.1042/BJ20021321

48. Ozturk N, Singh I, Mehta A, Braun T, Barreto G. HMGA proteins as modulators of chromatin structure during transcriptional activation. *Front Cell Dev Biol*. 2014;2(MAR):1-9. doi:10.3389/fcell.2014.00005

49. Aravind L, Landsman D. AT-hook motifs identified in a wide variety of DNA-binding proteins. *Nucleic Acids Res*. 1998;26(19):4413-4421. doi:10.1093/nar/26.19.4413

50. Pero R, Lembo F, Palmieri EA, et al. PATZ attenuates the RNF4-mediated enhancement of androgen receptor-dependent transcription. *J Biol Chem*. 2002;277(5):3280-3285. doi:10.1074/jbc.M109491200

51. Valentino T, Palmieri D, Vitiello M, Pierantoni GM, Fusco a, Fedele M. PATZ1 interacts with p53 and regulates expression of p53-target genes enhancing apoptosis or cell survival based on the cellular context. *Cell Death Dis*. 2013;4(12):e963. doi:10.1038/cddis.2013.500

52. Sakaguchi S, Hainberger D, Tizian C, et al. MAZR and Runx Factors Synergistically Repress ThPOK during CD8 + T Cell Lineage Development . *J Immunol*. 2015;195(6):2879-2887. doi:10.4049/jimmunol.1500387

53. He X, Park K, Kappes DJ. The Role of ThPOK in Control of CD4/CD8 Lineage Commitment. *Annu Rev Immunol*. 2010;28(1):295-320. doi:10.1146/annurev.immunol.25.022106.141715

54. Sakaguchi S, Hombauer M, Bilic I, et al. The zinc-finger protein MAZR is part of the transcription factor network that controls the CD4 versus CD8 lineage fate of double-positive thymocytes. *Nat Immunol*. 2010;11(5):442-448. doi:10.1038/ni.1860

55. Bilic I, Koesters C, Unger B, et al. Negative regulation of CD8 expression via Cd8 enhancer-mediated recruitment of the zinc finger protein MAZR. *Nat Immunol*. 2006;7(4):392-400. doi:10.1038/ni1311

56. Fedele M, Franco R, Salvatore G, et al. PATZ1 gene has a critical role in the spermatogenesis and testicular tumours. 2008;(January):39-47. doi:10.1002/path

57. O'Hara L, Smith LB. Androgen receptor roles in spermatogenesis and infertility. *Best Pract Res Clin Endocrinol Metab*. 2015;29(4):595-605. doi:10.1016/j.beem.2015.04.006

58. Cousminer DL, Stergiakouli E, Berry DJ, et al. Genome-wide association study of sexual maturation in males and females highlights a role for body mass and menarche loci in male puberty. *Hum Mol Genet*. 2014;23(16):4452-4464. doi:10.1093/hmg/ddu150

59. Hernandez-Segura A, de Jong T V., Melov S, Guryev V, Campisi J, Demaria M. Unmasking Transcriptional Heterogeneity in Senescent Cells. *Curr Biol*. 2017;27(17):2652-2660.e4. doi:10.1016/j.cub.2017.07.033

60. Cho JH, Kim MJ, Kim KJ, Kim J-R. POZ/BTB and AT-hook-containing zinc finger protein 1 (PATZ1) inhibits endothelial cell senescence through a p53 dependent pathway. *Cell Death Differ*. 2012;19(4):703-712. doi:10.1038/cdd.2011.142

61. Tritz R, Mueller BM, Hickey MJ, et al. siRNA Down-regulation of the PATZ1 Gene in Human Glioma Cells Increases Their Sensitivity to Apoptotic Stimuli. *Cancer Ther*. 2008;6(B):865-876. http://www.ncbi.nlm.nih.gov/pubmed/19081762

62. Keskin N, Deniz E, Eryilmaz J, et al. PATZ1 Is a DNA Damage-Responsive Transcription Factor That Inhibits p53 Function. *Mol Cell Biol*. 2015;35(10):1741-1753. doi:10.1128/MCB.01475-14

63. Nichols J, Zevnik B, Anastassiadis K, et al. Formation of pluripotent stem cells in the mammalian embryo depends on the POU transcription factor Oct4. *Cell*. 1998;95(3):379-391. doi:10.1016/S0092-8674(00)81769-9

64. Avilion AA, Nicolis SK, Pevny LH, Perez L, Vivian N, Lovell-Badge R. Multipotent cell lineages in early mouse development depend on SOX2 function. *Genes Dev*. 2003;17(1):126-140. doi:10.1101/gad.224503

65. Chambers I, Colby D, Robertson M, et al. Functional expression cloning of Nanog, a pluripotency sustaining factor in embryonic stem cells. *Cell*. 2003;113(5):643-655. doi:10.1016/S0092-8674(03)00392-1

66. Mitsui K, Tokuzawa Y, Itoh H, et al. The homeoprotein nanog is required for maintenance of pluripotency in mouse epiblast and ES cells. *Cell*. 2003;113(5):631-642. doi:10.1016/S0092-8674(03)00393-3

67. Nishiyama A, Xin L, Sharov AA, et al. Uncovering Early Response of Gene Regulatory Networks in ESCs by Systematic Induction of Transcription Factors. *Cell Stem Cell*. 2009;5(4):420-433. doi:10.1016/j.stem.2009.07.012

68. Oliviero G, Munawar N, Watson A, et al. The variant Polycomb Repressor Complex 1 component PCGF1 interacts with a pluripotency sub-network that includes DPPA4, a regulator of embryogenesis. *Sci Rep*. 2015;5(November):1-11.

doi:10.1038/srep18388

69. Takahashi K, Yamanaka S. Induction of Pluripotent Stem Cells from Mouse Embryonic and Adult Fibroblast Cultures by Defined Factors. *Cell*. 2006;126(4):663-676. doi:10.1016/j.cell.2006.07.024

70. Ma H, Ow JR, Tan BCP, et al. The dosage of Patz1 modulates reprogramming process. *Sci Rep*. 2014;4:1-12. doi:10.1038/srep07519

71. Pero R, Palmieri D, Angrisano T, et al. POZ-, AT-hook-, and zinc finger-containing protein (PATZ) interacts with human oncogene B cell lymphoma 6 (BCL6) and is required for its negative autoregulation. *J Biol Chem*. 2012;287(22):18308-18317. doi:10.1074/jbc.M112.346270

72. Franco R, Scognamiglio G, Valentino E, et al. PATZ1 expression correlates positively with BAX and negatively with BCL6 and survival in human diffuse large B cell lymphomas. *Oncotarget*. 2016;7(37):59158-59172. doi:10.18632/oncotarget.10993

73. Ho MY, Liang CM, Liang SM. PATZ1 induces PP4R2 to form a negative feedback loop on IKK/ NF-κB signaling in lung cancer. *Oncotarget*. 2016;7(32):52255-52269. doi:10.18632/oncotarget.10427

74. Iesato A, Nakamura T, Izumi H, Uehara T, Ito KI. PATZ1 knockdown enhances malignant phenotype in thyroid epithelial follicular cells and thyroid cancer cells. *Oncotarget*. 2017;8(47):82754-82772. doi:10.18632/oncotarget.19787

75. Chiappetta G, Valentino T, Vitiello M, et al. PATZ1 acts as a tumor suppressor in thyroid cancer via targeting p53-dependent genes involved in EMT and cell migration. *Oncotarget*. 2015;6(7):5310-5323. doi:10.18632/oncotarget.2776

76. Zhao C, Yan M, Li C, Feng Z. POZ/BTB and AT-hook-containing zinc finger protein 1 (PATZ1) suppresses progression of ovarian cancer and serves as an independent prognosis factor. *Med Sci Monit*. 2018;24:4262-4270. doi:10.12659/MSM.908766

77. Tian X, Sun D, Zhang Y, Zhao S, Xiong H, Fang J. Zinc finger protein 278, a potential oncogene in human colorectal cancer. *Acta Biochim Biophys Sin (Shanghai)*. 2008;40(4):289-296. doi:10.1111/j.1745-7270.2008.00405.x

78. Kawamata N, Miki T, Fukuda T, Hirosawa S, Aoki N. The organization of the BCL6 gene. *Leukemia*. 1994;8(8):1327-1330. http://www.ncbi.nlm.nih.gov/pubmed/8057668

79. Dent AL, Shaffer AL, Yu X, Allman D, Staudt LM. Control of Inflammation, Cytokine Expression, and Germinal Center Formation by BCL-6. *Science (80-)*. 1997;276(5312):589-592. doi:10.1126/science.276.5312.589

80. Jardin F, Ruminy P, Bastard C, Tilly H. The BCL6 proto-oncogene: a leading role during germinal center development and lymphomagenesis. *Pathol Biol*. 2007;55(1):73-83. doi:10.1016/j.patbio.2006.04.001

81. Chen Z, Brand NJ, Chen A, et al. Fusion between a novel Krüppel-like zinc finger gene and the retinoic acid receptor-alpha locus due to a variant t(11;17) translocation associated with acute promyelocytic leukaemia. *EMBO J*. 1993;12(3):1161-1167. doi:10.1002/j.1460-2075.1993.tb05757.x

82. Guadagno E, Vitiello M, Francesca P, et al. PATZ1 is a new prognostic marker of

glioblastoma associated with the stem-like phenotype and enriched in the proneural subtype. *Oncotarget*. 2017;8(35):59282-59300. doi:10.18632/oncotarget.19546

83. Passariello A, Errico ME, Donofrio V, et al. PATZ1 is overexpressed in pediatric glial tumors and correlates with worse event-free survival in high-grade gliomas. *Cancers (Basel)*. 2019;11(10):1-13. doi:10.3390/cancers11101537

84. Chen J, Li Y, Yu TS, et al. A restricted cell population propagates glioblastoma growth after chemotherapy. *Nature*. 2012;488(7412):522-526. doi:10.1038/nature11287

85. Chen R an, Sun X mian, Yan C you, et al. Hyperglycemia-induced PATZ1 negatively modulates endothelial vasculogenesis via repression of FABP4 signaling. *Biochem Biophys Res Commun*. 2016;477(4):548-555. doi:10.1016/j.bbrc.2016.06.052

86. Dhaouadi N, Li JY, Feugier P, et al. Computational identification of potential transcriptional regulators of TGF-ß1 in human atherosclerotic arteries. *Genomics*. 2014;103(5-6):357-370. doi:10.1016/j.ygeno.2014.05.001

87. Eliwa H, Belzung C, Surget A. Adult hippocampal neurogenesis: Is it the alpha and omega of antidepressant action? *Biochem Pharmacol*. 2017;141:86-99. doi:10.1016/j.bcp.2017.08.005

88. Xu F, Yang J, Chen J, et al. Differential co-expression and regulation analyses reveal different mechanisms underlying major depressive disorder and subsyndromal symptomatic depression. *BMC Bioinformatics*. 2015;16(1):1-10. doi:10.1186/s12859-015-0543-y

89. Padlan EA. Anatomy of the antibody molecule. *Mol Immunol*. 1994;31(3):169-217. doi:10.1016/0161-5890(94)90001-9

90. Hamers-Casterman C, Atarhouch T, Muyldermans S, et al. Naturally occurring antibodies devoid of light chains. *Nature*. 1993;363(6428):446-448. doi:10.1038/363446a0

91. Greenberg AS, Avila D, Hughes M, Hughes A, McKinney EC, Flajnik MF. A new antigen receptor gene family that undergoes rearrangement and extensive somatic diversification in sharks. *Nature*. 1995;374(6518):168-173. doi:10.1038/374168a0

92. Muyldermans S, Atarhouch T, Saldanha J, Barbosa JARG, Hamers R. Sequence and structure of V H domain from naturally occurring camel heavy chain immunoglobulins lacking light chains. *"Protein Eng Des Sel*. 1994;7(9):1129-1135. doi:10.1093/protein/7.9.1129

93. Chothia C, Boswell DR, Lesk AM. The outline structure of the T-cell alpha beta receptor. *EMBO J*. 1988;7(12):3745-3755. doi:10.1002/j.1460-2075.1988.tb03258.x

94. Davies DR, Metzger H. Structural Basis of Antibody Function. *Annu Rev Immunol*. 1983;1(1):87-115. doi:10.1146/annurev.iy.01.040183.000511

95. Alzari PM, Lascombe MB, Poljak RJ. Three-Dimensional Structure of Antibodies. *Annu Rev Immunol*. 1988;6(1):555-580. doi:10.1146/annurev.iy.06.040188.003011

96. Chothia C, Lesk AM, Gherardi E, et al. Structural repertoire of the human VH segments. *J Mol Biol*. 1992;227(3):799-817. doi:10.1016/0022-2836(92)90224-8

97. Desmyter A, Transue TR, Ghahroudi MA, et al. Crystal structure of a camel single-

domain VH antibody fragment in complex with lysozyme. *Nat Struct Mol Biol*. 1996;3(9):803-811. doi:10.1038/nsb0996-803

98. Lesk AM, Chothia C. Elbow motion in the immunoglobulins involves a molecular ball-and-socket joint. *Nature*. 1988;335(6186):188-190. doi:10.1038/335188a0

99. Davies J, Riechmann L. 'Camelising' human antibody fragments: NMR studies on VH domains. *FEBS Lett*. 1994;339(3):285-290. doi:10.1016/0014-5793(94)80432-X

100. Chothia C, Novotný J, Bruccoleri R, Karplus M. Domain association in immunoglobulin molecules. *J Mol Biol*. 1985;186(3):651-663. doi:10.1016/0022-2836(85)90137-8

101. Jung S-H, Pastan I, Lee B. Design of interchain disulfide bonds in the framework region of the Fv fragment of the monoclonal antibody B3. *Proteins Struct Funct Genet*. 1994;19(1):35-47. doi:10.1002/prot.340190106

102. Reiter Y, Brinkmann U, Webber KO, Jung S-H, Lee B, Pastan I. Engineering interchain disulfide bonds into conserved framework regions of Fv fragments: improved biochemical characteristics of recombinant immunotoxins containing disulfide-stabilized Fv. *Protein Eng*. 1994;7(5):697-704. doi:10.1093/protein/7.5.697

103. Conrath K., Wernery U, Muyldermans S, Nguyen V. Emergence and evolution of functional heavy-chain antibodies in Camelidae. *Dev Comp Immunol*. 2003;27(2):87-103. doi:10.1016/S0145-305X(02)00071-X

104. Nguyen VK, Hamers R, Wyns L, Muyldermans S. Camel heavy-chain antibodies: diverse germline VHH and specific mechanisms enlarge the antigen-binding repertoire. *EMBO J*. 2000;19(5):921-930. doi:10.1093/emboj/19.5.921

105. De Genst E, Silence K, Decanniere K, et al. Molecular basis for the preferential cleft recognition by dromedary heavy-chain antibodies. *Proc Natl Acad Sci*. 2006;103(12):4586-4591. doi:10.1073/pnas.0505379103

106. Arbabi Ghahroudi M, Desmyter A, Wyns L, Hamers R, Muyldermans S. Selection and identification of single domain antibody fragments from camel heavy-chain antibodies. *FEBS Lett*. 1997;414(3):521-526. doi:10.1016/S0014-5793(97)01062-4

107. Jespers L, Schon O, Famm K, Winter G. Aggregation-resistant domain antibodies selected on phage by heat denaturation. *Nat Biotechnol*. 2004;22(9):1161-1165. doi:10.1038/nbt1000

108. Christ D, Famm K, Winter G. Repertoires of aggregation-resistant human antibody domains. *Protein Eng Des Sel*. 2007;20(8):413-416. doi:10.1093/protein/gzm037

109. Moutel S, Bery N, Bernard V, et al. NaLi-H1: A universal synthetic library of humanized nanobodies providing highly functional antibodies and intrabodies. *Elife*. 2016;5:1-31. doi:10.7554/eLife.16228

110. Emmerson CD, Vlist Els J. van der, Braam MR, et al. Enhancement of polymeric immunoglobulin receptor transcytosis by biparatopic vhh. *PLoS One*. 2011;6(10):1-10. doi:10.1371/journal.pone.0026299

111. Els Conrath K, Lauwereys M, Wyns L, Muyldermans S. Camel Single-domain Antibodies as Modular Building Units in Bispecific and Bivalent Antibody Constructs. *J Biol Chem*. 2001;276(10):7346-7350. doi:10.1074/jbc.M007734200

112. Chames P, Baty D. Bispecific antibodies for cancer therapy. *MAbs*. 2009;1(6):539-547. doi:10.4161/mabs.1.6.10015

113. Chakravarty R, Goel S, Cai W. Nanobody: The "magic bullet" for molecular imaging? *Theranostics*. 2014;4(4):386-398. doi:10.7150/thno.8006

114. Rothbauer U, Zolghadr K, Tillib S, et al. Targeting and tracing antigens in live cells with fluorescent nanobodies. *Nat Methods*. 2006;3(11):887-889. doi:10.1038/nmeth953

115. Cortez-Retamozo V, Backmann N, Senter PD, et al. Efficient Cancer Therapy with a Nanobody-Based Conjugate. *Cancer Res*. 2004;64(8):2853-2857. doi:10.1158/0008-5472.CAN-03-3935

116. Conrath K, Vanhollebeke B, Pays E, et al. Experimental therapy of African trypanosomiasis with a nanobody-conjugated human trypanolytic factor. 2006;12(5):580-584. doi:10.1038/nm1395

117. Coppieters K, Dreier T, Silence K, et al. Formatted Anti – Tumor Necrosis Factor ␣ VHH Proteins Derived From Camelids Show Superior Potency and Targeting to Inflamed Joints in a Murine Model of Collagen-Induced Arthritis. 2006;54(6):1856-1866. doi:10.1002/art.21827

118. Jittavisutthikul S, Thanongsaksrikul J, Thueng-in K, et al. Humanized-VHH Transbodies that Inhibit HCV Protease and Replication. *Viruses*. 2015;7(4):2030-2056. doi:10.3390/v7042030

119. Vincke C, Loris R, Saerens D, Martinez-Rodriguez S, Muyldermans S, Conrath K. General Strategy to Humanize a Camelid Single-domain Antibody and Identification of a Universal Humanized Nanobody Scaffold. *J Biol Chem*. 2009;284(5):3273-3284. doi:10.1074/jbc.M806889200

120. Pardon E, Laeremans T, Triest S, et al. A general protocol for the generation of Nanobodies for structural biology. *Nat Protoc*. 2014;9(3):674-693. doi:10.1038/nprot.2014.039

121. Muyldermans S. Nanobodies: Natural Single-Domain Antibodies. *Annu Rev Biochem*. 2013;82(1):775-797. doi:10.1146/annurev-biochem-063011-092449

122. Goldman ER, Anderson GP, Liu JL, et al. Facile Generation of Heat-Stable Antiviral and Antitoxin Single Domain Antibodies from a Semisynthetic Llama Library. *Anal Chem*. 2006;78(24):8245-8255. doi:10.1021/ac0610053

123. Zimmermann I, Egloff P, Hutter CA, et al. Synthetic single domain antibodies for the conformational trapping of membrane proteins. *Elife*. 2018;7:e34317. doi:10.7554/eLife.34317

124. Olichon A, de Marco A. Preparation of a Naïve Library of Camelid Single Domain Antibodies. In: *Methods in Molecular Biology*. Vol 911. ; 2012:65-78. doi:10.1007/978-1-61779-968-6_5

125. Yan J, Wang P, Zhu M, et al. Characterization and applications of Nanobodies against human procalcitonin selected from a novel naïve Nanobody phage display library. *J Nanobiotechnology*. 2015;13(1):33. doi:10.1186/s12951-015-0091-7

126. Muruganandam A, Tanha J, Narang S, Stanimirovic D. Selection of phage-displayed llama single-domain antibodies that transmigrate across human blood-brain barrier endothelium. *FASEB J*. 2002;16(2):1-22. doi:10.1096/fj.01-0343fje

127. Monegal A, Ami D, Martinelli C, et al. Immunological applications of single-domain llama recombinant antibodies isolated from a naïve library. *Protein Eng Des Sel*. 2009;22(4):273-280. doi:10.1093/protein/gzp002

128. Wang Y, Fan Z, Shao L, et al. Nanobody-derived nanobiotechnology tool kits for diverse biomedical and biotechnology applications. *Int J Nanomedicine*. 2016;Volume 11:3287-3303. doi:10.2147/IJN.S107194

129. McMahon C, Baier AS, Pascolutti R, et al. Yeast surface display platform for rapid discovery of conformationally selective nanobodies. *Nat Struct Mol Biol*. 2018;25(3):289-296. doi:10.1038/s41594-018-0028-6

130. Ju M-S, Min S-W, Lee SM, et al. A synthetic library for rapid isolation of humanized single-domain antibodies. *Biotechnol Bioprocess Eng*. 2017;22(3):239-247. doi:10.1007/s12257-017-0082-7

131. Woods J. Selection of Functional Intracellular Nanobodies. *SLAS Discov*. 2019;24(7):703-713. doi:10.1177/2472555219853235

132. Ryckaert S, Pardon E, Steyaert J, Callewaert N. Isolation of antigen-binding camelid heavy chain antibody fragments (nanobodies) from an immune library displayed on the surface of Pichia pastoris. *J Biotechnol*. 2010;145(2):93-98. doi:10.1016/j.jbiotec.2009.10.010

133. Boder ET, Wittrup KD. Yeast surface display for screening combinatorial polypeptide libraries. *Nat Biotechnol*. 1997;15(6):553-557. doi:10.1038/nbt0697-553

134. Matz J, Hérate C, Bouchet J, et al. Selection of Intracellular Single-Domain Antibodies Targeting the HIV-1 Vpr Protein by Cytoplasmic Yeast Two-Hybrid System. Goldman ER, ed. *PLoS One*. 2014;9(12):e113729. doi:10.1371/journal.pone.0113729

135. Visintin M, Meli GA, Cannistraci I, Cattaneo A. Intracellular antibodies for proteomics. *J Immunol Methods*. 2004;290(1-2):135-153. doi:10.1016/j.jim.2004.04.014

136. Pellis M, Pardon E, Zolghadr K, et al. A bacterial-two-hybrid selection system for one-step isolation of intracellularly functional Nanobodies. *Arch Biochem Biophys*. 2012;526(2):114-123. doi:10.1016/j.abb.2012.04.023

137. Schmidt FI, Hanke L, Morin B, et al. Phenotypic lentivirus screens to identify functional single domain antibodies. *Nat Microbiol*. 2016;1(8):16080. doi:10.1038/nmicrobiol.2016.80

138. Rossotti M, Tabares S, Alfaya L, Leizagoyen C, Moron G, González-Sapienza G. Streamlined method for parallel identification of single domain antibodies to membrane receptors on whole cells. *Biochim Biophys Acta - Gen Subj*. 2015;1850(7):1397-1404. doi:10.1016/j.bbagen.2015.03.009

139. Hanes J, Jermutus L, Plückthun A. [24] Selecting and evolving functional proteins in vitro by ribosome display. In: *Methods in Enzymology*. Vol 328. ; 2000:404-430. doi:10.1016/S0076-6879(00)28409-7

140. Roberts RW, Szostak JW. RNA-peptide fusions for the in vitro selection of peptides and proteins. *Proc Natl Acad Sci U S A*. 1997;94(23):12297-12302. doi:10.1073/pnas.94.23.12297

141. de Marco A. Recombinant expression of nanobodies and nanobody-derived immunoreagents. *Protein Expr Purif*. 2020;172(March):105645. doi:10.1016/j.pep.2020.105645

142. de Marco A. Recent contributions in the field of the recombinant expression of disulfide bonded protein in bacteria. *Microb Cell Fact*. 2012;11(1):129. doi:10.1186/1475-2859-11-129

143. Thie H, Schirrmann T, Paschke M, Dübel S, Hust M. SRP and Sec pathway leader peptides for antibody phage display and antibody fragment production in E. coli. *N Biotechnol*. 2008;25(1):49-54. doi:10.1016/j.nbt.2008.01.001

144. Salema V, Fernández LÁ. High yield purification of nanobodies from the periplasm of E. coli as fusions with the maltose binding protein. *Protein Expr Purif*. 2013;91(1):42-48. doi:10.1016/j.pep.2013.07.001

145. Schlapschy M, Skerra A. Periplasmic Chaperones Used to Enhance Functional Secretion of Proteins in E. coli. In: *Methods in Molecular Biology*. Vol 705. ; 2011:211-224. doi:10.1007/978-1-61737-967-3_12

146. Veggiani G, de Marco A. Improved quantitative and qualitative production of single-domain intrabodies mediated by the co-expression of Erv1p sulfhydryl oxidase. *Protein Expr Purif*. 2011;79(1):111-114. doi:10.1016/j.pep.2011.03.005

147. Djender S, Schneider A, Beugnet A, et al. Bacterial cytoplasm as an effective cell compartment for producing functional VHH-based affinity reagents and Camelidae IgG-like recombinant antibodies. *Microb Cell Fact*. 2014;13(1):140. doi:10.1186/s12934-014-0140-1

148. Olichon A, Surrey T. Selection of Genetically Encoded Fluorescent Single Domain Antibodies Engineered for Efficient Expression in Escherichia coli. *J Biol Chem*. 2007;282(50):36314-36320. doi:10.1074/jbc.M704908200

149. Ruano-Gallego D, Fraile S, Gutierrez C, Fernández LÁ. Screening and purification of nanobodies from E. coli culture supernatants using the hemolysin secretion system. *Microb Cell Fact*. 2019;18(1):47. doi:10.1186/s12934-019-1094-0

150. Bobkov V, Zarca AM, Van Hout A, et al. Nanobody-Fc constructs targeting chemokine receptor CXCR4 potently inhibit signaling and CXCR4-mediated HIV-entry and induce antibody effector functions. *Biochem Pharmacol*. 2018;158(May):413-424. doi:10.1016/j.bcp.2018.10.014

151. Godakova, Noskov, Vinogradova, et al. Camelid VHHs Fused to Human Fc Fragments Provide Long Term Protection Against Botulinum Neurotoxin A in Mice. *Toxins (Basel)*. 2019;11(8):464. doi:10.3390/toxins11080464

152. Liu Y, Huang H. Expression of single-domain antibody in different systems. *Appl Microbiol Biotechnol*. 2018;102(2):539-551. doi:10.1007/s00253-017-8644-3

153. Kaur S, Venktaraman G, Jain M, Senapati S, Garg PK, Batra SK. Recent trends in antibody-based oncologic imaging. *Cancer Lett*. 2012;315(2):97-111.

doi:10.1016/j.canlet.2011.10.017

154. Keyaerts M, Xavier C, Heemskerk J, et al. Phase I Study of 68 Ga-HER2-Nanobody for PET/CT Assessment of HER2 Expression in Breast Carcinoma. *J Nucl Med*. 2016;57(1):27-33. doi:10.2967/jnumed.115.162024

155. Keyaerts M, Xavier C, Everaert H, et al. Phase II trial of HER2-PET/CT using 68Ga-anti-HER2 VHH1 for characterization of HER2 presence in brain metastases of breast cancer patients. *Ann Oncol*. 2019;30(May):iii25-iii26. doi:10.1093/annonc/mdz095.081

156. Xavier C, Blykers A, Laoui D, et al. Clinical Translation of [68Ga]Ga-NOTA-anti-MMR-sdAb for PET/CT Imaging of Protumorigenic Macrophages. *Mol Imaging Biol*. 2019;21(5):898-906. doi:10.1007/s11307-018-01302-5

157. Bridoux J, Broos K, Lecocq Q, et al. Anti-Human PD-L1 Nanobody for Immuno-PET Imaging: Validation of a Conjugation Strategy for Clinical Translation. *Biomolecules*. 2020;10(10):1388. doi:10.3390/biom10101388

158. Ingram JR, Blomberg OS, Rashidian M, et al. Anti–CTLA-4 therapy requires an Fc domain for efficacy. *Proc Natl Acad Sci*. 2018;115(15):3912-3917. doi:10.1073/pnas.1801524115

159. Caveliers V, Cortez-Retamozo V, Lahoutte T, et al. 99mTc-Labeled Nanobodies: A New Type of Targeted Probes for Imaging Antigen Expression. *Curr Radiopharm*. 2008;1(1):37-41. doi:10.2174/1874471010801010037

160. Uchański T, Pardon E, Steyaert J. Nanobodies to study protein conformational states. *Curr Opin Struct Biol*. 2020;60:117-123. doi:10.1016/j.sbi.2020.01.003

161. Staus DP, Strachan RT, Manglik A, et al. Allosteric nanobodies reveal the dynamic range and diverse mechanisms of G-protein-coupled receptor activation. *Nature*. 2016;535(7612):448-452. doi:10.1038/nature18636

162. Strauss M, Schotte L, Karunatilaka KS, Filman DJ, Hogle JM. Cryo-electron Microscopy Structures of Expanded Poliovirus with VHHs Sample the Conformational Repertoire of the Expanded State. Dermody TS, ed. *J Virol*. 2017;91(3):1-22. doi:10.1128/JVI.01443-16

163. Bannas P, Hambach J, Koch-Nolte F. Nanobodies and Nanobody-Based Human Heavy Chain Antibodies As Antitumor Therapeutics. *Front Immunol*. 2017;8(NOV):1-13. doi:10.3389/fimmu.2017.01603

164. Scully M, Cataland SR, Peyvandi F, et al. Caplacizumab Treatment for Acquired Thrombotic Thrombocytopenic Purpura. *N Engl J Med*. 2019;380(4):335-346. doi:10.1056/NEJMoa1806311

165. De Munter S, Ingels J, Goetgeluk G, et al. Nanobody Based Dual Specific CARs. *Int J Mol Sci*. 2018;19(2):403. doi:10.3390/ijms19020403

166. Weiss, Verrips. Nanobodies that Neutralize HIV. *Vaccines*. 2019;7(3):77. doi:10.3390/vaccines7030077

167. Bouchet J, Basmaciogullari SE, Chrobak P, et al. Inhibition of the Nef regulatory protein of HIV-1 by a single-domain antibody. *Blood*. 2011;117(13):3559-3568. doi:10.1182/blood-2010-07-296749

168. Heng BC, Cao T. Making cell-permeable antibodies (Transbody) through fusion of protein transduction domains (PTD) with single chain variable fragment (scFv) antibodies: Potential advantages over antibodies expressed within the intracellular environment (Intrabody). *Med Hypotheses*. 2005;64(6):1105-1108. doi:10.1016/j.mehy.2005.01.011

169. Thueng-in K, Thanongsaksrikul J, Srimanote P, et al. Cell Penetrable Humanized-VH/VHH That Inhibit RNA Dependent RNA Polymerase (NS5B) of HCV. Pagano JS, ed. *PLoS One*. 2012;7(11):e49254. doi:10.1371/journal.pone.0049254

170. Mix KA, Lomax JE, Raines RT, States U, States U, States U. Cytosolic Delivery of Proteins by Bioreversible Esterification. *J Am Chem Soc*. 2018;139(41):14396-14398. doi:10.1021/jacs.7b06597.Cytosolic

171. Bruce VJ, McNaughton BR. Inside Job: Methods for Delivering Proteins to the Interior of Mammalian Cells. *Cell Chem Biol*. 2017;24(8):924-934. doi:10.1016/j.chembiol.2017.06.014

172. Zolghadr K, Gregor J, Leonhardt H, Rothbauer U. Case Study on Live Cell Apoptosis-Assay Using Lamin-Chromobody Cell-Lines for High-Content Analysis. In: *Single Domain Antibodies*. Vol 911. Humana Press; 2012:569-575. doi:10.1007/978-1-61779-968-6_36

173. Rajan M, Mortusewicz O, Rothbauer U, et al. Generation of an alpaca-derived nanobody recognizing γ-H2AX. *FEBS Open Bio*. 2015;5(1):779-788. doi:10.1016/j.fob.2015.09.005

174. Schiavon CR, Zhang T, Zhao B, et al. Actin chromobody imaging reveals sub-organellar actin dynamics. *Nat Methods*. 2020;17(9):917-921. doi:10.1038/s41592-020-0926-5

175. Keller B-M, Maier J, Weldle M, Segan S, Traenkle B, Rothbauer U. A Strategy to Optimize the Generation of Stable Chromobody Cell Lines for Visualization and Quantification of Endogenous Proteins in Living Cells. *Antibodies*. 2019;8(1):10. doi:10.3390/antib8010010

176. Maier J, Traenkle B, Rothbauer U. Real-time analysis of epithelial-mesenchymal transition using fluorescent single-domain antibodies. *Sci Rep*. 2015;5(1):13402. doi:10.1038/srep13402

177. Keller B-M, Maier J, Secker K-A, et al. Chromobodies to Quantify Changes of Endogenous Protein Concentration in Living Cells. *Mol Cell Proteomics*. 2018;17(12):2518-2533. doi:10.1074/mcp.TIR118.000914

178. Burgess A, Lorca T, Castro A. Quantitative Live Imaging of Endogenous DNA Replication in Mammalian Cells. Pelling A, ed. *PLoS One*. 2012;7(9):e45726. doi:10.1371/journal.pone.0045726

179. Prole DL, Taylor CW. A genetically encoded toolkit of functionalized nanobodies against fluorescent proteins for visualizing and manipulating intracellular signalling. *BMC Biol*. 2019;17(1):41. doi:10.1186/s12915-019-0662-4

180. Kossatz S, Pirovano G, Demétrio P, et al. PARP1 as a biomarker for early detection and intraoperative tumor delineation in epithelial cancers-first-in-human results. *Nat*

Biomed Eng. 2020;4:272–285. doi:10.1101/663385

181. Buchfellner A, Yurlova L, Nüske S, et al. A New Nanobody-Based Biosensor to Study Endogenous PARP1 In Vitro and in Live Human Cells. *PLoS One*. 2016;11(3):e0151041. doi:10.1371/journal.pone.0151041

182. Bethuyne J, De Gieter S, Zwaenepoel O, et al. A nanobody modulates the p53 transcriptional program without perturbing its functional architecture. *Nucleic Acids Res*. 2014;42(20):12928-12938. doi:10.1093/nar/gku962

183. Van M V., Fujimori T, Bintu L. Nanobody-mediated control of gene expression and epigenetic memory. *Nat Commun*. 2021;12(1):537. doi:10.1038/s41467-020-20757-1

184. Caussinus E, Kanca O, Affolter M. Fluorescent fusion protein knockout mediated by anti-GFP nanobody. *Nat Struct Mol Biol*. 2012;19(1):117-121. doi:10.1038/nsmb.2180

185. Piepoli S, Nogay L, Akkose U, et al. Sibling rivalry among the ZBTB transcription factor family : homo vs . heterodimers. Published online 2021. doi:10.1101/2021.12.17.472994

186. Wang F, Li Z-F, Yang Y-Y, et al. Chemiluminescent Enzyme Immunoassay and Bioluminescent Enzyme Immunoassay for Tenuazonic Acid Mycotoxin by Exploitation of Nanobody and Nanobody−Nanoluciferase Fusion. Published online 2020. doi:10.1021/acs.analchem.0c02338

187. Barakat S, Berksoz M, Zahedimaram P, Piepoli S, Erman B. Nanobodies as molecular imaging probes. *Free Radic Biol Med*. 2022;182(February):260-275. doi:10.1016/j.freeradbiomed.2022.02.031

188. Longhin E, Grønberg C, Hu Q, et al. Isolation and Characterization of Nanobodies against a Zinc-Transporting P-Type ATPase. *Antibodies*. 2018;7(4):39. doi:10.3390/antib7040039

189. Löw C, Yau YH, Pardon E, et al. Nanobody Mediated Crystallization of an Archeal Mechanosensitive Channel. *PLoS One*. 2013;8(10):1-14. doi:10.1371/journal.pone.0077984

190. Piepoli S, Alt AO, Atilgan C, Mancini EJ, Erman B. Structural analysis of the PATZ1 BTB domain homodimer. *Acta Crystallogr Sect D Struct Biol*. 2020;76(6):581-593. doi:10.1107/S2059798320005355

191. Lee PS, Yoshida R, Ekiert DC, et al. Heterosubtypic antibody recognition of the influenza virus hemagglutinin receptor binding site enhanced by avidity. *Proc Natl Acad Sci U S A*. 2012;109(42):17040-17045. doi:10.1073/pnas.1212371109

192. Zhao Y, Li Y, Wu X, et al. Identification of anti-CD16a single domain antibodies and their application in bispecific antibodies. *Cancer Biol Ther*. 2020;21(1):72-80. doi:10.1080/15384047.2019.1665953

193. Zolghadr K, Rothbauer U, Leonhardt H. The Fluorescent Two-Hybrid (F2H) Assay for Direct Analysis of Protein–Protein Interactions in Living Cells. In: Suter B, Wanker EE, eds. *Methods in Molecular Biology (Clifton, N.J.)*. Vol 812. Methods in Molecular Biology. Humana Press; 2012:275-282. doi:10.1007/978-1-61779-455-1_16

194. Yurlova L, Derks M, Buchfellner A, et al. The Fluorescent Two-Hybrid Assay to Screen for Protein–Protein Interaction Inhibitors in Live Cells. *J Biomol Screen*. 2014;19(4):516-525. doi:10.1177/1087057113518067

195. Reisinger H, Willibald AE, Ae S, Ae HK, Kunert R. Serum-free transfection of CHO cells with chemically defined transfection systems and investigation of their potential for transient and stable transfection. doi:10.1007/s10616-009-9224-x

196. Yang J, Liu H, Zhang X. Design, preparation and application of nucleic acid delivery carriers. *Biotechnol Adv*. 2014;32(4):804-817. doi:10.1016/j.biotechadv.2013.11.004

197. Wurm FM. Production of recombinant protein therapeutics in cultivated mammalian cells. *Nat Biotechnol*. 2004;22(11):1393-1398. doi:10.1038/nbt1026

198. Finn GK, Kurz BW, Cheng RZ, Shmookler Reis RJ. Homologous plasmid recombination is elevated in immortally transformed cells. *Mol Cell Biol*. 1989;9(9):4009-4017. doi:10.1128/mcb.9.9.4009-4017.1989

199. Elegheert J, Behiels E, Bishop B, et al. Lentiviral transduction of mammalian cells for fast, scalable and high-level production of soluble and membrane proteins. *Nat Protoc*. 2018;13(12):2991-3017. doi:10.1038/s41596-018-0075-9

200. Akhtar W, de Jong J, Pindyurin A V., et al. Chromatin Position Effects Assayed by Thousands of Reporters Integrated in Parallel. *Cell*. 2013;154(4):914-927. doi:10.1016/j.cell.2013.07.018

201. Papapetrou EP, Schambach A. Gene Insertion Into Genomic Safe Harbors for Human Gene Therapy. *Mol Ther*. 2016;24(4):678-684. doi:10.1038/mt.2016.38

202. Trastoy MO, Defais M, Larminat F. Resistance to the antibiotic Zeocin by stable expression of the Sh ble gene does not fully suppress Zeocin-induced DNA cleavage in human cells. *Mutagenesis*. 2005;20(2):111-114. doi:10.1093/mutage/gei016

203. Xia W, Bringmann P, McClary J, et al. High levels of protein expression using different mammalian CMV promoters in several cell lines. *Protein Expr Purif*. 2006;45(1):115-124. doi:10.1016/j.pep.2005.07.008

204. Lo C-A, Greben AW, Chen BE. Generating stable cell lines with quantifiable protein production using CRISPR/Cas9-mediated knock-in. *Biotechniques*. 2017;62(4):165-174. doi:10.2144/000114534

205. Gezen M. Identification of The Targets of The Human Transcription Factor PATZ1. Published online 2022.

206. Wu D, Si W, Wang M, Lv S, Ji A, Li Y. Hydrogen sulfide in cancer: Friend or foe? *Nitric Oxide*. 2015;50:38-45. doi:10.1016/j.niox.2015.08.004

207. Wang L, Shi H, Zhang X, et al. I157172, a novel inhibitor of cystathionine γ-lyase, inhibits growth and migration of breast cancer cells via SIRT1-mediated deacetylation of STAT3. *Oncol Rep*. 2019;41(1):427-436. doi:10.3892/or.2018.6798

208. Jurkowska H, Wróbel M. Cystathionine Promotes the Proliferation of Human Astrocytoma U373 Cells. *Anticancer Res*. 2018;38(6):3501-3505. doi:10.21873/anticanres.12621

209. Kai-Yuan Chen, Xiaojing Liu, Pengcheng Bu, et al. A metabolic signature of colon

cancer initiating cells. In: *2014 36th Annual International Conference of the IEEE Engineering in Medicine and Biology Society*. IEEE; 2014:4759-4762. doi:10.1109/EMBC.2014.6944688

210. Gasi D, Van Der Korput HA, Douben HC, et al. Overexpression of Full-Length ETV1 Transcripts in Clinical Prostate Cancer Due to Gene Translocation. *PLoS One*. 2011;6(1):16332. doi:10.1371/journal.pone.0016332

211. Jang BG, Lee HE, Kim WH. ETV1 mRNA is specifically expressed in gastrointestinal stromal tumors. *Virchows Arch*. 2015;467(4):393-403. doi:10.1007/s00428-015-1813-9

APPENDIX A

Chemicals

Chemicals and Media Components	Supplier Company
2-Mercaptoethanol	Sigma, Germany
2xTY agar	sigma
2xTY medium	sigma
Acetic Acid	Merck, Germany
Acid Washed Glass Beads	Sigma, Germany
Acrylamide/Bis-acrylamide	Sigma, Germany
Agarose	peQLab, Germany
Ammonium Persulfate	Sigma, Germany
Ampicillin Sodium Salt	CellGro, USA
Bacto Agar	BD, USA
Bacto Tryptone	BD, USA
Boric Acid	Molekula, UK
Bromophenol Blue	Sigma, Germany
Chloramphenicol	Gibco, USA
Coomassie Blue Brilliant Blue R	Sigma, Germany
D-Glucose	Sigma, Germany
Distilled water	Milipore, France
DMEM	PAN, Germany
DMSO	Sigma, Germany
DNA Gel Loading Solution, 5X	Quality Biological, Inc, USA
EDTA	Applichem, Germany
Ethanol	Riedel-de Haen, Germany
Ethidium Bromide	Sigma, Germany
Fetal Bovine Serum	Thermo Fischer Scientific, USA
Fetal Bovine Serum (FBS)	Biological Industries, Israel
Glycerol Anhydrous	Applichem, Germany
Glycine	Applichem, Germany
HBSS	CellGro, USA
HEPES	Applichem, Germany
HisPure Cobalt Superflow Agarose	Thermo Fischer Scientific, USA
Hydrochloric Acid	Merck, Germany
Imidazole	Sigma, Germany
IPTG	Fermentas, USA
Isopropanol	Riedel-de Haén, Germany

Kanamycin Sulfate	Gibco, USA
LB Agar	BD, USA
LB Broth	BD, USA
Liquid nitrogen	Karbogaz, Turkey
M9, Minimal Salts	sigma
Methanol	Riedel-de Haen, Germany
PBS	Thermo Fischer Scientific, USA
PEG-6000	sigma
Penicillin-Streptomycin	Sigma, Germany
Phenol-Chloroform-Isoamylalcohol	Amersco, USA
PIPES	Sigma, Germany
Potassium Acetate	Merck Millipore, USA
Protease Tablets (EDTA-free)	Roche, Germany
RNase A	Roche, Germany
SDS Pure	Applichem, Germany
Skim Milk Powder	Fluka, Germany
Sodium Azide	Amresco, USA
Sodium Chloride	Applichem, Germany
TCEP	Sigma, Germany
TEMED	Applichem, Germany
Tris Buffer Grade	Amresco, USA
Tris Hydrochloride	Amresco, USA
Trypan Blue Solution	Thermo Fischer Scientific, USA
Tween20	Sigma, Germany

APPENDIX B

Equipment Used in the Study

Equipment	Company
AKTA pure chromatography system	Cytiva
Autoclave	Hirayama,Hiclave HV-110,Japan
Balance	Isolab, Germany
BD Influx Cell Sorter	BD Biosciences
Bioruptor ® Pico sonication device	Diagenode
Centrifuge	5418R Eppendorf, Germany 5702 Eppendorf, Germany 5415R Eppendorf, Germany Allegra X-15R, Beckman Coulter, USA Sorvall Lynx 6000, Thermo Scientific, USA
CO2 Incubator	Binder,Germany
Countless II Automated Cell Counter	Thermo Fischer Scientific, USA
Deepfreeze	-80^{o}C, Forma,Thermo ElectronCorp.,USA -20^{o}C, Bosch,Turkey
Distilled Water	Millipore, Elix-S, France
Electrophoresis Apparatus	VWR, USA Biorad Inc., USA
Filter Membranes	Millipore,USA
Freezing Container	Mr. Frosty, Thermo Fischer Scientific, USA
Gel Documentation	Gel Doc EZ, Biorad, USA
Heater	ThermomixerComfort,Eppendorf,Germany
Hematocytometer	Neubauer Improved, Isolab, Germany
Ice Machine	AF20, Scotsman Inc., USA
Incubator	Innova 44, New Brunswick Scientific USA
Infinite 200 multimode microplate reader.	TECAN
Laminar Flow	HeraSafe HS15, Heraeus, Germany HeraSafe HS12, Heraeus, Germany
Liquid Nitrogen Tank	Taylor-Wharton,3000RS, USA
Magnetic Stirrer	SB162, Stuart, UK
Microliter Pipettes	Thermo Fischer Scientific, USA
Microscope	Olympus CK40, Japan ZEISS Axio Observer Z1
Microwave Oven	Bosch,Turkey

pH meter	SevenCompact, Mettler Toledo, USA
PikoReal™ Real-Time PCR System	Thermo Scientific
Refrigerator	Bosch,Turkey Arcelik, Turkey Panasonic, Japan
Sonics-VibraCell™ sonicator	SONICS
Spectrophotometer	NanoDrop 2000, Thermo Fischer Scientific, USA Ultrospec 2100 pro, Amersham Biosciences, UK
Surface Plasmon Resonance System	BIACORE T200, GE Healthcare Life Sciences, USA
Thermocycler	C1000 Touch, Biorad, USA PTC-200, MJ Reseach Inc., Canada
Vortex	VWR, USA
Water Bath	Innova 3100, New Brunswick Scientific, USA

APPENDIX C

Molecular Biology Kits

Kits	Company
NucleoSpin Gel and PCR Clean-up	Macherey-Nagel, USA
Plasmid DNA purification (NucleoBond® Xtra Midi / Maxi)	Macherey-Nagel, USA
ZymoPure Plasmid Maxiprep Kit	Zymo Research, USA

APPENDIX D

Protein and DNA Molecular Weight Marker

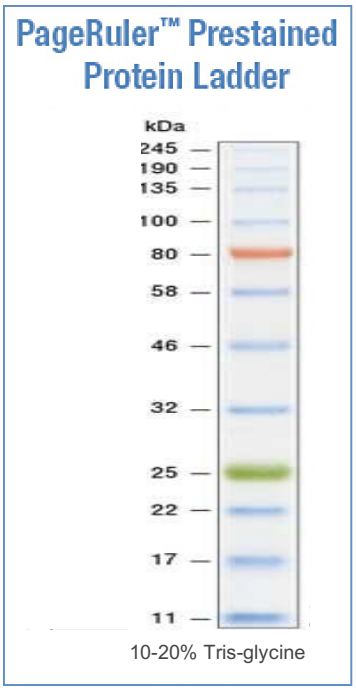

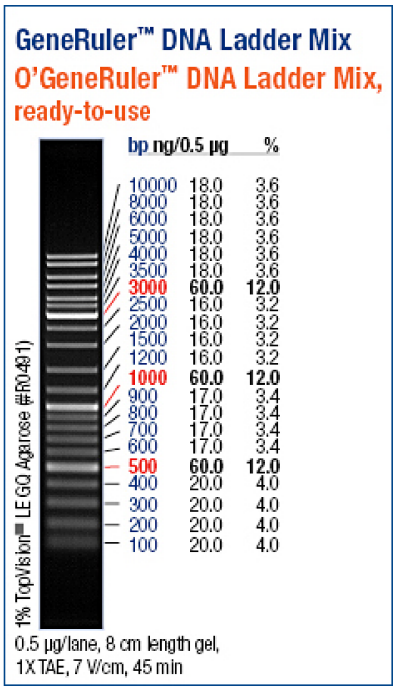

APPENDIX E

General panning protocol for anti-c-myc magnetic beads with soluble antigens

(Adapted from the lab of Prof. Ario de Marco)

Day 1:

b) Coating of the beads with the antigens

- Aliquot 50 µL of anti-c-myc magnetic beads in microtubes for each antigen to be used for negative and positive. Wash them 3 times with 1 mL of PBS 1X.
- Resuspend the beads in 50 µL of PBS 1X then add 50 µg each antigen and incubate under rotation overnight 4 ºC.

b) Inoculate 50 mL of minimal medium (MM) with TG1 cells and grow overnight at 37 ºC.

Day 2:

a) Blocking

Reagents: PBST-milk (PBS pH 7,4; 0,1% Tween20; 2% skim milk)

- Block 1 phage aliquot (10^{11}-10^{12} phages): add 1 mL of PBST-milk to the phages and incubate 30 min at 4 ºC under rotation.
- Block 50 µl of anti-c-myc magnetic beads: wash the beads 3 times with 1 mL of PBS then resuspend in 1 mL of PBST-milk and incubate 30 min at 4ºC under rotation.
- Block 4 (15 mL) tubes for washing step: add 5 mL of PBST-milk and incubate 30 min at 4 ºC with rotation.
- Block antigen loaded beads (from day1): first recover the beads on a magnetic stand then wash 3 times with 1 mL of PBS 1X to remove excess antigen then resuspend in 1 mL of PBST-milk and incubate 30 min at 4 ºC with rotation.

b) Panning:

i. Elimination of beads binders:

- Spin the phages for 5 min under 3000 g at 4 ºC to eliminate inactive phages.
- Recover the blocked beads on a magnet stand.

- Resuspend the beads with the phage supernatant (active phages) and incubate 60 min under rotation at 4 ºC.

ii. Negative selection:

- Place the blocked beads (from previous step) on a magnet stand. The supernatant is the phage library depleted from bead binders.
- Recover the blocked beads loaded with the negative selection antigen on a magnet stand and wash once with PBS 1X.
- Resuspend the negative selection beads with phage library depleted from bead binders and incubate 60 min under rotation at 4 ºC.
- Repeat the same steps with each negative selection antigen.

iii. Positive selection:

- Place the negative selection tube (from previous step) on a magnet stand. The supernatant is the phage library depleted from binders to antigens used for negative selection.
- Recover the blocked beads loaded with the positive selection antigen on a magnet stand and wash once with PBS 1X.
- Resuspend the positive selection beads with phage library depleted from binders to antigens used for negative selection and incubate 2 h under rotation at 4 ºC.

c) Inoculate 50 mL of 2xYT medium with 500 µL of overnight grown TG1 pre-culture and grow it at 37 ºC until OD_{600nm} is 0.5 (2-3 h).

d) Washing:

- Discard the blocking solution from 4 (15 mL) tubes and keep them on ice.
- Recover positive selection beads on a magnetic stand and resuspend in 250 µl PBS 1X. Wash the beads by adding them to the first washing tube loaded with 5 mL of PBS 1X.
- Recover the beads on a magnetic stand and repeat the wash using the same tube for 5 times.
- at the 5^{th} wash add only 2.5 mL of PBD 1X and transfer the beads to the second washing tube loaded with 2.5 mL of PBD 1X.

- Repeat the washes in the same manner with the third and fourth washing tubes. In total 20 washes will be performed.
- Discard the supernatant after the last wash.

e) Elution of phages

Reagents: Elution solution: Glycine 0,1 M pH 2,2. Neutralization solution: Tris-HCl 1 M pH 9,1.

- Add 900 µL of elution solution to the beads then transfer to a new 1.5 mL microtube and incubate 10 min with gentle shaking at 4 ºC.
- Place the tube on a magnetic stand and transfer the supernatant to a new 1.5 mL microtube then add 250 µL of neutralization solution (total volume 1150 µL).
- Add 10% glycerol to the 400 µL of eluted phages for formation of (*selected phage stock*) and save at -80 ºC.
- Infect 9,25 mL of TG1 bacteria (OD_{600nm} = 0.5) with 750 µL of neutralized eluate and incubate at 37ºC without shaking for 30 min.
- Pellet the infected TG1 bacteria by centrifuging at 3000 rpm for 15 min then resuspend the pellet in 1.8 mL of 2xYT medium.
- Spread the culture on three large agar plates (2xYT, 1% glucose, Amp) (600 µL each) and incubate them overnight at 37 ºC. This step is for amplification of positive clones, therefore TG1 cells are grown in glucose containing media. Glucose repress LacZ promoter of phage coat protein (g3p- to which nanobodies are fused). This is to reduce possible toxicity effects of fusion protein on host cells. TG-1 cells don't have any resistance, but phage plasmid is Amp R therefore culturing infected TG11 cells is all time under Amp control.

If second round of bio-panning is not needed proceed to Day 5.

<u>Day 3:</u>

a) Phage amplification

- Recover the bacteria from the three large agar plates with 6 mL of (2xYT, 30% glycerol). Use a plastic stick to collect the bacteria. Start by first plate then pipette the 6 mL the second then the third plate.
- First culture: mix the collected bacteria gently and put 100 µL in 20-30 mL of (2xYT, 1% glucose, Amp) and incubate at 37 °C under shaking until OD_{600nm}=0.5 (~ 2 h).
- Make 2 aliquots of the remaining bacterial sample for formation of stock of (*selected phage in TG1 bacteria*) and save at -80 ºC.
- Second culture: when OD_{600nm}=0.5 is reached put 10 mL in a sterile tube and add 0,45 µL of helper phages and incubate for 30 min at 37 °C without shaking.

Note: ~1 bacterium/20 phages. OD_{600nm}=0.5 correspond to $4x10^8$ bacteria/mL ($80x10^8$ phages). This corresponds to $8x10^{10}$ phages for 10mL of bacteria. Helper phages in stock are $1.8x10^{14}$ pfu/mL, therefore 0,45µL of helper phages should be used.

- Centrifuge for 10 min at 3300 rpm at RT then resuspend the bacteria in 50 mL of [2xYT/Amp/Kan (without glucose)] and incubate overnight at 37°C with shaking.

Note 1: Phage helper assist packaging and secretion of phages from TG1 cells to the medium.

Note 2: Phage helpers are Ken R therefor after phage production with phage helpers we always grow under Amp and Ken control and without glucose.

Note 3: all work with phages and phage helper is done with **filtered tips.**

b) Coating of the beads with the antigen for the second round of panning as descried above.

<u>Day 4:</u>

a) Phage precipitation

Reagents: Precipitation solution (30% PEG-6000; 2.5 mL NaCl, filter 0.22um, keep on ice)**.**

- Centrifuge 50 mL of the overnight culture for 15 min at 5000 rpm at 4 °C.
- Transfer 40 mL of the supernatant (containing active phages) to a clean tube and add 8 mL of chilled precipitation solution, mix gently, incubate on ice for 60 min.
- Pellet active phages by centrifuging for 15 min at 5000 rpm at 4 °C.
- Wash the pellet with 1.8 mL of PBS 1X.
- Transfer to a 2 mL microtube and centrifuge 10 min at 13000 rpm at 4 °C.

- Use 100 µL of supernatant (active phages) for blocking and proceed with same steps described above for the second round of bio-panning.
- Use the rest of the supernatant to make two aliquots and save at -80 ºC.

Day 5:

a) Phages extraction for monoclonal screening

- Recover the bacteria from the 3 large Petri dishes with 6mL of (2xYT, 30% glycerol) as described above.
- Mix gently, transfer 50 µL to a new tube for miniprep and freeze the rest in 2 aliquots.
- Start the bacterial transformation using chemicompetent TG1 cells.
- Proceed to screening for potential binders with ELISA

APPENDIX F

General protocol for screening phages with ELISA

(Adapted from the lab of Prof. Ario de Marco)

Day1:

a) 100 colony amplification (of transformed bacteria) for screening

- Put 1 mL/well of medium (2xYT, 1% glucose, Amp) in a sterile 2 mL 96 well plate.
- Pick 93 random colonies from the transformation plate with sterile toothpicks.
- leave 3 empty wells (medium only) for negative control.
- Cover with "breathable" paper-film, grow overnight, 37 °C, shaking 150 rpm.

Day 2:

a) Prepare glycerol plates for stock:

In a sterile flat bottom 96 well plate, put 120 µL of medium (2xYT+ 50% glycerol).

b) Prepare plates for second culture:

In a new sterile 2 mL 96 plate, put 1 mL/well of medium (2xYT, 1% glucose, Amp).

c) Prepare antigen plates for ELISA:

In a 96 well ELISA plate, put 1 µL g of diluted antigen in 100 µL of PBS 1X for each well. Incubate overnight 4 °C.

d) In plate phage production:

- Transfer 80 µL of the preculture to the corresponding wells of both new plates. Remember to keep the last three wells for negative control.
- Save the plates for stock in -80 ºC and grow the second culture plates 2.5 h at 37 °C, shaking 150 rpm.
- When the OD_{600nm}=0.5 (~2.5 h) infect with helper phages. Add 45 µL /well (1:1000 dilution in 2xYT). Grow 30 min 37 °C, no shaking.
- Pellet the bacteria (3000 rpm, 15 min, 4 °C). Control wells should not have any pallets.
- Discard the supernatant by vacuum with new tip for each well then resuspend the bacteria in 1 mL of medium (2xYT+Amp+Kan). Grow overnight at 30 °C, with shaking 150 rpm.

Day3:

a) Blocking:

Reagents: (2% BSA in PBS, keep on ice)

i. Block the antigen plates:

Add 100 µL /well of blocking solution to overnight grown antigen plates after discarding PBS 1X.

ii. Block the produced phages:

- Pellet bacteria from overnight culture (3000 rpm, 15 min).
- In a new flat plate add 25 µL /well of blocking solution for each 100 µL of phages.
- Block (both antigen and phage plates) for 45 min at 4 °C.

b) Phages-antigen binding

- Discard the blocking solution from the antigen plate and add 100 µL of blocked phages.
- Add only PBS 1X to control wells.
- Incubate for 2 h at 4°C.

c) ELISA

- Wash the plates four times with PBS. Discard the waste each time just by inverting the plate.
- Add 100 µL /well of α-M13 HRP conjugated (diluted 1:5000 in 1% BSA in PBS 1X).
- Incubate 60 min at 4°C.
- Wash the plates four times with PBS. Make sure the plates do not dry after the last wash.
- Add 50 µL /well of ELISA substrate (TMB).
- Stop the reaction with 100 µL /well of H2SO4 1 N.
- Read the absorbance at 450 nm with the plate reader.
- Interesting clones that have significant difference between target and negative control in relation to empty well controls can be tested in triplicates using glycerol plate stocks.

Important notes:

1. Keep the bench clean and regularly wiped with 2% bleach to limit phage cross-contamination and only use filtered tips to prevent aerosol contaminations.

2. Phages are known to survive standard autoclaving conditions and are not removed by 0.22 μm filtration. Therefor they are either killed by heat-treating dry autoclaved materials in oven for 4 hs at 105 ^{o}C, or by incubation in 2% bleach for at least 1 h.

APPENDIX G

Elementary and confirmatory ELISA results of first bio-panning

	Elementary ELISA																		Confirmatory ELISA									
	NbPATZ1:AgPATZ1		NbPATZ1:AgPATZ2		NbPATZ1:AgMiz		NbPATZ2:AgPATZ1		NbPATZ2:AgPATZ2		NbPATZ2:Ag Miz		NbMiz:AgPATZ1		NbMiz:AgPATZ2		NbMiz:AgMiz		NbPATZ1:AgPATZ1						NbPATZ1:AgMiz					
	original	corrected	original	corrected	original	corrected	original	corrected	original	corrected	original	corrected	original	corrected	original	corrected	original	corrected	1	corrected	2	corrected	3	corrected	1	corrected	2	corrected	3	corrected
A1	0,04	0,00	0,05	-0,04	0,05	0,00	0,05	0,00	0,04	0,00	0,04	0,00	0,05	0,00	0,05	0,00	0,04	-0,15										
A2	0,04	0,00	0,05	-0,04	0,05	0,00	0,98	0,94	0,65	0,60	1,13	1,09	0,18	0,12	0,15	0,11	0,09	-0,10										
A3	0,96	0,92	0,96	0,87	0,05	0,00	0,05	0,00	0,06	0,01	0,05	0,01	0,22	0,17	0,22	0,17	0,14	-0,06	1,08	0,99	1,01	0,93	1,05	0,96	0,98	0,90	1,00	0,92	1,01	0,93
A4	0,04	0,00	0,05	-0,03	0,11	0,06	0,35	0,30	0,19	0,14	0,51	0,46	0,53	0,48	0,58	0,54	0,40	0,20										
A5	0,05	0,00	0,05	-0,04	0,06	0,01	0,05	0,00	0,05	0,00	0,05	0,00	0,55	0,50	0,58	0,53	0,37	0,18										
A6	0,04	0,00	0,04	-0,04	0,48	0,43	0,05	0,00	0,05	0,00	0,05	0,00	0,67	0,62	0,73	0,68	0,39	0,20	0,66	0,57	0,71	0,63	0,61	0,52	0,64	0,56	0,64	0,55	0,70	0,62
A7	0,05	0,01	0,05	-0,04	0,31	0,26	0,05	0,00	0,05	0,00	0,04	0,00	0,64	0,59	0,67	0,62	0,26	0,07	0,51	0,43	0,52	0,43	0,37	0,28	0,37	0,28	0,29	0,20	0,32	0,24
A8	0,11	0,07	0,05	-0,04	0,24	0,19	0,73	0,68	0,58	0,53	0,92	0,87	0,09	0,04	0,08	0,04	0,07	-0,13	0,73	0,65	0,73	0,64	0,69	0,60	0,68	0,59	0,66	0,57	0,74	0,66
A9	0,09	0,05	0,05	-0,04	0,07	0,02	0,05	0,00	0,05	0,00	0,05	0,00	0,05	0,00	0,04	0,00	0,13	-0,06										
A10	0,05	0,00	0,05	-0,04	0,27	0,22	0,05	0,00	0,04	0,00	0,04	0,00	0,04	-0,01	0,05	0,00	0,04	-0,15	0,48	0,40	0,43	0,34	0,43	0,35	0,41	0,33	0,39	0,30	0,37	0,29
A11	0,04	0,00	0,09	0,00	0,13	0,09	0,04	-0,01	0,05	0,00	0,05	0,00	0,14	0,09	0,13	0,08	0,11	-0,08										
A12	0,05	0,00	0,05	-0,04	0,06	0,01	0,04	-0,01	0,05	0,00	0,05	0,01	0,08	0,03	0,07	0,03	0,07	-0,13										
B1	0,45	0,41	0,63	0,54	0,05	0,00	0,04	-0,01	0,05	0,00	0,05	0,00	0,05	0,00	0,05	0,00	0,05	-0,15	0,59	0,51	0,59	0,51	0,37	0,28	0,57	0,48	0,38	0,30	0,68	0,59
B2	0,05	0,00	0,05	-0,04	0,48	0,43	0,05	0,00	0,05	0,00	0,05	0,01	0,40	0,35	0,49	0,45	0,26	0,06	0,78	0,70	0,62	0,54	0,69	0,60	0,70	0,62	0,71	0,63	0,68	0,60
B3	0,14	0,09	0,15	0,06	0,05	0,00	0,05	0,00	0,04	0,00	0,05	0,00	0,07	0,02	0,05	0,00	0,04	-0,15										
B4	0,05	0,00	0,04	-0,04	0,20	0,15	0,05	0,00	0,05	0,00	0,06	0,01	0,35	0,30	0,48	0,44	0,26	0,07	0,62	0,53	0,61	0,52	0,65	0,56	0,56	0,48	0,43	0,34	0,66	0,58
B5	0,04	0,00	0,05	-0,04	0,05	0,00	0,30	0,25	0,31	0,26	0,57	0,53	0,42	0,37	0,62	0,57	0,36	0,17										
B6	0,08	0,04	0,09	0,00	0,57	0,52	0,06	0,02	0,06	0,02	0,07	0,02	0,06	0,01	0,11	0,06	0,07	-0,13	0,26	0,18	0,29	0,20	0,35	0,26	0,24	0,16	0,27	0,19	0,25	0,17
B7	0,04	-0,01	0,05	-0,04	0,25	0,20	0,04	0,00	0,04	0,00	0,12	0,08	0,15	0,10	0,17	0,12	0,12	-0,08	0,56	0,48	0,57	0,49	0,64	0,55	0,52	0,44	0,26	0,18	0,59	0,50
B8	0,05	0,00	0,05	-0,04	0,14	0,10	0,05	0,00	0,04	0,00	0,05	0,00	0,15	0,10	0,16	0,11	0,16	-0,04										
B9	0,05	0,01	0,04	-0,04	0,13	0,08	0,04	-0,01	0,04	0,00	0,05	0,00	0,16	0,11	0,19	0,14	0,33	0,13										
B10	0,04	0,00	0,05	-0,04	0,05	0,00	0,05	0,00	0,05	0,00	0,05	0,00	0,17	0,12	0,17	0,13	0,12	-0,07										
B11	0,05	0,00	0,05	-0,04	0,48	0,44	0,04	0,00	0,04	0,00	0,05	0,00	0,13	0,07	0,13	0,08	0,11	-0,08	0,45	0,37	0,45	0,37	0,49	0,40	0,40	0,32	0,49	0,41	0,47	0,38
B12	0,04	0,00	0,05	-0,04	0,24	0,19	0,04	0,00	0,04	0,00	0,05	0,00	0,50	0,45	0,53	0,48	0,40	0,20	0,65	0,56	0,64	0,55	0,63	0,54	0,58	0,49	0,52	0,44	0,75	0,66
C1	0,87	0,83	0,75	0,66	0,05	0,01	0,83	0,78	0,64	0,59	0,97	0,93	0,50	0,44	0,57	0,52	0,23	0,04	0,74	0,65	0,64	0,55	0,65	0,57	0,63	0,55	0,66	0,57	0,70	0,61
C2	0,05	0,00	0,05	-0,04	0,12	0,07	0,50	0,45	0,49	0,44	0,64	0,60	0,05	0,00	0,05	0,00	0,04	-0,15										
C3	0,04	0,00	0,05	-0,04	0,05	0,00	0,56	0,51	0,50	0,45	0,75	0,70	0,05	0,00	0,04	0,00	0,05	-0,15										
C4	0,21	0,16	0,23	0,14	0,05	0,00	0,13	0,08	0,11	0,06	0,23	0,19	0,34	0,29	0,49	0,45	0,31	0,11										
C5	0,14	0,09	0,16	0,07	0,57	0,52	0,42	0,37	0,57	0,53	0,78	0,74	0,09	0,04	0,12	0,07	0,09	-0,11	0,83	0,74	0,80	0,72	0,79	0,70	0,81	0,73	0,81	0,72	0,90	0,82
C6	0,04	0,00	0,05	-0,04	0,10	0,06	0,39	0,34	0,34	0,30	0,51	0,47	0,50	0,45	0,63	0,59	0,28	0,09										
C7	0,05	0,00	0,04	-0,04	0,14	0,10	0,05	0,01	0,05	0,00	0,06	0,01	0,07	0,02	0,07	0,03	0,08	-0,12										
C8	0,05	0,00	0,05	-0,04	0,09	0,04	0,64	0,59	0,49	0,45	0,73	0,68	0,06	0,01	0,07	0,02	0,06	-0,13										
C9	0,75	0,71	0,67	0,58	0,05	0,00	0,27	0,22	0,35	0,30	0,63	0,59	0,08	0,03	0,07	0,03	0,29	0,09	0,62	0,54	0,59	0,50	0,55	0,46	0,30	0,21	0,30	0,22	0,27	0,18
C10	0,04	0,00	0,05	-0,04	0,05	0,00	0,05	0,00	0,05	0,00	0,07	0,02	0,16	0,11	0,08	0,03	0,06	-0,14										
C11	0,40	0,36	0,51	0,42	0,05	0,00	0,29	0,24	0,53	0,48	0,81	0,76	0,05	0,00	0,04	0,00	0,05	-0,15	0,79	0,74	0,80	0,76	0,80	0,75	0,84	0,80	0,81	0,77	0,76	0,71
C12	0,04	0,00	0,05	-0,04	0,05	0,00	0,31	0,26	0,35	0,30	0,62	0,58	0,05	0,00	0,04	0,00	0,05	-0,15										
D1	0,06	0,01	0,07	-0,02	0,25	0,20	0,55	0,50	0,42	0,38	0,70	0,66	0,05	0,00	0,06	0,02	0,05	-0,15	0,75	0,70	0,78	0,73	0,70	0,66	0,78	0,73	0,69	0,64	0,82	0,77
D2	0,05	0,01	0,05	-0,03	0,12	0,07	0,43	0,39	0,31	0,27	0,45	0,40	0,13	0,08	0,30	0,25	0,11	-0,09										
D3	0,05	0,00	0,05	-0,04	0,04	-0,01	0,53	0,49	0,45	0,40	0,47	0,42	0,09	0,04	0,15	0,10	0,10	-0,10										
D4	0,05	0,00	0,05	-0,04	0,04	-0,01	0,65	0,60	0,42	0,37	0,86	0,81	0,22	0,16	0,22	0,17	0,11	-0,09										
D5	0,05	0,00	0,05	-0,04	0,05	0,00	0,65	0,60	0,53	0,49	0,76	0,71	0,15	0,10	0,26	0,21	0,22	0,03										
D6	0,06	0,01	0,07	-0,02	0,05	0,00	0,41	0,36	0,35	0,31	0,52	0,47	0,29	0,24	0,58	0,54	0,21	0,02										
D7	0,13	0,08	0,17	0,08	0,05	0,00	0,85	0,81	0,80	0,75	1,07	1,03	0,47	0,42	0,60	0,55	0,32	0,13										
D8	0,48	0,44	0,76	0,67	0,04	0,00	0,67	0,62	0,57	0,52	0,83	0,78	0,05	0,00	0,04	-0,01	0,04	-0,15	0,26	0,21	0,12	0,07	0,58	0,54	0,58	0,53	0,59	0,55	0,59	0,54
D9	0,71	0,66	0,27	0,18	0,06	0,01	0,26	0,21	0,43	0,39	0,63	0,58	0,65	0,59	0,80	0,75	0,35	0,15	0,69	0,64	0,69	0,65	0,65	0,61	0,24	0,20	0,20	0,15	0,26	0,21
D10	0,05	0,00	0,05	-0,04	0,05	0,00	0,14	0,09	0,13	0,09	0,31	0,26	0,65	0,60	0,94	0,89	0,33	0,13										
D11	0,93	0,89	1,08	0,99	0,05	0,00	0,37	0,33	0,34	0,29	0,72	0,67	0,05	0,00	0,05	0,00	0,04	-0,15	0,86	0,81	0,72	0,68	0,73	0,68	0,71	0,67	0,74	0,69	0,71	0,66
D12	0,05	0,00	0,05	-0,03	0,06	0,01	0,26	0,21	0,33	0,29	0,86	0,82	0,06	0,01	0,05	0,01	0,05	-0,14										
E1	0,05	0,01	0,07	-0,02	0,06	0,01	0,05	0,00	0,05	0,00	0,05	0,00	0,14	0,09	0,15	0,11	0,07	-0,13										
E2	0,05	0,00	0,05	-0,04	0,93	0,89	0,08	0,03	0,05	0,01	0,05	0,00	0,14	0,09	0,17	0,12	0,11	-0,09	0,08	0,03	0,11	0,06	0,05	0,00	0,09	0,04	0,05	0,00	0,07	0,02
E3	0,05	0,00	0,05	-0,04	0,05	0,01	0,06	0,01	0,06	0,01	0,06	0,01	0,08	0,03	0,05	0,01	0,09	-0,10										
E4	0,05	0,01	0,06	-0,03	0,17	0,12	0,05	0,00	0,05	0,00	0,05	0,00	0,42	0,37	0,47	0,42	0,25	0,06										
E5	0,05	0,00	0,06	-0,03	0,62	0,57	0,04	0,00	0,05	0,00	0,05	0,00	0,48	0,42	0,40	0,35	0,31	0,11	0,72	0,68	0,60	0,56	0,62	0,58	0,61	0,57	0,64	0,60	0,63	0,58
E6	0,04	0,00	0,05	-0,04	0,20	0,15	0,05	0,00	0,05	0,00	0,05	0,01	0,48	0,43	0,19	0,14	0,13	-0,06										
E7	0,04	0,00	0,05	-0,04	0,05	0,01	0,05	0,00	0,05	0,00	0,06	0,01	0,50	0,45	0,65	0,60	0,41	0,21										
E8	0,04	0,00	0,04	-0,05	0,05	0,00	0,17	0,12	0,23	0,19	0,43	0,38	0,12	0,06	0,12	0,08	0,07	-0,13										
E9	0,05	0,00	0,05	-0,04	0,05	0,00	0,24	0,19	0,22	0,18	0,62	0,57	0,05	0,00	0,05	0,00	0,05	-0,15										
E10	0,05	0,00	0,05	-0,04	0,05	0,00	0,08	0,03	0,05	0,00	0,05	0,00	0,05	0,00	0,05	0,00	0,04	-0,15										
E11	0,05	0,00	0,05	-0,04	0,05	0,00	0,52	0,47	0,40	0,35	0,80	0,75	0,05	0,00	0,05	0,00	0,04	-0,16										
E12	0,31	0,27	0,38	0,29	0,06	0,01	0,05	0,00	0,05	0,01	0,07	0,03	0,48	0,43	0,53	0,49	0,37	0,18	0,68	0,64	0,68	0,64	0,66	0,61	0,68	0,63	0,69	0,65	0,76	0,72
F1	0,05	0,00	0,06	-0,03	0,08	0,03	0,10	0,06	0,09	0,05	0,12	0,08	0,05	0,00	0,06	0,01	0,05	-0,14										
F2	0,06	0,02	0,08	-0,01	0,49	0,44	0,11	0,07	0,12	0,07	0,10	0,05	0,18	0,13	0,27	0,23	0,17	-0,03	0,05	0,01	0,05	0,00	0,05	0,01	0,05	0,01	0,05	0,00	0,06	0,01
F3	0,05	0,00	0,05	-0,03	0,05	0,00	0,07	0,02	0,08	0,03	0,08	0,03	0,07	0,02	0,06	0,01	0,05	-0,15										
F4	0,05	0,00	0,05	-0,04	0,68	0,63	0,66	0,61	0,50	0,45	0,94	0,89	0,36	0,31	0,46	0,41	0,43	0,23	0,33	0,29	0,32	0,27	0,35	0,30	0,29	0,24	0,28	0,24	0,31	0,26
F5	0,05	0,00	0,05	-0,04	0,19	0,14	0,58	0,54	0,05	0,00	0,82	0,78	0,13	0,08	0,16	0,11	0,13	-0,07										
F6	0,04	0,00	0,05	-0,04	0,05	0,01	0,31	0,26	0,28	0,24	0,58	0,54	0,08	0,03	0,22	0,18	0,07	-0,13										
F7	0,04	0,00	0,05	-0,04	0,05	0,00	0,17	0,12	0,18	0,14	0,51	0,46	0,44	0,39	0,48	0,44	0,28	0,08										
F8	0,77	0,73	0,86	0,78	0,15	0,10	0,04	-0,01	0,04	0,00	0,05	0,00	0,05	0,00	0,04	0,00	0,04	-0,15	0,83	0,78	0,66	0,61	0,70	0,65	0,65	0,61	0,67	0,62	0,66	0,61
F9	0,50	0,46	0,04	-0,04	0,22	0,17	0,04	0,00	0,05	0,00	0,05	0,00	0,05	0,00	0,05	0,00	0,05	-0,15	0,54	0,49	0,57	0,53	0,54	0,49	0,13	0,08	0,10	0,05	0,11	0,06
F10	0,05	0,00	0,05	-0,04	0,04	0,00	0,04	0,00	0,04	0,00	0,05	0,01	0,05	0,00	0,05	0,01	0,05	-0,15										
F11	0,05	0,00	0,05	-0,04	0,04	0,00	0,10	0,06	0,08	0,04	0,20	0,15	0,05	0,00	0,08	0,03	0,05	-0,15										
F12	0,04	0,00	0,05	-0,04	0,61	0,56	0,05	0,00	0,05	0,00	0,06	0,01	0,68	0,63	0,82	0,78	0,57	0,38	0,70	0,65	0,59	0,54	0,60	0,56	0,59	0,55	0,62	0,57	0,62	0,57
G1	0,94	0,90	0,45	0,36	0,09	0,04	0,05	0,00	0,08	0,04	0,06	0,01	0,48	0,43	0,53	0,49	0,28	0,08	0,63	0,59	0,64	0,59	0,61	0,56	0,24	0,20	0,21	0,17	0,24	0,19
G2	0,83	0,78	0,94	0,85	0,04	0,00	0,09	0,05	0,10	0,06	0,17	0,13	0,06	0,01	0,09	0,05	0,08	-0,12	0,90	0,85	0,78	0,73	0,85	0,80	0,34	0,30	0,41	0,36	0,44	0,39
G3	0,05	0,01	0,08	-0,01	0,05	0,00	0,07	0,02	0,08	0,03	0,17	0,13	0,05	-0,01	0,05	0,00	0,04	-0,15										
G4	0,17	0,13	0,28	0,19	0,04	-0,01	0,48	0,43	0,51	0,46	0,75	0,70	0,06	0,01	0,07	0,02	0,06	-0,14										
G5	0,17	0,13	0,30	0,21	0,05	0,00	0,08	0,03	0,12	0,07	0,13	0,08	0,12	0,07	0,13	0,08	0,20	0,00										
G6	0,53	0,49	0,79	0,70	0,12	0,07	0,37	0,32	0,55	0,50	0,79	0,74	0,49	0,43	0,67	0,62	0,40	0,20	0,87	0,81	0,95	0,89	0,11	0,05	0,41	0,35	0,10	0,05	0,78	0,73
G7	1,04	0,99	1,38	1,29	0,07	0,02	0,05	0,00	0,04	0,00	0,05	0,00	0,18	0,13	0,24	0,20	0,18	-0,01	1,13	1,07	0,79	0,73	0,85	0,79	0,97	0,92	0,94	0,88	0,96	0,90
G8	0,04	0,00	0,05	-0,03	0,05	0,00	0,54	0,49	0,55	0,50	0,84	0,79	0,27	0,22	0,24	0,20	0,16	-0,03										
G9	0,29	0,24	0,51	0,42	0,05	0,00	0,14	0,09	0,13	0,09	0,30	0,25	0,18	0,13	0,22	0,18	0,04	-0,16	0,06	0,00	0,05	-0,01	0,06	0,00	0,06	0,00	0,06	0,01	0,05	-0,01
G10	0,05	0,00	0,06	-0,03	0,05	0,00	0,49	0,45	0,42	0,37	0,80	0,75	0,19	0,13	0,22	0,18	0,14	-0,05										
G11	0,80	0,76	1,11	1,02	0,05	0,00	0,05	0,00	0,05	0,00	0,06	0,02	0,06	0,01	0,06	0,02	0,05	-0,14	0,81	0,75	0,68	0,62	0,70	0,64	0,68	0,62	0,71	0,65	0,70	0,64
G12	0,05	0,00	0,05	-0,04	0,62	0,57	0,56	0,51	0,65	0,61	0,89	0,85	0,05	0,00	0,05	0,01	0,05	-0,15	0,11	0,05	0,08	0,03	0,11	0,05	0,10	0,04	0,14	0,08	0,09	0,04
H1	0,06	0,01	0,24	0,15	0,06	0,01	0,49	0,44	0,56	0,52	0,70	0,66	0,64	0,59	0,62	0,57	0,40	0,21										
H2	0,23	0,19	0,40	0,31	0,06	0,01	0,44	0,40	0,49	0,44	0,54	0,49	0,10	0,05	0,15	0,11	0,12	-0,07	0,29	0,24	0,29	0,24	0,29	0,23	0,33	0,27	0,32	0,26	0,29	0,23
H3	0,64	0,60	0,58	0,49	0,08	0,03	0,55	0,51	0,65	0,60	0,90	0,85	0,37	0,32	0,75	0,71	0,27	0,08	0,05	0,00	0,08	0,02	0,06	0,01	0,06	0,00	0,09	0,03	0,06	0,00
H4	0,09	0,04	0,16	0,07	0,05	0,01	0,09	0,04	0,10	0,06	0,22	0,18	0,32	0,27	0,49	0,44	0,29	0,10										
H5	0,46	0,41	0,57	0,48	0,05	0,00	0,78	0,73	0,48	0,44	0,82	0,77	0,43	0,37	0,43	0,38	0,29	0,09	0,85	0,79	0,85	0,80	0,69	0,64	0,85	0,79	0,74	0,68	0,66	0,60
H6	0,89	0,84	0,84	0,75	0,05	0,00	0,40	0,35	0,51	0,47	0,73	0,69	0,42	0,37	0,67	0,62	0,29	0,10	1,85	1,79	1,85	1,80	1,69	1,64	1,85	1,79	1,74	1,68	1,66	1,60
H7	1,00	0,95	0,85	0,76	0,05	0,00	0,32	0,27	0,47	0,42	0,84	0,79	0,40	0,35	0,50	0,45	0,28	0,08	0,67	0,61	0,67	0,61	0,11	0,05	0,64	0,58	0,11	0,05	0,86	0,80
H8	0,05	0,01	0,37	0,28	0,05	0,01	0,04	0,00	0,05	0,00	0,05	0,00	0,18	0,12	0,23	0,18	0,13	-0,07	0,06	0,00	0,06	0,00	0,06	0,00	0,06	0,01	0,06	0,00	0,08	0,02
H9	0,20	0,15	0,25	0,16	0,06	0,01	0,05	0,00	0,04	0,00	0,05	0,00	0,05	0,00	0,06	0,01	0,12	-0,08										
H10	0,05	0,00	0,16	0,07	1,43	1,38	0,05	0,00	0,05	0,00	0,05	0,00	0,05	0,00	0,05	0,00	0,05	-0,15										
H11	0,05	0,00	0,05	-0,04	0,05	0,00	0,05	0,00	0,05	0,00	0,05	0,00	0,05	0,00	0,05	0,00	0,05	-0,15										
H12	0,04	0,00	0,05	-0,03	0,05	0,00	0,05	0,00	0,05	0,00	0,04	-0,01	0,06	0,00	0,05	0,00	0,05	-0,15										

Original absolute values of absorbance and corrected values (blank subtracted) are shown.

APPENDIX H

Elementary and confirmatory ELISA results of second bio-panning

	Elementary ELISA						Confirmatory ELISA															
	NbPATZ1:AgPATZ1		NbPATZ1:AgPATZ2		NbPATZ1:AgMiz		NbPATZ1:AgPATZ1						NbPATZ1:AgPATZ2						NbPATZ1:AgMiz					
	original	corrected	original	corrected	original	corrected	original 1	corrected 1	original 2	corrected 2	original 3	corrected 3	original 1	corrected 1	original 2	corrected 2	original 3	corrected 3	original 1	corrected 1	original 2	corrected 2	original 3	corrected 3
A1	0,05	0,00	0,05	0,00	0,05	-0,01																		
A2	0,07	0,02	0,11	0,06	0,14	0,08																		
A3	0,38	0,33	0,06	0,01	0,06	0,00	0,81	0,76	0,61	0,57	0,89	0,85	0,52	0,47	0,32	0,27	0,20	0,15	0,21	0,16	0,12	0,07	0,23	0,18
A4	0,06	0,01	0,04	0,00	0,05	-0,01																		
A5	0,37	0,32	0,16	0,11	0,08	0,02	0,24	0,19	0,29	0,25	0,28	0,24	0,10	0,05	0,11	0,06	0,11	0,06	0,07	0,02	0,08	0,03	0,08	0,03
A6	0,34	0,29	0,31	0,27	0,24	0,18																		
A7	0,15	0,10	0,19	0,14	0,10	0,04																		
A8	0,32	0,27	0,25	0,20	0,22	0,16																		
A9	0,04	-0,01	0,04	0,00	0,05	-0,01																		
A10	0,05	0,00	0,05	0,00	0,05	-0,01																		
A11	0,05	0,00	0,04	0,00	0,16	0,10																		
A12	0,04	-0,01	0,05	0,00	0,27	0,21	0,10	0,05	0,06	0,02	0,12	0,08	0,40	0,35	0,38	0,33	0,42	0,36	0,13	0,08	0,19	0,14	0,26	0,21
B1	0,05	-0,01	0,05	0,00	0,05	-0,01																		
B2	0,06	0,01	0,05	0,00	0,07	0,01																		
B3	0,05	0,00	0,04	0,00	0,04	-0,02																		
B4	0,04	-0,01	0,04	0,00	0,07	0,01																		
B5	0,04	-0,01	0,04	0,00	0,05	-0,01																		
B6	0,04	-0,01	0,04	-0,01	0,04	-0,02																		
B7	0,04	-0,01	0,04	-0,01	0,05	-0,01																		
B8	0,05	0,00	0,05	0,00	0,05	-0,01																		
B9	0,05	0,00	0,11	0,07	0,11	0,05																		
B10	0,04	-0,01	0,08	0,03	0,08	0,02																		
B11	0,04	-0,01	0,05	0,00	0,05	-0,01																		
B12	0,26	0,21	0,17	0,13	0,53	0,47	0,57	0,52	0,59	0,54	0,79	0,74	0,82	0,77	0,77	0,71	0,78	0,73	0,58	0,53	0,58	0,53	0,63	0,58
C1	0,05	0,00	0,04	-0,01	0,05	-0,01																		
C2	0,35	0,30	0,61	0,56	0,54	0,48	0,53	0,49	0,56	0,52	0,51	0,47	1,40	1,35	1,04	0,99	1,03	0,97	0,90	0,85	0,76	0,71	0,79	0,74
C3	0,30	0,25	0,12	0,07	0,09	0,03	0,48	0,44	0,58	0,53	0,57	0,53	0,40	0,35	0,47	0,42	0,44	0,39	0,19	0,14	0,36	0,31	0,21	0,16
C4	0,05	0,00	0,09	0,04	0,13	0,07																		
C5	0,04	-0,01	0,05	0,00	0,05	-0,01																		
C6	0,04	-0,01	0,04	-0,01	0,04	-0,02																		
C7	0,04	-0,01	0,04	-0,01	0,06	0,01																		
C8	0,45	0,40	0,06	0,02	0,11	0,05	0,43	0,39	0,41	0,37	0,42	0,38	0,26	0,20	0,23	0,18	0,33	0,28	0,09	0,04	0,21	0,16	0,39	0,33
C9	0,06	0,01	0,08	0,03	0,12	0,06																		
C10	0,25	0,20	0,06	0,02	0,07	0,01	0,49	0,45	0,51	0,46	0,52	0,47	0,19	0,14	0,18	0,13	0,15	0,10	0,08	0,03	0,11	0,06	0,11	0,05
C11	0,20	0,15	0,27	0,22	0,32	0,26	0,61	0,57	0,53	0,49	0,54	0,49	1,37	1,32	0,06	0,01	1,03	0,98	0,74	0,68	0,75	0,70	0,86	0,80
C12	0,05	0,00	0,07	0,02	0,20	0,14																		
D1	0,07	0,02	0,05	0,00	0,05	-0,01																		
D2	0,15	0,10	0,26	0,22	0,23	0,17	0,25	0,21	0,27	0,23	0,25	0,20	0,74	0,68	0,93	0,88	0,87	0,82	0,61	0,56	0,53	0,48	0,53	0,48
D3	0,05	0,00	0,05	0,00	0,04	-0,02																		
D4	0,04	-0,01	0,05	0,00	0,05	-0,01																		
D5	0,04	-0,01	0,04	-0,01	0,05	-0,01																		
D6	0,04	-0,01	0,04	-0,01	0,05	-0,01																		
D7	0,04	-0,01	0,04	-0,01	0,04	-0,02																		
D8	0,04	-0,01	0,05	0,00	0,06	0,00																		
D9	0,05	0,00	0,05	0,00	0,05	-0,01																		
D10	0,12	0,07	0,34	0,29	0,46	0,40	0,40	0,36	0,39	0,34	0,34	0,30	1,01	0,96	0,85	0,80	1,04	0,99	0,56	0,51	0,64	0,59	0,60	0,55
D11	0,06	0,01	0,06	0,01	0,09	0,03																		
D12	0,32	0,27	0,10	0,05	0,24	0,18	0,61	0,56	0,60	0,55	0,65	0,61	0,43	0,37	0,44	0,38	0,30	0,25	0,13	0,07	0,17	0,12	0,16	0,11
E1	0,31	0,26	0,06	0,01	0,06	0,00	0,59	0,55	0,54	0,50	0,58	0,53	0,12	0,06	0,15	0,10	0,16	0,11	0,16	0,11	0,09	0,04	0,08	0,03
E2	0,51	0,46	0,25	0,20	0,11	0,05	0,63	0,58	0,73	0,68	0,69	0,65	0,64	0,59	0,70	0,65	0,65	0,60	0,28	0,23	0,27	0,22	0,24	0,19
E3	0,07	0,02	0,08	0,03	0,07	0,01																		
E4	0,07	0,02	0,06	0,01	0,11	0,05																		
E5	0,21	0,16	0,08	0,03	0,17	0,11																		
E6	0,29	0,24	0,10	0,05	0,09	0,03	0,71	0,66	0,69	0,65	0,71	0,66	0,77	0,71	0,46	0,41	0,73	0,67	0,03	-0,02	0,49	0,44	0,50	0,45
E7	0,30	0,25	0,09	0,04	0,11	0,05	0,64	0,60	0,59	0,55	0,65	0,61	0,56	0,51	0,54	0,49	0,46	0,40	0,31	0,26	0,30	0,25	0,28	0,22
E8	0,35	0,30	0,22	0,17	0,18	0,12																		
E9	0,04	-0,01	0,04	-0,01	0,06	0,00																		
E10	0,05	0,00	0,12	0,07	0,08	0,02																		
E11	0,34	0,29	0,29	0,25	0,33	0,27																		
E12	0,05	0,00	0,21	0,17	0,37	0,31	0,35	0,30	0,08	0,03	0,08	0,04	0,75	0,70	0,70	0,65	0,69	0,64	0,27	0,22	0,28	0,23	0,22	0,17
F1	0,11	0,06	0,07	0,02	0,06	0,00																		
F2	0,49	0,44	0,21	0,16	0,11	0,05	0,64	0,60	0,69	0,65	0,69	0,65	0,62	0,56	0,53	0,48	0,64	0,59	0,25	0,20	0,22	0,17	0,25	0,20
F3	0,48	0,43	0,17	0,13	0,17	0,11	0,70	0,65	0,66	0,62	0,70	0,65	0,59	0,54	0,39	0,33	0,58	0,53	0,47	0,42	0,49	0,44	0,44	0,39
F4	0,04	-0,01	0,04	0,00	0,05	-0,01																		
F5	0,05	-0,01	0,05	0,00	0,04	-0,02																		
F6	0,32	0,27	0,23	0,18	0,27	0,21																		
F7	0,05	0,00	0,04	0,00	0,05	-0,01																		
F8	0,32	0,27	0,10	0,06	0,10	0,04	0,66	0,62	0,65	0,60	0,66	0,61	0,34	0,28	0,57	0,52	0,29	0,24	0,24	0,19	0,26	0,21	0,17	0,11
F9	0,25	0,20	0,05	0,00	0,08	0,02	0,62	0,58	0,62	0,57	0,61	0,56	0,31	0,26	0,26	0,20	0,26	0,21	0,07	0,02	0,06	0,01	0,08	0,02
F10	0,09	0,04	0,14	0,09	0,14	0,08																		
F11	0,39	0,34	0,50	0,46	0,48	0,42	0,69	0,64	0,75	0,70	0,68	0,63	1,57	1,52	1,80	1,75	1,73	1,68	0,69	0,64	0,77	0,71	0,65	0,59
F12	0,04	-0,01	0,05	0,00	0,16	0,10																		
G1	0,64	0,59	0,46	0,41	0,27	0,21	0,67	0,63	0,74	0,69	0,71	0,66	0,57	0,52	0,82	0,76	0,94	0,89	0,37	0,32	0,42	0,37	0,36	0,31
G2	0,05	0,00	0,04	0,00	0,05	-0,01																		
G3	0,05	0,00	0,05	0,00	0,05	-0,01																		
G4	0,05	0,00	0,05	0,00	0,05	-0,01																		
G5	0,04	-0,01	0,04	0,00	0,05	-0,01																		
G6	0,05	0,00	0,06	0,01	0,07	0,01																		
G7	0,05	0,00	0,05	0,00	0,06	0,00																		
G8	0,32	0,26	0,15	0,11	0,22	0,16																		
G9	0,28	0,23	0,14	0,09	0,16	0,10																		
G10	0,05	0,00	0,04	0,00	0,05	-0,01																		
G11	0,05	0,00	0,07	0,02	0,16	0,10																		
G12	0,05	0,00	0,08	0,04	0,06	0,00																		
H1	0,11	0,06	0,05	0,00	0,06	0,00																		
H2	0,07	0,02	0,05	0,00	0,06	0,00																		
H3	0,51	0,46	0,25	0,20	0,10	0,04	0,66	0,62	0,51	0,47	0,64	0,60	0,35	0,30	0,80	0,75	0,60	0,54	0,23	0,18	0,26	0,21	0,20	0,15
H4	0,50	0,45	0,32	0,27	0,41	0,35	0,77	0,72	0,73	0,69	0,73	0,69	0,81	0,76	0,86	0,81	0,78	0,72	0,70	0,65	0,89	0,84	0,71	0,66
H5	0,05	0,00	0,05	0,00	0,05	-0,01																		
H6	0,53	0,48	0,20	0,15	0,31	0,25	0,70	0,65	0,73	0,68	0,69	0,64	0,65	0,60	0,64	0,59	0,37	0,32	0,52	0,47	0,49	0,44	0,53	0,48
H7	0,05	0,00	0,05	0,01	0,05	-0,01																		
H8	0,05	0,00	0,04	0,00	0,06	0,00																		
H9	0,06	0,01	0,17	0,12	0,27	0,21	0,08	0,04	0,08	0,04	0,08	0,04	0,35	0,29	0,31	0,26	0,52	0,47	0,54	0,49	0,58	0,53	0,30	0,25
H10	0,05	0,00	0,13	0,08	0,07	0,01	0,04	0,00	0,04	0,00	0,04	0,00	0,06	0,00	0,05	0,00	0,05	0,00	0,06	0,00	0,05	0,00	0,05	0,00
H11	0,05	0,00	0,22	0,17	0,05	-0,01																		
H12	0,05	0,00	0,05	0,00	0,19	0,13																		

Original absolute values of absorbance and corrected values (blank subtracted) are shown.

APPENDIX I

Maps of plasmids

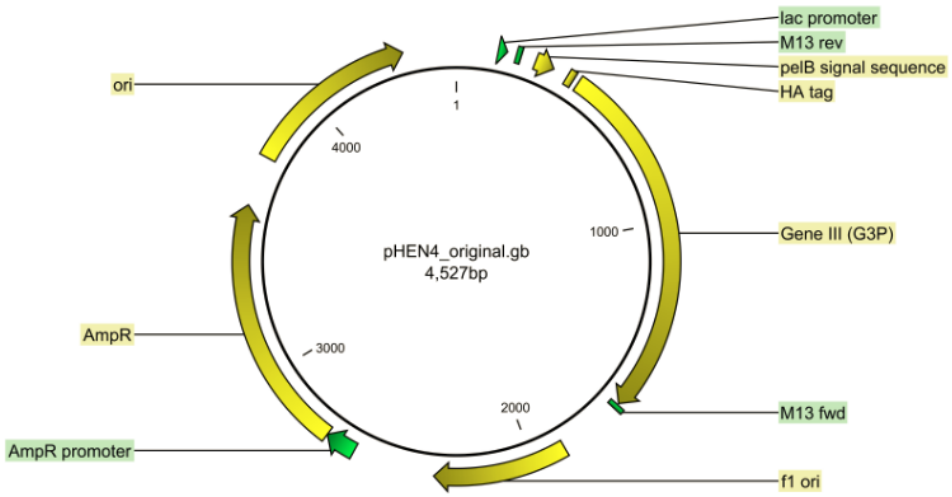

The map of pHEN4 plasmid

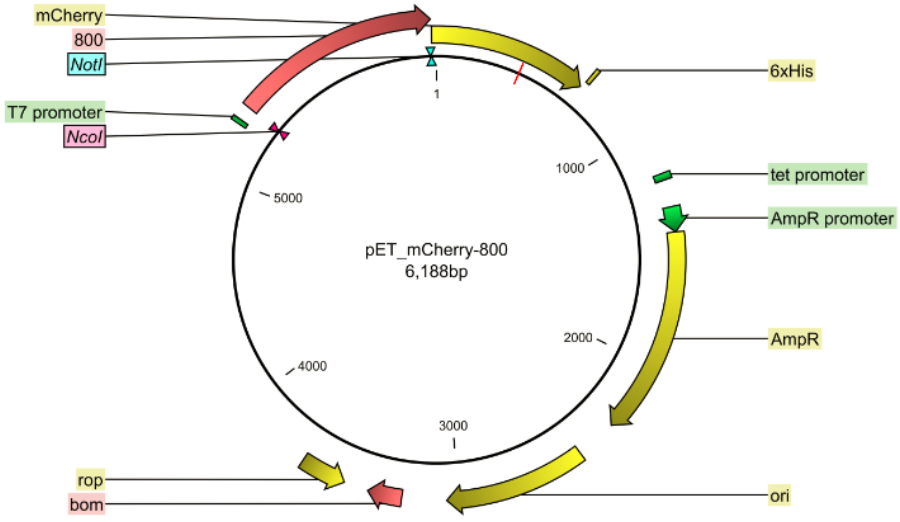

The map of pET_mCherry-800 plasmid

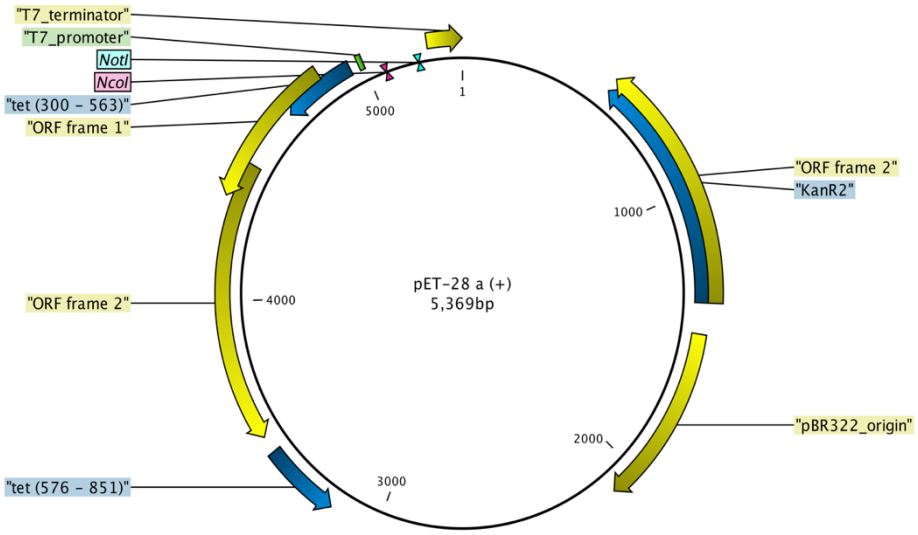

The map of pET-28a (+) plasmid

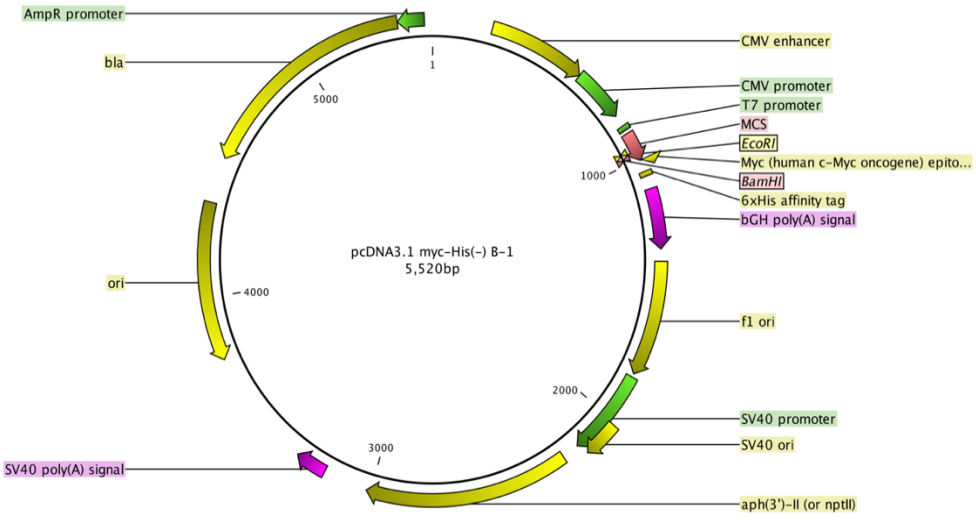

The map of pcDNA3.1 Myc His B (-) plasmid

APPENDIX J

Nanobody DNA Sequences

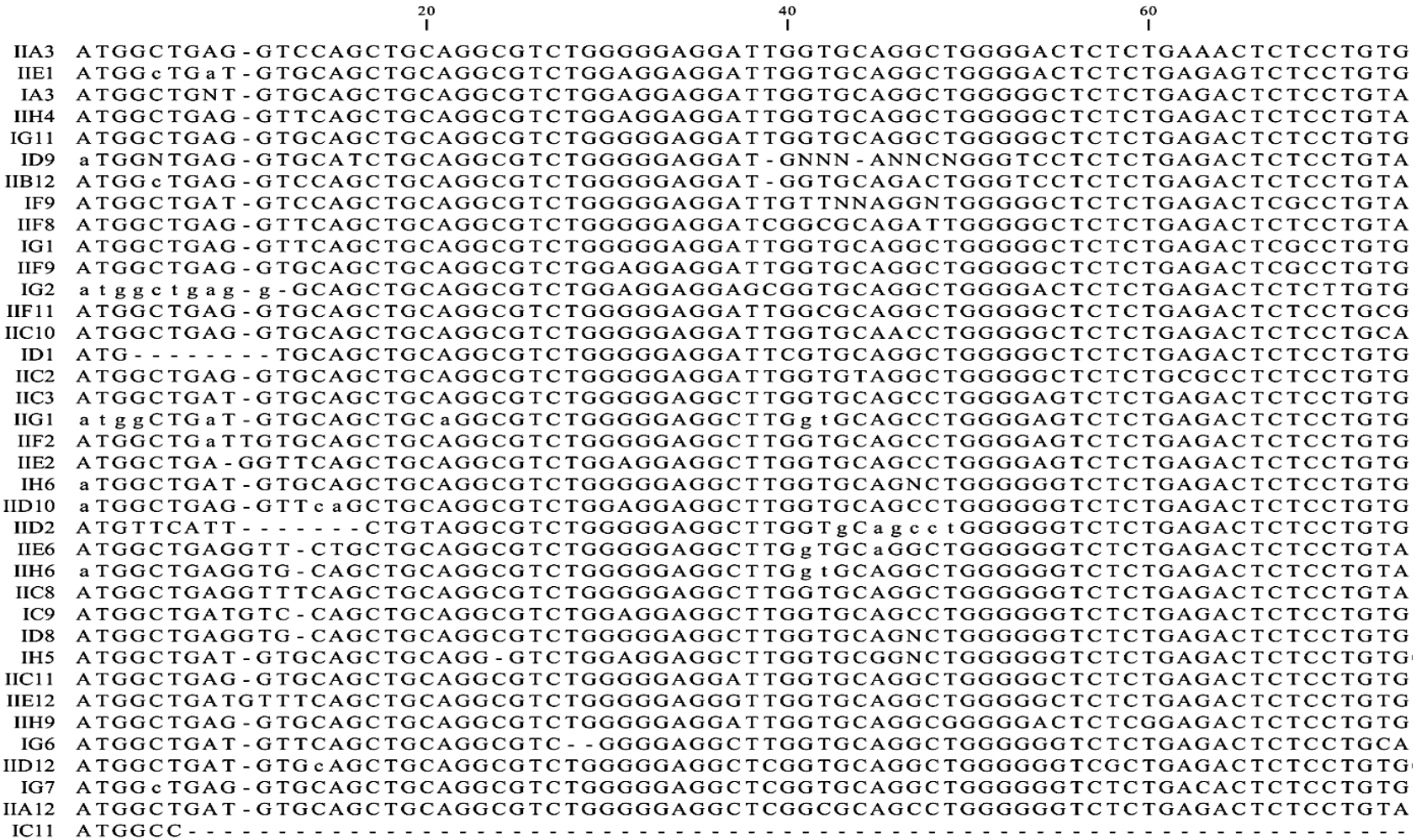

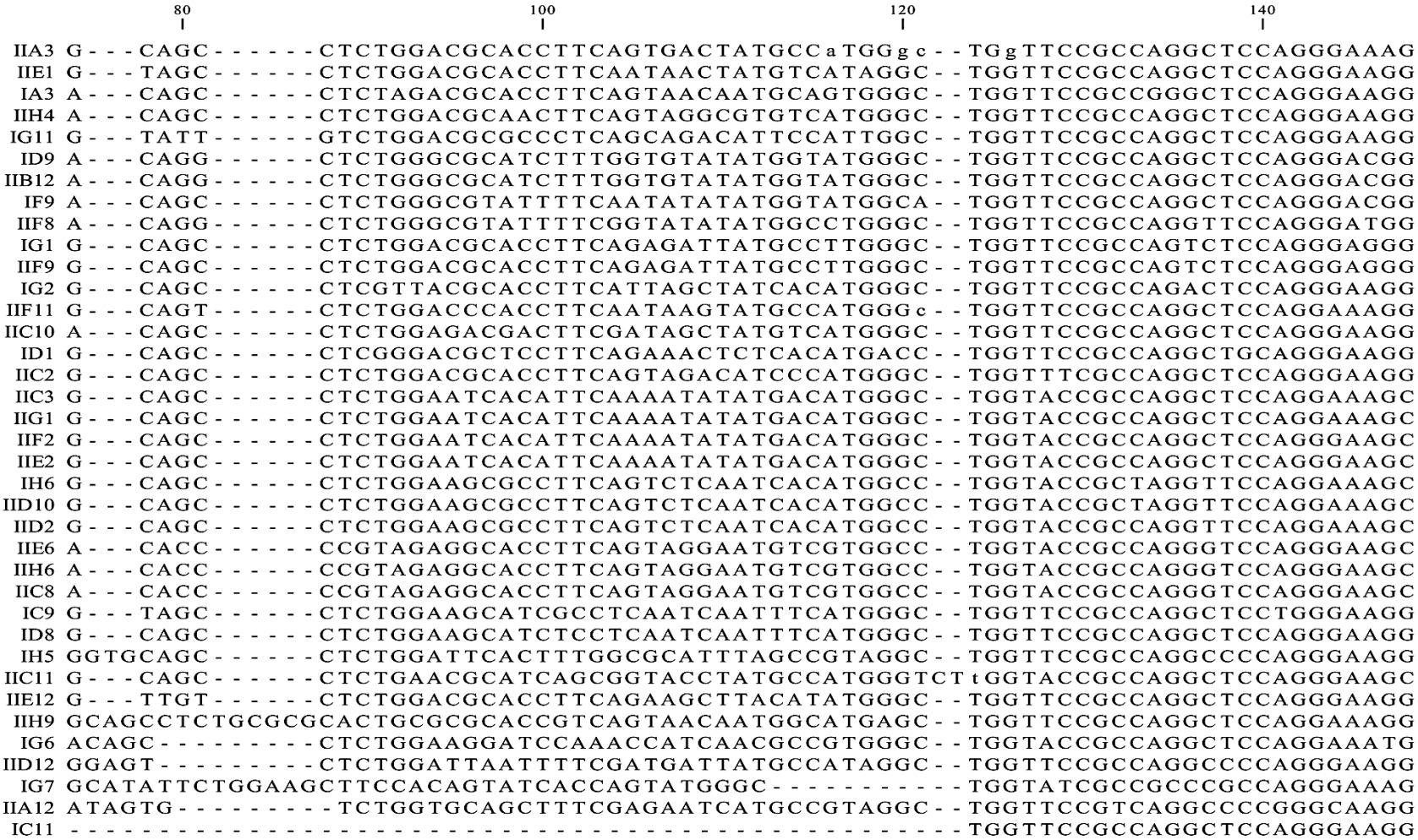
80
100
120
140
IIA3 G - - - CAGC - - - - - - - CTCTGGACGCACCTTCAGTGACTATGCC a TGG g c - - TG g TTCCGCCAGGCTCCAGGGAAAG
IIE1 G - - - TAGC - - - - - - - CTCTGGACGCACCTTCAATAACTATGTCATAGGC - - TGGTTCCGCCAGGCTCCAGGGAAGG
IA3 A - - - CAGC - - - - - - - CTCTAGACGCACCTTCAGTAACAATGCAGTGGGC - - TGGTTCCGCCGGGCTCCAGGGAAGG
IIH4 A - - - CAGC - - - - - - - CTCTGGACGCAACTTCAGTAGGCGTGTCATGGGC - - TGGTTCCGCCAGGCTCCAGGGAAGG
IG11 G - - - TATT - - - - - - - GTCTGGACGCGCCCTCAGCAGACATTCCATTGGC - - TGGTTCCGCCAGGCTCCAGGGAAGG
ID9 A - - - CAGG - - - - - - - CTCTGGGCGCATCTTTGGTGTATATGGTATGGGC - - TGGTTCCGCCAGGCTCCAGGGACGG
IIB12 A - - - CAGG - - - - - - - CTCTGGGCGCATCTTTGGTGTATATGGTATGGGC - - TGGTTCCGCCAGGCTCCAGGGACGG
IF9 A - - - CAGC - - - - - - - CTCTGGGCGTATTTTCAATATATATGGTATGGCA - - TGGTTCCGCCAGGCTCCAGGGACGG
IIF8 A - - - CAGG - - - - - - - CTCTGGGCGTATTTTCGGTATATATGGCCTGGGC - - TGGTTCCGCCAGGTTCCAGGGATGG
IG1 G - - - CAGC - - - - - - - CTCTGGACGCACCTTCAGAGATTATGCCTTGGGC - - TGGTTCCGCCAGTCTCCAGGGAGGG
IIF9 G - - - CAGC - - - - - - - CTCTGGACGCACCTTCAGAGATTATGCCTTGGGC - - TGGTTCCGCCAGTCTCCAGGGAGGG
IG2 G - - - CAGC - - - - - - - CTCGTTACGCACCTTCATTAGCTATCACATGGGC - - TGGTTCCGCCAGACTCCAGGGAAGG
IIF11 G - - - CAGT - - - - - - - CTCTGGACCCACCTTCAATAAGTATGCCATGGG c - - TGGTTCCGCCAGGCTCCAGGAAAGG
IIC10 A - - - CAGC - - - - - - - CTCTGGAGACGACTTCGATAGCTATGTCATGGGC - - TGGTTCCGCCAGGCTCCAGGGAAGG
ID1 G - - - CAGC - - - - - - - CTCGGGACGCTCCTTCAGAAACTCTCACATGACC - - TGGTTCCGCCAGGCTGCAGGGAAGG
IIC2 G - - - CAGC - - - - - - - CTCTGGACGCACCTTCAGTAGACATCCCATGGGC - - TGGTTTCGCCAGGCTCCAGGGAAGG
IIC3 G - - - CAGC - - - - - - - CTCTGGAATCACATTCAAAATATATGACATGGGC - - TGGTACCGCCAGGCTCCAGGAAAGC
IIG1 G - - - CAGC - - - - - - - CTCTGGAATCACATTCAAAATATATGACATGGGC - - TGGTACCGCCAGGCTCCAGGAAAGC
IIF2 G - - - CAGC - - - - - - - CTCTGGAATCACATTCAAAATATATGACATGGGC - - TGGTACCGCCAGGCTCCAGGGAAGC
IIE2 G - - - CAGC - - - - - - - CTCTGGAATCACATTCAAAATATATGACATGGGC - - TGGTACCGCCAGGCTCCAGGGAAGC
IH6 G - - - CAGC - - - - - - - CTCTGGAAGCGCCTTCAGTCTCAATCACATGGCC - - TGGTACCGCTAGGTTCCAGGAAAGC
IID10 G - - - CAGC - - - - - - - CTCTGGAAGCGCCTTCAGTCTCAATCACATGGCC - - TGGTACCGCTAGGTTCCAGGAAAGC
IID2 G - - - CAGC - - - - - - - CTCTGGAAGCGCCTTCAGTCTCAATCACATGGCC - - TGGTACCGCCAGGTTCCAGGAAAGC
IIE6 A - - - CACC - - - - - - - CCGTAGAGGCACCTTCAGTAGGAATGTCGTGGCC - - TGGTACCGCCAGGGTCCAGGGAAGC
IIH6 A - - - CACC - - - - - - - CCGTAGAGGCACCTTCAGTAGGAATGTCGTGGCC - - TGGTACCGCCAGGGTCCAGGGAAGC
IIC8 A - - - CACC - - - - - - - CCGTAGAGGCACCTTCAGTAGGAATGTCGTGGCC - - TGGTACCGCCAGGGTCCAGGGAAGC
IC9 G - - - TAGC - - - - - - - CTCTGGAAGCATCGCCTCAATCAATTTCATGGGC - - TGGTTCCGCCAGGCTCCTGGGAAGG
ID8 G - - - CAGC - - - - - - - CTCTGGAAGCATCTCCTCAATCAATTTCATGGGC - - TGGTTCCGCCAGGCTCCAGGGAAGG
IH5 GGTGCAGC - - - - - - - CTCTGGATTCACTTTGGCGCATTTAGCCGTAGGC - - TGGTTCCGCCAGGCCCCAGGGAAGG
IIC11 G - - - CAGC - - - - - - - CTCTGAACGCATCAGCGGTACCTATGCCATGGGTCT t GGTACCGCCAGGCTCCAGGGAAGC
IIE12 G - - - TTGT - - - - - - - CTCTGGACGCACCTTCAGAAGCTTACATATGGGC - - TGGTTCCGCCAGGCTCCAGGGAAGG
IIH9 GCAGCCTCTGCGCGCACTGCGCGCACCGTCAGTAACAATGGCATGAGC - - TGGTTCCGCCAGGCTCCAGGAAAGG
IG6 ACAGC - - - - - - - - - CTCTGGAAGGATCCAAACCATCAACGCCGTGGGC - - TGGTACCGCCAGGCTCCAGGAAATG
IID12 GGAGT - - - - - - - - - CTCTGGATTAATTTTCGATGATTATGCCATAGGC - - TGGTTCCGCCAGGCCCCAGGGAAGG
IG7 GCATATTCTGGAAGCTTCCACAGTATCACCAGTATGGGC - - - - - - - - - - TGGTATCGCCGCCCGCCAGGGAAAG
IIA12 ATAGTG - - - - - - - - - TCTGGTGCAGCTTTCGAGAATCATGCCGTAGGC - - TGGTTCCGTCAGGCCCCGGGCAAGG
IC11 - TGGTTCCGCCAGGCTCCAGGGAAGG

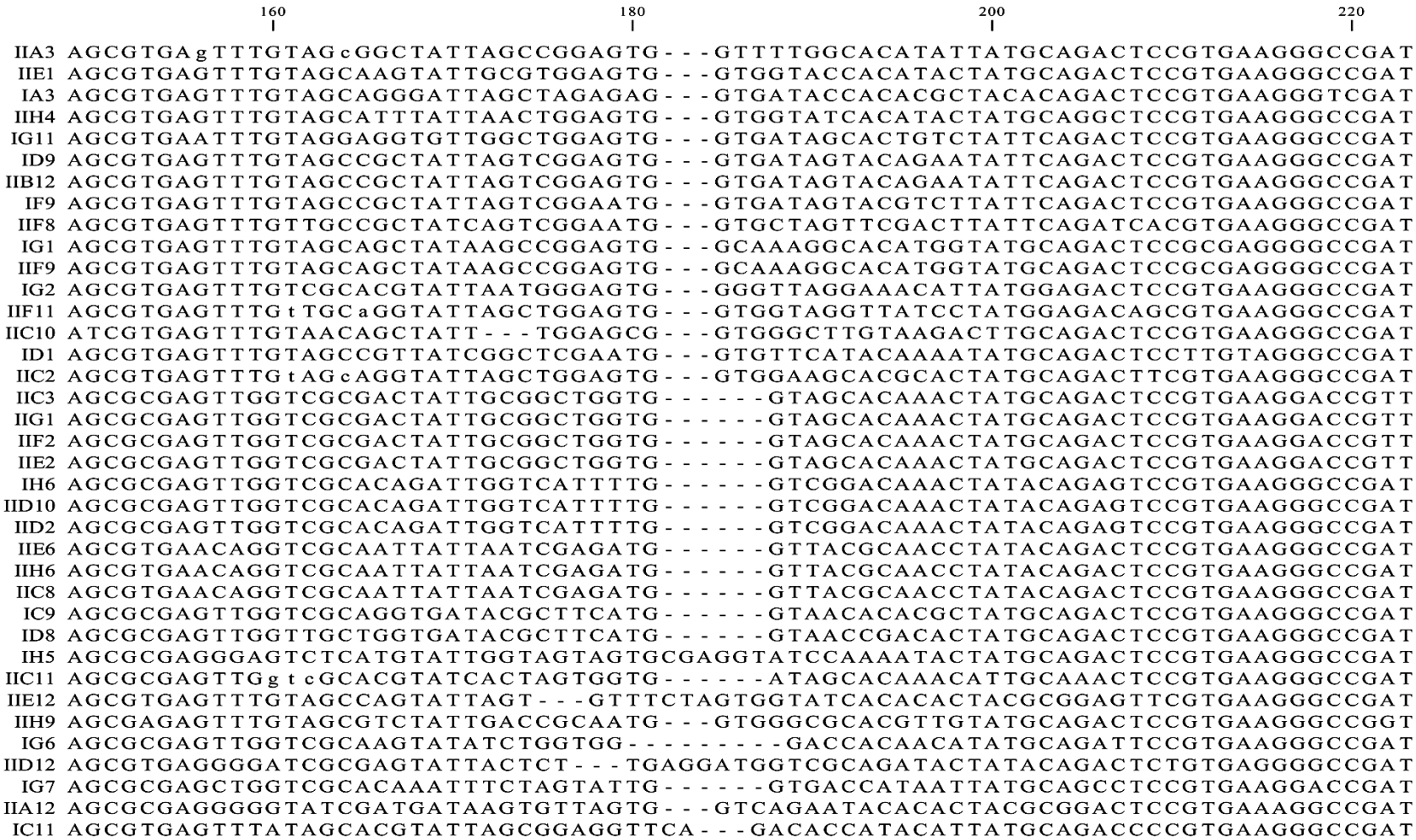
160
180
200
220
IIA3 AGCGTGAgTTTGTAGcGGCTATTAGCCGGAGTG---GTTTTGGCACATATTATGCAGACTCCGTGAAGGGCCGAT
IIE1 AGCGTGAGTTTGTAGCAAGTATTGCGTGGAGTG---GTGGTACCACATACTATGCAGACTCCGTGAAGGGCCGAT
IA3 AGCGTGAGTTTGTAGCAGGGATTAGCTAGAGAG---GTGATACCACACGCTACACAGACTCCGTGAAGGGTCGAT
IIH4 AGCGTGAGTTTGTAGCATTTATTAACTGGAGTG---GTGGTATCACATACTATGCAGGCTCCGTGAAGGGCCGAT
IG11 AGCGTGAATTTGTAGGAGGTGTTGGCTGGAGTG---GTGATAGCACTGTCTATTCAGACTCCGTGAAGGGCCGAT
ID9 AGCGTGAGTTTGTAGCCGCTATTAGTCGGAGTG---GTGATAGTACAGAATATTCAGACTCCGTGAAGGGCCGAT
IIB12 AGCGTGAGTTTGTAGCCGCTATTAGTCGGAGTG---GTGATAGTACAGAATATTCAGACTCCGTGAAGGGCCGAT
IF9 AGCGTGAGTTTGTAGCCGCTATTAGTCGGAATG---GTGATAGTACGTCTTATTCAGACTCCGTGAAGGGCCGAT
IIF8 AGCGTGAGTTTGTTGCCGCTATCAGTCGGAATG---GTGCTAGTTCGACTTATTCAGATCACGTGAAGGGCCGAT
IG1 AGCGTGAGTTTGTAGCAGCTATAAGCCGGAGTG---GCAAAGGCACATGGTATGCAGACTCCGCGAGGGGCCGAT
IIF9 AGCGTGAGTTTGTAGCAGCTATAAGCCGGAGTG---GCAAAGGCACATGGTATGCAGACTCCGCGAGGGGCCGAT
IG2 AGCGTGAGTTTGTCGCACGTATTAATGGGAGTG---GGGTTAGGAAACATTATGGAGACTCCGTGAAGGGCCGAT
IIF11 AGCGTGAGTTTGtTGCaGGTATTAGCTGGAGTG---GTGGTAGGTTATCCTATGGAGACAGCGTGAAGGGCCGAT
IIC10 ATCGTGAGTTTGTAACAGCTATT---TGGAGCG---GTGGGCTTGTAAGACTTGCAGACTCCGTGAAGGGCCGAT
ID1 AGCGTGAGTTTGTAGCCGTTATCGGCTCGAATG---GTGTTCATACAAAATATGCAGACTCCTTGTAGGGCCGAT
IIC2 AGCGTGAGTTTGtAGcAGGTATTAGCTGGAGTG---GTGGAAGCACGCACTATGCAGACTTCGTGAAGGGCCGAT
IIC3 AGCGCGAGTTGGTCGCGACTATTGCGGCTGGTG------GTAGCACAAACTATGCAGACTCCGTGAAGGACCGTT
IIG1 AGCGCGAGTTGGTCGCGACTATTGCGGCTGGTG------GTAGCACAAACTATGCAGACTCCGTGAAGGACCGTT
IIF2 AGCGCGAGTTGGTCGCGACTATTGCGGCTGGTG------GTAGCACAAACTATGCAGACTCCGTGAAGGACCGTT
IIE2 AGCGCGAGTTGGTCGCGACTATTGCGGCTGGTG------GTAGCACAAACTATGCAGACTCCGTGAAGGACCGTT
IH6 AGCGCGAGTTGGTCGCACAGATTGGTCATTTTG------GTCGGACAAACTATACAGAGTCCGTGAAGGGCCGAT
IID10 AGCGCGAGTTGGTCGCACAGATTGGTCATTTTG------GTCGGACAAACTATACAGAGTCCGTGAAGGGCCGAT
IID2 AGCGCGAGTTGGTCGCACAGATTGGTCATTTTG------GTCGGACAAACTATACAGAGTCCGTGAAGGGCCGAT
IIE6 AGCGTGAACAGGTCGCAATTATTAATCGAGATG------GTTACGCAACCTATACAGACTCCGTGAAGGGCCGAT
IIH6 AGCGTGAACAGGTCGCAATTATTAATCGAGATG------GTTACGCAACCTATACAGACTCCGTGAAGGGCCGAT
IIC8 AGCGTGAACAGGTCGCAATTATTAATCGAGATG------GTTACGCAACCTATACAGACTCCGTGAAGGGCCGAT
IC9 AGCGCGAGTTGGTCGCAGGTGATACGCTTCATG------GTAACACACGCTATGCAGACTCCGTGAAGGGCCGAT
ID8 AGCGCGAGTTGGTTGCTGGTGATACGCTTCATG------GTAACCGACACTATGCAGACTCCGTGAAGGGCCGAT
IH5 AGCGCGAGGGAGTCTCATGTATTGGTAGTAGTGCGAGGTATCCAAAATACTATGCAGACTCCGTGAAGGGCCGAT
IIC11 AGCGCGAGTTGgtcGCACGTATCACTAGTGGTG------ATAGCACAAACATTGCAAACTCCGTGAAGGGCCGAT
IIE12 AGCGTGAGTTTGTAGCCAGTATTAGT---GTTTCTAGTGGTATCACACACTACGCGGAGTTCGTGAAGGGCCGAT
IIH9 AGCGAGAGTTTGTAGCGTCTATTGACCGCAATG---GTGGGCGCACGTTGTATGCAGACTCCGTGAAGGGCCGGT
IG6 AGCGCGAGTTGGTCGCAAGTATATCTGGTGG---------GACCACAACATATGCAGATTCCGTGAAGGGCCGAT
IID12 AGCGTGAGGGGATCGCGAGTATTACTCT---TGAGGATGGTCGCAGATACTATACAGACTCTGTGAGGGGCCGAT
IG7 AGCGCGAGCTGGTCGCACAAATTTCTAGTATTG------GTGACCATAATTATGCAGCCTCCGTGAAGGACCGAT
IIA12 AGCGCGAGGGGGTATCGATGATAAGTGTTAGTG---GTCAGAATACACACTACGCGGACTCCGTGAAAGGCCGAT
IC11 AGCGTGAGTTTATAGCACGTATTAGCGGAGGTTCA---GACACCATACATTATGCAGACCCCGTGAAGGGCCGAT

```
                          240                 260                 280
                           |                   |                   |
IIA3  TCACCATCTCCAGAGACAACGCCAACAACACGGCGTATCTGCACATGAACAGCCTGCAACCTGAAGACACGGCCG
IIE1  TCACCATCTCCAGAGACGACGCCAAGAACACGGTGTCGCTGCAAATGAACAGCCTGAAACCTGAGGACACGGCCG
IA3   TCATCATCTCCAGAGACAACGCCAAGAACACGGTGTATCTGCAAATGAACAGCCTGAAACCTGGGGACGCGGCCG
IIH4  TCACCATCTCCAGAGACAACGTCAAGAACACGGTGTATCTGCAAATGAACAGCCTGAAACCTGAGGACACGGCCA
IG11  TCTCCATCTCCAGAGACAACGCCAAGAACACGGTGTATCTGCAAATGAACAGTCTGAAACCTGAGGACACGGCCG
ID9   TCGCCATCTCCAGAGACAATTCCAAGAACACGGTGACTCTGCAAATGAACAGCCTGACACCTGAGGACACGGCCG
IIB12 TCGCCATCTCCAGAGACAATTCCAAGAACACGGTGACTCTGCAAATGAACAGCCTGACACCTGAGGACACGGCCG
IF9   TCGCCATCTCCAGAGACAACTCCAAGAACACGGTGTCTCTGCAAATGAACAGCCTGACACCTGAGGACACGGCCA
IIF8  TCGCCATCTCCAGAGACAACTCCAAGAACACGGTGTCTCTACAAATGAACAGTCTAGTACCTGAGGATTCGGCCG
IG1   TCACGATCTTCAGAGATGACGCCAAGAGCACGGTGTATCTACAAATGAACAGCCTGAAACCAGAGGACACGGCCC
IIF9  TCACGATCTTCAGAGATGACGCCAAGAGCACGGTGTATCTACAAATGAACAGCCTGAAACCAGAGGACACGGCCC
IG2   TCACCATCTCCAGAGACAACTCCAAGAACACGGTGTATCTACAAATGAACAGCCTGAAACCTGAGGACACGGCCG
IIF11 TTACCATCTCCAGAGACAACGCCAAGAACACGGTGTCTCTGCAAATGAACAGCCTGAAACCTGAGGACACGGCCG
IIC10 TCACCATCTCCAGAGACAACCCCAGGAACACGATATATCTGCAAATGAACAGCCTGAAATCTGAGGACACGGCCG
ID1   TCACGATCTCCAGAAACAACGACGACAATGCGGTGTATCTACAAATGAACAGCCTGAAACCTGAGGACACGGCCG
IIC2  TCACCATTTCCACAAACAACGCCAAGAACACGGTGTATCTGAAAATGGACAGCCTGAAACCTGAAGACACGGCCG
IIC3  TCACCATCTCCAGAGACAACACCAAGAACACGGTGTATCTGCAAATGAACAGCCTAAAACCTGAGGACACGGCCG
IIG1  TCACCATCTCCAGAGACAACACCAAGAACACGGTGTATCTGCAAATGAACAGCCTAAAACCTGAGGACACGGCCG
IIF2  TCACCATCTCCAGAGACAACACCAAGAACACGGTGTATCTGCAAATGAACAGCCTAAAACCTGAGGACACGGCCG
IIE2  TCACCATCTCCAGAGACAACACCAAGAACACGGTGTATCTGCAAATGAACAGCCTAAAACCTGAGGACACGGCCG
IH6   TCACCATCTCCAGAGACGACGCCAAGAACACGCTGTATCTGCAAATGAACGGCCTTAAACCTGAGGATTCGGCTG
IID10 TCACCATCTCCAGAGACGACGCCAAGAACACGCTGTATCTGCAAATGAACGGCCTTAAACCTGAGGACTCGGCCG
IID2  TCACCATCTCCAGAGACGACGCCAAGAACACGCTGTATCTGCAAATGAACGGCCTTAAACCTGAGGACTCGGCCG
IIE6  TCACCGCCTCCAGAGACAACGCCAAGAACACGGTGTATCTTCAAATGAACAACCTGAAACCTGAGGATACGGCCG
IIH6  TCACCGCCTCCAGAGACAACGCCAAGAACACGGTGTATCTTCAAATGAACAACCTGAAACCTGAGGATACGGCCG
IIC8  TCACCATCTCCAGAGACAACGCCAACAATACGGTGTATCTGCAAATGAACAGCCTGAAACCTGAGGACACGGCCG
IC9   TCACCATCTCCAGAGACAACGCCAACAATACGGTGTATCTGCAAATGAACAGCCTGAAACCTGAGGACACGGCCG
ID8   TCACCATCTCCAGAGACAACGCCAACAACACGGTGTATCTGCAAATGAACAATCTAGAACCTGAGGACACGGCCG
IH5   TCACCATCTCCAGAGCCGATGACAAGAACACGGTGTATCTGGAAATGAACAACCTGAAACCTGAGGATACGGCCG
IIC11 TCACCATCTCCAGAGACAACGCTAAGAACACGGTGTATCTACAAATGAACACCCTGAAACCTGAGGACACAGCCG
IIE12 TCACCGTTTCTGGGGACCACGCCAAGAACACAGTGTACCTGCGAATGGACAGCCTGAAACCTGAGGACACGGCCG
IIH9  TCACCATCTCCAGAGACAATGCCAAGAACACGGTGTATCTCCAAATGAACAACCTGAAACCTGAGGACACGGCCG
IG6   TCACCATCTCCGGAGACAACGCCAAGCGCACGTTCCATCTGCAAATGACCGGCCTGAAACCTGACGACACAGCCA
IID12 TCTCCATCTCCACAAACAACGCCAAGAACACGGTATATCTCCAAATGAACAGCCTGAAGCCTGAGGACACGGCCG
IG7   TCACCATCGCCAGAGACAGCGCCAAGCACACGCTGTATCTGCACATGAACAGCCTGAAACCTGAGGACACAGCCG
IIA12 TCACTATCTCCAGAGACAACACCAAGAACACGGTGTGGCTGCAGATGAACAACCTGAGACCTGAGGACACGGCCG
IC11  TCACCATCTCCAGAGACAACACCAAGAACACGGGGTATCTGCAAATGAACGGCCTGAAACCTGAGGACACGGCCG
```

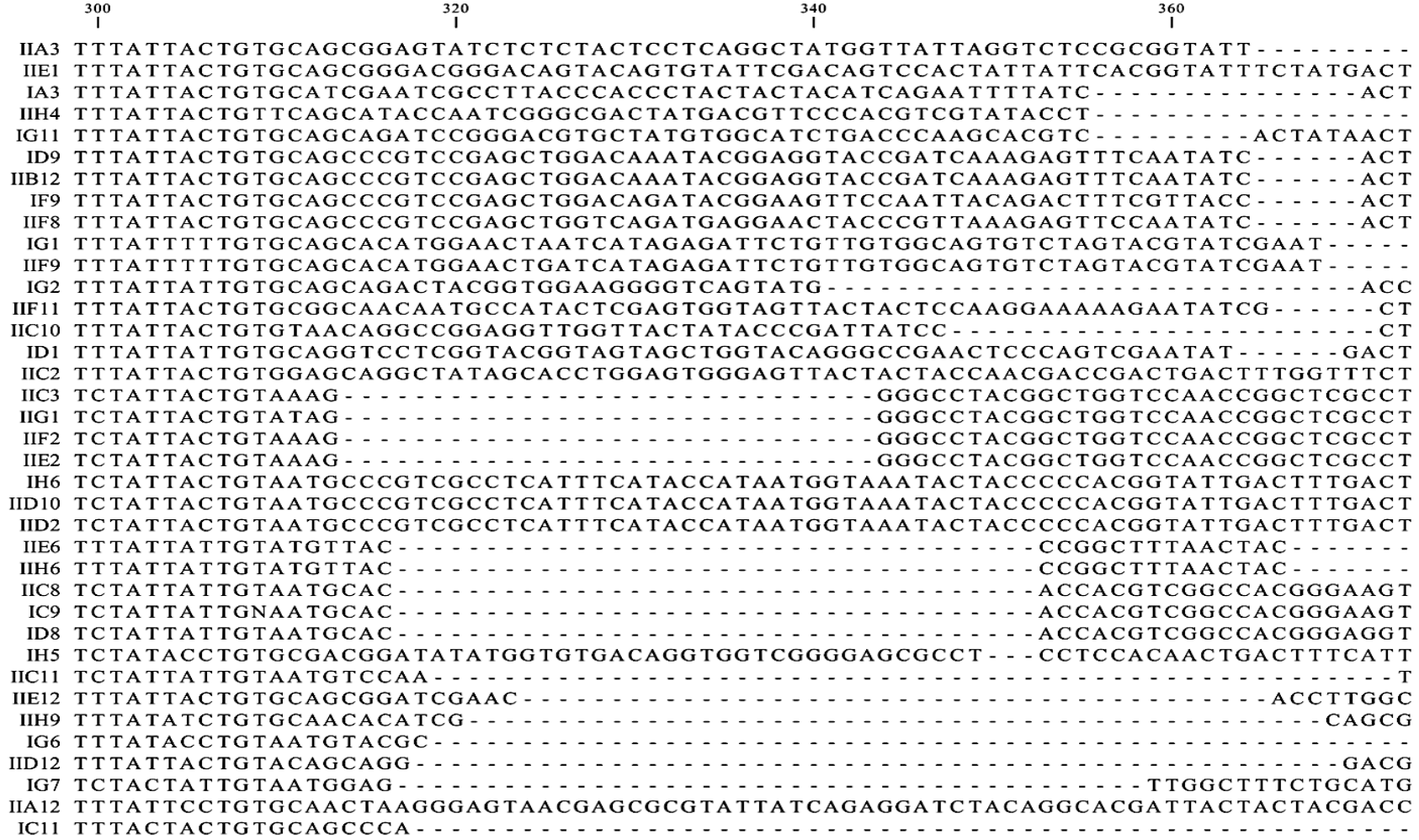
300
320
340
360
IIA3 TTTATTACTGTGCAGCGGAGTATCTCTCTACTCCTCAGGCTATGGTTATTAGGTCTCCGCGGTATT---------
IIE1 TTTATTACTGTGCAGCGGGACGGGACAGTACAGTGTATTCGACAGTCCACTATTATTCACGGTATTTCTATGACT
IA3 TTTATTACTGTGCATCGAATCGCCTTACCCACCCTACTACTACATCAGAATTTTATC---------------ACT
IIH4 TTTATTACTGTTCAGCATACCAATCGGGCGACTATGACGTTCCCACGTCGTATACCT-----------------
IG11 TTTATTACTGTGCAGCAGATCCGGGACGTGCTATGTGGCATCTGACCCAAGCACGTC---------ACTATAACT
ID9 TTTATTACTGTGCAGCCCGTCCGAGCTGGACAAATACGGAGGTACCGATCAAAGAGTTTCAATATC------ACT
IIB12 TTTATTACTGTGCAGCCCGTCCGAGCTGGACAAATACGGAGGTACCGATCAAAGAGTTTCAATATC------ACT
IF9 TTTATTACTGTGCAGCCCGTCCGAGCTGGACAGATACGGAAGTTCCAATTACAGACTTTCGTTACC------ACT
IIF8 TTTATTACTGTGCAGCCCGTCCGAGCTGGTCAGATGAGGAACTACCCGTTAAAGAGTTCCAATATC------ACT
IG1 TTTATTTTTGTGCAGCACATGGAACTAATCATAGAGATTCTGTTGTGGCAGTGTCTAGTACGTATCGAAT-----
IIF9 TTTATTTTTGTGCAGCACATGGAACTGATCATAGAGATTCTGTTGTGGCAGTGTCTAGTACGTATCGAAT-----
IG2 TTTATTATTGTGCAGCAGACTACGGTGGAAGGGGTCAGTATG-----------------------------ACC
IIF11 TTTATTACTGTGCGGCAACAATGCCATACTCGAGTGGTAGTTACTACTCCAAGGAAAAAGAATATCG------CT
IIC10 TTTATTACTGTGTAACAGGCCGGAGGTTGGTTACTATACCCGATTATCC-----------------------CT
ID1 TTTATTATTGTGCAGGTCCTCGGTACGGTAGTAGCTGGTACAGGGCCGAACTCCCAGTCGAATAT------GACT
IIC2 TTTATTACTGTGGAGCAGGCTATAGCACCTGGAGTGGGAGTTACTACTACCAACGACCGACTGACTTTGGTTTCT
IIC3 TCTATTACTGTAAAG-----------------------------GGGCCTACGGCTGGTCCAACCGGCTCGCCT
IIG1 TCTATTACTGTATAG-----------------------------GGGCCTACGGCTGGTCCAACCGGCTCGCCT
IIF2 TCTATTACTGTAAAG-----------------------------GGGCCTACGGCTGGTCCAACCGGCTCGCCT
IIE2 TCTATTACTGTAAAG-----------------------------GGGCCTACGGCTGGTCCAACCGGCTCGCCT
IH6 TCTATTACTGTAATGCCCGTCGCCTCATTTCATACCATAATGGTAAATACTACCCCCACGGTATTGACTTTGACT
IID10 TCTATTACTGTAATGCCCGTCGCCTCATTTCATACCATAATGGTAAATACTACCCCCACGGTATTGACTTTGACT
IID2 TCTATTACTGTAATGCCCGTCGCCTCATTTCATACCATAATGGTAAATACTACCCCCACGGTATTGACTTTGACT
IIE6 TTTATTATTGTATGTTAC-----------------------------------CCGGCTTTAACTAC-------
IIH6 TTTATTATTGTATGTTAC-----------------------------------CCGGCTTTAACTAC-------
IIC8 TCTATTATTGTAATGCAC-----------------------------------ACCACGTCGGCCACGGGAAGT
IC9 TCTATTATTGNAATGCAC-----------------------------------ACCACGTCGGCCACGGGAAGT
ID8 TCTATTATTGTAATGCAC-----------------------------------ACCACGTCGGCCACGGGAGGT
IH5 TCTATACCTGTGCGACGGATATATGGTGTGACAGGTGGTCGGGGAGCGCCT---CCTCCACAACTGACTTTCATT
IIC11 TCTATTATTGTAATGTCCAA---T
IIE12 TTTATTACTGTGCAGCGGATCGAAC---ACCTTGGC
IIH9 TTTATATCTGTGCAACACATCG---CAGCG
IG6 TTTATACCTGTAATGTACGC---
IID12 TTTATTACTGTACAGCAGG---GACG
IG7 TCTACTATTGTAATGGAG-----------------------------------TTGGCTTTCTGCATG
IIA12 TTTATTCCTGTGCAACTAAGGGAGTAACGAGCGCGTATTATCAGAGGATCTACAGGCACGATTACTACTACGACC
IC11 TTTACTACTGTGCAGCCCA---

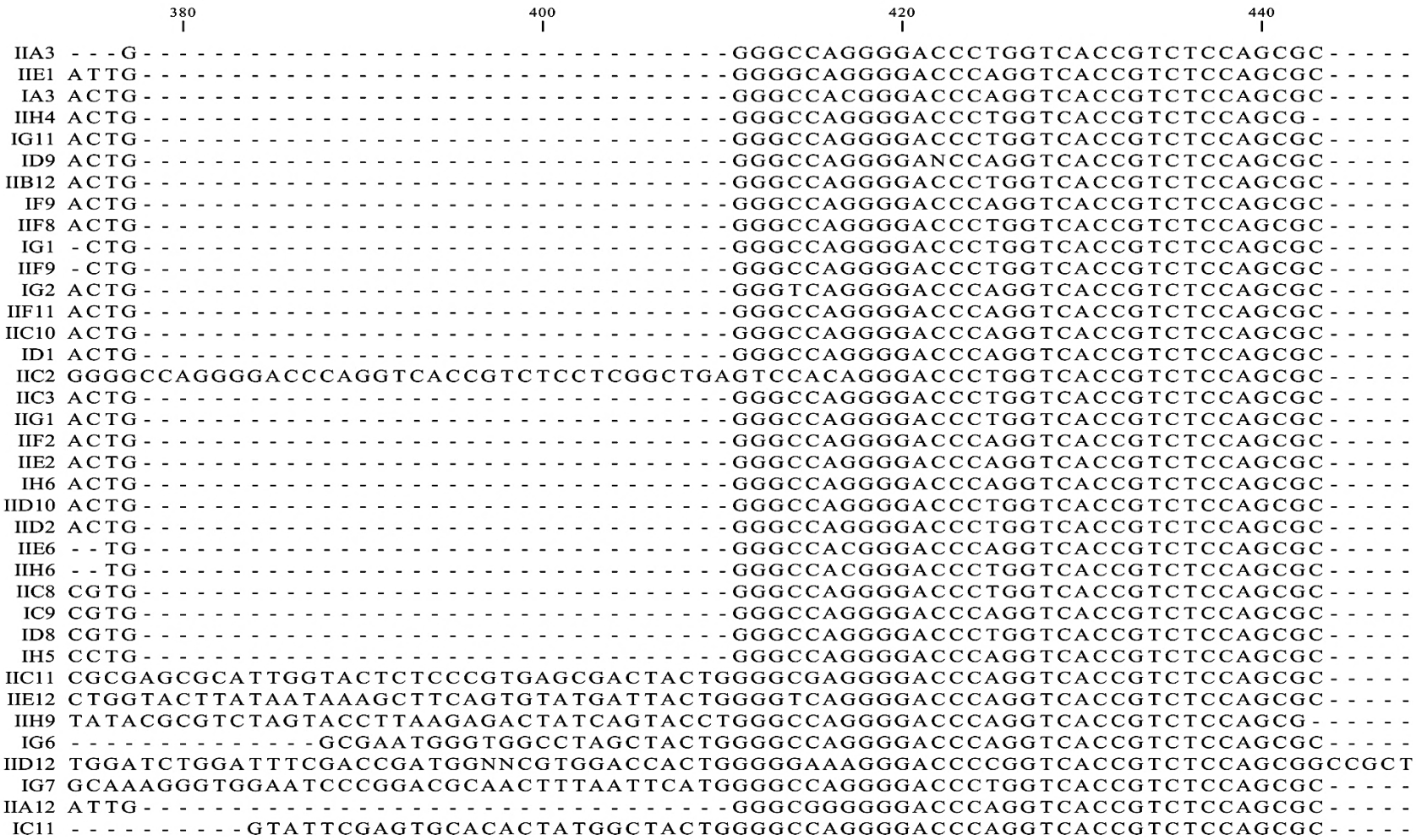
380
400
420
440
IIA3 ---G----------GGGCCAGGGGACCCTGGTCACCGTCTCCAGCGC-----
IIE1 ATTG----------GGGGCAGGGGACCCAGGTCACCGTCTCCAGCGC-----
IA3 ACTG----------GGGCCACGGGACCCAGGTCACCGTCTCCAGCGC-----
IIH4 ACTG----------GGGCCAGGGGACCCTGGTCACCGTCTCCAGCG------
IG11 ACTG----------GGGCCAGGGGACCCTGGTCACCGTCTCCAGCGC-----
ID9 ACTG----------GGGCCAGGGGANCCAGGTCACCGTCTCCAGCGC-----
IIB12 ACTG----------GGGCCAGGGGACCCTGGTCACCGTCTCCAGCGC-----
IF9 ACTG----------GGGCCAGGGGACCCAGGTCACCGTCTCCAGCGC-----
IIF8 ACTG----------GGGCCAGGGGACCCTGGTCACCGTCTCCAGCGC-----
IG1 -CTG----------GGGCCAGGGGACCCTGGTCACCGTCTCCAGCGC-----
IIF9 -CTG----------GGGCCAGGGGACCCTGGTCACCGTCTCCAGCGC-----
IG2 ACTG----------GGGTCAGGGGACCCAGGTCACCGTCTCCAGCGC-----
IIF11 ACTG----------GGGCCAGGGGACCCAGGTCACCGTCTCCAGCGC-----
IIC10 ACTG----------GGGCCAGGGGACCCAGGTCACCGTCTCCAGCGC-----
ID1 ACTG----------GGGCCAGGGGACCCAGGTCACCGTCTCCAGCGC-----
IIC2 GGGGCCAGGGGACCCAGGTCACCGTCTCCTCGGCTGAGTCCACAGGGACCCTGGTCACCGTCTCCAGCGC-----
IIC3 ACTG----------GGGCCAGGGGACCCTGGTCACCGTCTCCAGCGC-----
IIG1 ACTG----------GGGCCAGGGGACCCTGGTCACCGTCTCCAGCGC-----
IIF2 ACTG----------GGGCCAGGGGACCCAGGTCACCGTCTCCAGCGC-----
IIE2 ACTG----------GGGCCAGGGGACCCAGGTCACCGTCTCCAGCGC-----
IH6 ACTG----------GGGCCAGGGGACCCAGGTCACCGTCTCCAGCGC-----
IID10 ACTG----------GGGCCAGGGGACCCTGGTCACCGTCTCCAGCGC-----
IID2 ACTG----------GGGCCAGGGGACCCTGGTCACCGTCTCCAGCGC-----
IIE6 --TG----------GGGCCACGGGACCCAGGTCACCGTCTCCAGCGC-----
IIH6 --TG----------GGGCCACGGGACCCTGGTCACCGTCTCCAGCGC-----
IIC8 CGTG----------GGGCCAGGGGACCCTGGTCACCGTCTCCAGCGC-----
IC9 CGTG----------GGGCCAGGGGACCCAGGTCACCGTCTCCAGCGC-----
ID8 CGTG----------GGGCCAGGGGACCCTGGTCACCGTCTCCAGCGC-----
IH5 CCTG----------GGGCCAGGGGACCCAGGTCACCGTCTCCAGCGC-----
IIC11 CGCGAGCGCATTGGTACTCTCCCGTGAGCGACTACTGGGGCGAGGGGACCCAGGTCACCGTCTCCAGCGC-----
IIE12 CTGGTACTTATAATAAAGCTTCAGTGTATGATTACTGGGGTCAGGGGACCCAGGTCACCGTCTCCAGCGC-----
IIH9 TATACGCGTCTAGTACCTTAAGAGACTATCAGTACCTGGGCCAGGGGACCCAGGTCACCGTCTCCAGCG------
IG6 ----------GCGAATGGGTGGCCTAGCTACTGGGGCCAGGGGACCCAGGTCACCGTCTCCAGCGC-----
IID12 TGGATCTGGATTTCGACCGATGGNNCGTGGACCACTGGGGGAAAGGGACCCCGGTCACCGTCTCCAGCGGCCGCT
IG7 GCAAAGGGTGGAATCCCGGACGCAACTTTAATTCATGGGGCCAGGGGACCCTGGTCACCGTCTCCAGCGC-----
IIA12 ATTG----------GGGCGGGGGGACCCAGGTCACCGTCTCCAGCGC-----
IC11 ----------GTATTCGAGTGCACACTATGGCTACTGGGGCCAGGGGACCCAGGTCACCGTCTCCAGCGC-----

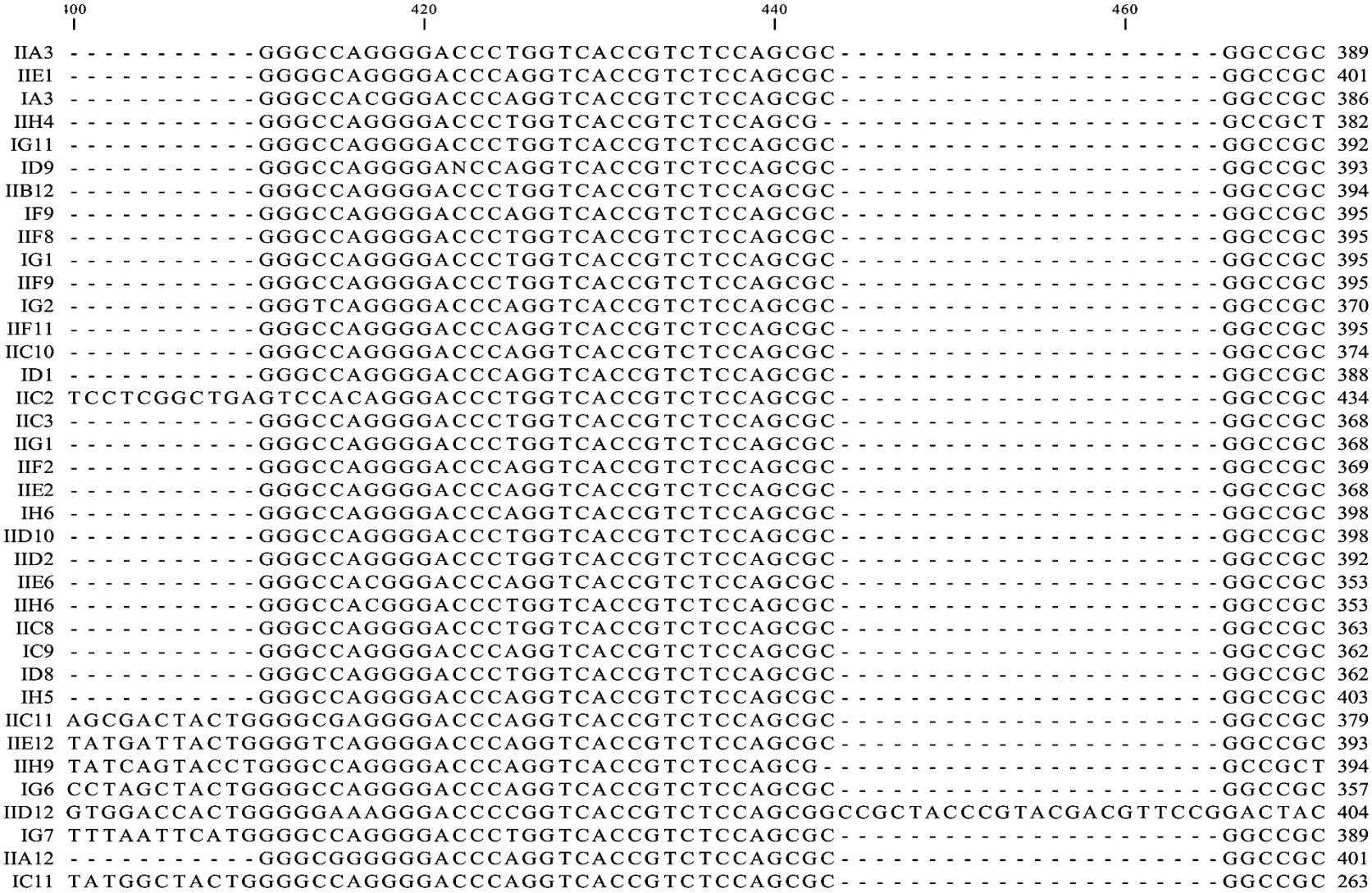
100
420
440
460
IIA3 ----------GGGCCAGGGGACCCTGGTCACCGTCTCCAGCGC----------GGCCGC 389
IIE1 ----------GGGGCAGGGGACCCAGGTCACCGTCTCCAGCGC----------GGCCGC 401
IA3 ----------GGGCCACGGGACCCAGGTCACCGTCTCCAGCGC----------GGCCGC 386
IIH4 ----------GGGCCAGGGGACCCTGGTCACCGTCTCCAGCG----------GCCGCT 382
IG11 ----------GGGCCAGGGGACCCTGGTCACCGTCTCCAGCGC----------GGCCGC 392
ID9 ----------GGGCCAGGGGANCCAGGTCACCGTCTCCAGCGC----------GGCCGC 393
IIB12 ----------GGGCCAGGGGACCCTGGTCACCGTCTCCAGCGC----------GGCCGC 394
IF9 ----------GGGCCAGGGGACCCAGGTCACCGTCTCCAGCGC----------GGCCGC 395
IIF8 ----------GGGCCAGGGGACCCTGGTCACCGTCTCCAGCGC----------GGCCGC 395
IG1 ----------GGGCCAGGGGACCCTGGTCACCGTCTCCAGCGC----------GGCCGC 395
IIF9 ----------GGGCCAGGGGACCCTGGTCACCGTCTCCAGCGC----------GGCCGC 395
IG2 ----------GGGTCAGGGGACCCAGGTCACCGTCTCCAGCGC----------GGCCGC 370
IIF11 ----------GGGCCAGGGGACCCAGGTCACCGTCTCCAGCGC----------GGCCGC 395
IIC10 ----------GGGCCAGGGGACCCAGGTCACCGTCTCCAGCGC----------GGCCGC 374
ID1 ----------GGGCCAGGGGACCCAGGTCACCGTCTCCAGCGC----------GGCCGC 388
IIC2 TCCTCGGCTGAGTCCACAGGGACCCTGGTCACCGTCTCCAGCGC----------GGCCGC 434
IIC3 ----------GGGCCAGGGGACCCTGGTCACCGTCTCCAGCGC----------GGCCGC 368
IIG1 ----------GGGCCAGGGGACCCTGGTCACCGTCTCCAGCGC----------GGCCGC 368
IIF2 ----------GGGCCAGGGGACCCAGGTCACCGTCTCCAGCGC----------GGCCGC 369
IIE2 ----------GGGCCAGGGGACCCAGGTCACCGTCTCCAGCGC----------GGCCGC 368
IH6 ----------GGGCCAGGGGACCCAGGTCACCGTCTCCAGCGC----------GGCCGC 398
IID10 ----------GGGCCAGGGGACCCTGGTCACCGTCTCCAGCGC----------GGCCGC 398
IID2 ----------GGGCCAGGGGACCCTGGTCACCGTCTCCAGCGC----------GGCCGC 392
IIE6 ----------GGGCCACGGGACCCAGGTCACCGTCTCCAGCGC----------GGCCGC 353
IIH6 ----------GGGCCACGGGACCCTGGTCACCGTCTCCAGCGC----------GGCCGC 353
IIC8 ----------GGGCCAGGGGACCCTGGTCACCGTCTCCAGCGC----------GGCCGC 363
IC9 ----------GGGCCAGGGGACCCAGGTCACCGTCTCCAGCGC----------GGCCGC 362
ID8 ----------GGGCCAGGGGACCCTGGTCACCGTCTCCAGCGC----------GGCCGC 362
IH5 ----------GGGCCAGGGGACCCAGGTCACCGTCTCCAGCGC----------GGCCGC 403
IIC11 AGCGACTACTGGGGCGAGGGGACCCAGGTCACCGTCTCCAGCGC----------GGCCGC 379
IIE12 TATGATTACTGGGGTCAGGGGACCCAGGTCACCGTCTCCAGCGC----------GGCCGC 393
IIH9 TATCAGTACCTGGGCCAGGGGACCCAGGTCACCGTCTCCAGCG----------GCCGCT 394
IG6 CCTAGCTACTGGGGCCAGGGGACCCAGGTCACCGTCTCCAGCGC----------GGCCGC 357
IID12 GTGGACCACTGGGGGAAAGGGACCCCGGTCACCGTCTCCAGCGGCCGCTACCCGTACGACGTTCCGGACTAC 404
IG7 TTTAATTCATGGGGCCAGGGGACCCTGGTCACCGTCTCCAGCGC----------GGCCGC 389
IIA12 ----------GGGCGGGGGGACCCAGGTCACCGTCTCCAGCGC----------GGCCGC 401
IC11 TATGGCTACTGGGGCCAGGGGACCCAGGTCACCGTCTCCAGCGC----------GGCCGC 263